National Library of Canada
Bibliothèque nationale du Canada

Canadian Theses Service
Service des thèses canadiennes

Ottawa, Canada
K1A 0N4

NOTICE

The quality of this microform is heavily dependent upon the quality of the original thesis submitted for microfilming. Every effort has been made to ensure the highest quality of reproduction possible.

If pages are missing, contact the university which granted the degree.

Some pages may have indistinct print especially if the original pages were typed with a poor typewriter ribbon or if the university sent us an inferior photocopy.

Reproduction in full or in part of this microform is governed by the Canadian Copyright Act, R.S.C. 1970, c. C-30, and subsequent amendments.

AVIS

La qualité de cette microforme dépend grandement de la qualité de la thèse soumise au microfilmage. Nous avons tout fait pour assurer une qualité supérieure de reproduction.

S'il manque des pages, veuillez communiquer avec l'université qui a conféré le grade.

La qualité d'impression de certaines pages peut laisser à désirer, surtout si les pages originales ont été dactylographiées à l'aide d'un ruban usé ou si l'université nous a fait parvenir une photocopie de qualité inférieure.

La reproduction, même partielle, de cette microforme est soumise à la Loi canadienne sur le droit d'auteur, SRC 1970, c. C-30, et ses amendements subséquents.

NL-339 (r. 88/04) c

Canada

University of Alberta

A Single Phase, Unity Power Factor, Soft Switching, Resonant Tank Boost Rectifier with Tank Phase Controlled Input Current

by

Lawrence Joseph Borle

A Thesis submitted to the Faculty of Graduate Studies and Research in partial fullfilment of the Requirements for the Degree of

Master of Science

Department of Electrical Engineering

Edmonton, Alberta

Fall 1991

National Library of Canada
Bibliothèque nationale du Canada

Canadian Theses Service
Service des thèses canadiennes

Ottawa, Canada
K1A 0N4

The author has granted an irrevocable non-exclusive licence allowing the National Library of Canada to reproduce, loan, distribute or sell copies of his/her thesis by any means and in any form or format, making this thesis available to interested persons.

The author retains ownership of the copyright in his/her thesis. Neither the thesis nor substantial extracts from it may be printed or otherwise reproduced without his/her permission.

L'auteur a accordé une licence irrévocable et non exclusive permettant à la Bibliothèque nationale du Canada de reproduire, prêter, distribuer ou vendre des copies de sa thèse de quelque manière et sous quelque forme que ce soit pour mettre des exemplaires de cette thèse à la disposition des personnes intéressées.

L'auteur conserve la propriété du droit d'auteur qui protège sa thèse. Ni la thèse ni des extraits substantiels de celle-ci ne doivent être imprimés ou autrement reproduits sans son autorisation.

ISBN 0-315-70166-8

Canada

University of Alberta

RELEASE FORM

Name of Author:	Lawrence Joseph Borle
Title of Thesis:	A Single Phase, Unity Power Factor, Soft Switching, Resonant Tank Boost Rectifier with Tank Phase Controlled Input Current
Degree:	Master of Science
Year This Thesis Granted:	Fall 1991

Permission is hereby granted to THE UNIVERSITY OF ALBERTA LIBRARY to reproduce single copies of this thesis and to lend or sell such copies for private, scholarly or scientific research purposes only.

The author reserves other publication rights, and neither the thesis nor extensive extracts from it may be printed or otherwise reproduced without the author's written permission.

Lawrence Borle

Lawrence Borle

Permanent Address: 4005 - 42 Street
Stony Plain, Alberta
T0E 2G0

Date: 1991 - July - 31

University of Alberta

Faculty of Graduate Studies and Research

The undersigned certify they have read, and recommend to the Faculty of Graduate Studies and Research for acceptance, a thesis entitled "A SINGLE PHASE, UNITY POWER FACTOR, SOFT SWITCHING, RESONANT TANK BOOST RECTIFIER, WITH TANK PHASE CONTROLLED INPUT CURRENT", submitted by LAWRENCE JOSEPH BORLE in partial fulfillment of the requirements for the degree of MASTER of SCIENCE in ELECTRICAL ENGINEERING.

John C. Salmon

Dr. John Salmon, Supervisor

Keith Stromsmoe

Dr. Keith Stromsmoe, Committee Member

Duane Szafron

Dr. Duane Szafron, Committee Member

Date: 30th July 1991

Abstract

A single phase, soft-switched resonant tank boost rectifer (RTBR) with sinusoidal input current is presented. The RTBR has a boost converter topology which employs a continuously resonating L-C tank circuit in series with the switch to provide input current control and soft switching. A linear relationship exists between the phase of the resonant tank oscillation at switch turn-on and the resulting average input current for the switching period. The input current is forced to follow a sinusoidal reference waveform by timing the turn-on of the switch in successive switching periods to coincide with the appropriate tank phase. The tank capacitance provides zero-voltage-switching (ZVS) at the turn-off of the switch. Discontinuous current in the boost inductor provides zero-current-switching (ZCS) at turn-on.

As an introduction to the subject rectifier, unity power factor ac to dc power converters are reviewed. The basic operation of existing hard-switched and resonant switch-mode rectifier topologies is explained.

The operation of the RTBR is studied using a mathematical simulation. DC steady-state operation is found to be very close to ac line cycle operation in the simulation. The performance of the circuit is found to be dependent on the quality factor of the resonant tank.

The phase control technique is used together with a current estimator in an experimental prototype circuit. Experimental results are obtained from an 800 watt rectifier switching at 20 kilohertz using an IGBT switch. Performance with unity power factor, low current distortion, is demonstrated.

Acknowledgment

I would like to thank the Alberta Microelectronic Center for their financial contribution, without which this work would have been severely curtailed.

Thanks also to the many people at the University of Alberta who have helped me overcome many obstacles;

- To my supervisor, Dr. John Salmon for his technical guidance at many crucial points in the work in this thesis, and for providing high quality facilities and equipment.
- To Eric, Dan and Stuart, my fellow grad students, who gave of their knowledge and of their humor.
- To Albert, who was always ready with his practical expertise.
- To Herb and Bernie in the machine shop who promptly performed much of the metal work required to build the RTBR prototype.

Finally, I would like to thank my friends and family for their support, patience and understanding.

Contents

List of Tables ix

List of Figures x

Symbols xiii

1 Introduction 1
- 1.1 Performance Parameters . . . 1
  - 1.1.1 Power Factor . . . 1
  - 1.1.2 Total Harmonic Distortion . . . 2
- 1.2 Utility Harmonics . . . 3
  - 1.2.1 Sources of Harmonics . . . 3
  - 1.2.2 Effects of Harmonics . . . 3
  - 1.2.3 Harmonic Standards . . . 4
- 1.3 AC to DC Power Conversion . . . 5

2 Switch-mode Rectifiers 8
- 2.1 Boost Rectifier . . . 10
  - 2.1.1 Current Control . . . 10
  - 2.1.2 Variations . . . 13
- 2.2 Buck Rectifier . . . 16
  - 2.2.1 Current Control . . . 18
  - 2.2.2 Variations . . . 19
- 2.3 Buck-Boost Rectifier . . . 21
  - 2.3.1 Current Control . . . 22
  - 2.3.2 Variations . . . 22
- 2.4 Three Switched-Network Rectifiers . . . 23
- 2.5 Controlled Bridge Rectifiers . . . 23
  - 2.5.1 Half Bridge Rectifiers . . . 24
  - 2.5.2 Full Bridge Rectifiers . . . 25
  - 2.5.3 Current Control . . . 27

3 Resonant Switch-Mode Rectifiers **28**
3.1 Switching Losses . . . 28
3.2 Resonant Circuits . . . 29
3.2.1 Resonant DC to DC Converters . . . 30
3.2.2 Quasi-resonant Converters . . . 31
3.2.3 Resonant Rectifiers . . . 32
3.3 Resonant Boost Rectifiers . . . 34
3.4 Disadvantages of Existing Resonant Switch-mode Rectifiers . . . 39

4 Resonant Tank Boost Rectifier **40**
4.1 Overview . . . 40
4.2 Power Circuit Operation . . . 41
4.3 On Period . . . 43
4.4 Off Period . . . 48
4.5 Control System . . . 50
4.5.1 Tank Phase Window . . . 51
4.5.2 Inner Current Control Loop . . . 53
4.5.3 Outer Voltage Control Loop . . . 55
4.5.4 Forced Commutation . . . 56
4.6 Continuous Operation . . . 57
4.6.1 Steady-State Operation . . . 57

5 Simulation of the RTBR **60**
5.1 DCSteadyState . . . 60
5.1.1 Program Description . . . 61
5.1.2 Circuit Variable Formulae . . . 65
5.1.3 Switching Period Calculations . . . 66
5.2 ACLineCycle . . . 67
5.2.1 Program Description . . . 67
5.2.2 Circuit Variable Formulae . . . 70
5.2.3 Switching Period Calculations . . . 70
5.3 Simulation Results . . . 71
5.3.1 Average Input Pulse Current . . . 73
5.3.2 Peak Input Pulse Current . . . 77
5.3.3 Time at Switch Turn-off . . . 78
5.3.4 Tank Phase at Turn-off . . . 78
5.3.5 Peak Tank Voltage . . . 82
5.3.6 Switching Cycle Tank Loss . . . 84
5.3.7 Pulse Efficiency . . . 84
5.3.8 Switching Frequency . . . 86

5.4 Simulation Limitations 88
5.4.1 Undamped On Period Calculations 88
5.4.2 Estimation of Losses 88
5.4.3 Switching Transients 88

6 Prototype Design and Performance **89**
6.1 Design Criteria 89
6.2 Component Selection and Design 91
6.3 Control System Design 100
6.4 Experimental Accuracy 103
6.5 Verification of the Simulation Accuracy 104
6.6 Experimental Results 111
6.6.1 Zero Current and Zero Voltage Switching 111
6.6.2 Closed Loop Power Factor 111
6.6.3 Open Loop Power Factor 114
6.6.4 Efficiency 114

7 Conclusion **116**
7.1 RTBR Performance 116
7.1.1 Advantages 117
7.1.2 Disadvantages 117
7.1.3 Transient Operation 118
7.2 Suggestions for Further Work 119

References **121**

A DCSteadyState Simulation Program Listing **126**

B ACLineCycle Simulation Program Listing **135**

C Control Circuit Schematic Diagram **144**

List of Tables

5.1 Simulation and Prototype Per Unit Base Parameters 72
5.2 Simulation Base Case Component Values 72
5.3 Component Values Changed from the Base Case for $Z_t = 0.159$ . . . 72
5.4 Comparison of Average Input Currents Determined in **DCSteady-State** and **ACLineCycle** 75

6.1 Prototype RTBR Design Values 90
6.2 Prototype RTBR Simulation Component Values 92
6.3 Prototype RTBR Components 99

List of Figures

1.1 Diode Bridge LC Rectifier 5
1.2 Common Rectifier Input Current Waveforms 6
1.3 Relationship Between Distortion and Current Harmonic Factor . . . 6

2.1 Boost Rectifier 10
2.2 Boost Rectifier Modes of Operation 11
2.3 Latos and Bosack Boost Rectifier 14
2.4 Split Capacitor Boost Rectifier 14
2.5 Switch-Mode Rectifier 15
2.6 Half-Bridge Boost Rectifier 15
2.7 Coupled-Inductor Boost Rectifier 16
2.8 Buck Rectifier 17
2.9 Buck Rectifier Modes of Operation 17
2.10 Simplified Buck Rectifier 18
2.11 Pulse-Width Controlled AC to DC Converter 19
2.12 Coupled-Inductor Buck Rectifier 20
2.13 Buck Rectifier with Energy-Balancing Filter 20
2.14 Buck-Boost Rectifier 21
2.15 Buck-Boost Rectifier Modes of Operation 22
2.16 Coupled-Inductor Buck-Boost Rectifier 23
2.17 Modified Cuk Three Switched-Network Rectifier 24
2.18 Half-Bridge Rectifier 25
2.19 Half-Bridge Rectifier Modes of Operation 25
2.20 Full Bridge Rectifier 26
2.21 Full Bridge Rectifier Modes of Operation 26

3.1 Full Bridge Series Resonant DC to DC Converter 30
3.2 Half Bridge Parallel Resonant DC to DC Converter 31
3.3 Zero Current Resonant Switches 32
3.4 Zero Voltage Resonant Switches 32
3.5 Half Bridge Series Resonant Rectifier 33
3.6 Full Bridge Series Resonant Rectifier 33

3.7 Tuned Class D Rectifier 34
3.8 Series Resonant Rectifier 35
3.9 Four-Resonant-State Rectifier 35
3.10 "Modified" Boost Resonant Rectifier 36
3.11 ACRDCL Boost Rectifier 37
3.12 Zero-Current-Switching Quasi-Resonant Boost Rectifier 37
3.13 Voltage and Current Waveforms of the ZCS-Quasi-Resonant Rectifier 38

4.1 Resonant Tank Boost Rectifier 40
4.2 RTBR Voltage and Current Waveforms 42
4.3 Resonant Tank Boost Rectifier with Component Resistances 43
4.4 "On Period" RTBR Circuit 44
4.5 "Off Period" RTBR Circuit 48
4.6 Basic Control of the RTBR 51
4.7 Average Input Current $i_{b_{av}}$ versus RT Phase at Turn-on 52
4.8 Turn-On Phase Window 52
4.9 Open Loop Current Control of the RTBR 54
4.10 Average Input Current $i_{b_{av}}$ in a Half Line Cycle 55
4.11 RTBR Voltage, Current, and Energy Waveforms 58

5.1 DCSteadyState Simulation Flowchart 62
5.2 ACLineCycle Simulation Flowchart 68
5.3 DCSteadyState: Pulse Average Current $i_{b_{av}}$ versus RT Phase at Turn-on 74
5.4 ACLineCycle: Pulse Average Current $i_{b_{av}}$ versus Phase ϕ_V of V_{ac} . . 74
5.5 DCSteadyState: Pulse Average Current $i_{b_{av}}$ versus RT Phase at Turn-on 76
5.6 Pulse Peak Current Simulations 77
5.7 DCSteadyState: Time at Turn-off t_2 versus RT Phase at Turn-on . 79
5.8 ACLineCycle: Time at Turn-off t_2 versus Phase ϕ_V of V_{ac} 79
5.9 DCSteadyState: RT Phase at Turn-off β_2 versus RT Phase at Turn-on 80
5.10 ACLineCycle: RT Phase at Turn-off β_2 versus Phase ϕ_V of V_{ac} . . . 80
5.11 DCSteadyState: Peak Tank Voltage V_{tp} versus RT Phase at Turn-on 81
5.12 ACLineCycle: Peak Tank Voltage V_{tp} versus Phase ϕ_V of V_{ac} 82
5.13 DCSteadyState: Switching Cycle RT Loss P_t versus RT Phase at Turn-on 83
5.14 DCSteadyState: Pulse Efficiency η_p versus RT Phase at Turn-on . . 84
5.15 DCSteadyState: Pulse Efficiency η_e versus Phase ϕ_V of V_{ac} 85
5.16 DCSteadyState: Pulse Efficiency η_p versus Pulse Average Current $i_{b_{av}}$ 85
5.17 DCSteadyState: Switching Frequency f_{sw} versus Pulse Average Current $i_{b_{av}}$ 87

5.18 ACLineCycle: Switching Frequency f_{sw} versus Phase ϕ_V of V_{ac} . . . 87

6.1 Resonant Tank Boost Rectifier Components 92
6.2 Prototype Simulated Pulse Average Current, and RT Phase at Turn-off versus RT Phase at Turn-on 93
6.3 Prototype Simulated Switch Peak Current, Turn-off Time, and Switching Period versus RT Phase at Turn-on 95
6.4 Prototype Simulated Peak Tank Voltage V_{tp} versus Phase of V_{ac} . . 96
6.5 Output Capacitance Current at Input Voltage Crest 97
6.6 Complete Prototype RTBR Circuit 99
6.7 Control Overview 100
6.8 Comparison of Experimental Prototype RTBR Currents with the DCSteadyState Performance 105
6.9 Comparison of Experimental Prototype RTBR Peak Tank Voltage with the DCSteadyState Performance: V_{tp0} versus β_0 106
6.10 Comparison of Experimental Prototype RTBR Time Periods with the DCSteadyState Performance 107
6.11 Prototype RTBR Switching Cycle Voltage and Current Waveforms, $\beta_0 = 120°$, $V_{in} = 0.42$ pu 108
6.12 Simulated RTBR Switching Cycle Voltage and Current Waveforms, $\beta_0 = 120°$, $V_{in} = 0.42$ pu 108
6.13 Prototype RTBR Switching Cycle Voltage and Current Waveforms, $\beta_0 = 180°$, $V_{in} = 0.75$ pu 109
6.14 Simulated RTBR Switching Cycle Voltage and Current Waveforms, $\beta_0 = 180°$, $V_{in} = 0.75$ pu 109
6.15 Prototype RTBR Switching Cycle Voltage and Current Waveforms, $\beta_0 = 220°$, $V_{in} = 0.84$ pu 110
6.16 Simulated RTBR Switching Cycle Voltage and Current Waveforms, $\beta_0 = 220°$, $V_{in} = 0.84$ pu 110
6.17 RTBR Input Voltage and Current at Full Load 112
6.18 RTBR Input Current Harmonic Spectrum 112
6.19 RTBR Input Current Waveforms and Spectra with Closed Loop Current Control 113
6.20 RTBR Measured Input Current Distortion versus Load 113
6.21 RTBR Input Current Waveform and Spectrum with Open Loop Current Control 114
6.22 RTBR Measured Efficiency versus Load 115
6.23 Simulated Switching Cycle RT Loss P_t versus RT Phase at Turn-on 115

C.1 Control Circuit Schematic Diagram 145

Symbols

Symbol	*Description*
$\mathbf{A}$	On Period circuit characteristic matrix
ac	alternating current
$\mathbf{B}$	On Period circuit input matrix
c	Number of RT cycles in a switching period
CHF	Current Harmonic Factor
C_f	input filter capacitance
C_t	capacitance of the RT
C_o	output capacitance
D_b	boost diode
dc	direct current
DPF	Displacement Power Factor
D_{sw}	switch ultrafast diode
e_t	the energy contained in the RT
e_{t0}	e_t at time t_0
e_{t2}	e_t at time t_2
EMI	Electromagnetic Interference
FRS	Four-Resonant-State
i_b	current in L_b
$i_{b_{avg}}$	average i_b in one switching period
i_{b0}	i_b at time t_0
i_{b2}	i_b at time t_2
I_{dis}	distortion component of the current
I_n	nth harmonic current amplitude
I_s	rms value of the line current
i_t	current in L_t
i_{t0}	i_t at time t_0
i_{t2}	i_t at time t_2
GTO	Gate Turn-off Thyristor
k	ratio of L_t / $(L_b + L_t)$

L_b	boost inductance
L_s	inductance of the ac supply
L_t	inductance of the RT
P_t	power lost in the RT in a switching period
PF	Power Factor
PCC	Point of Common Coupling
PRC	Parallel Resonant Converter
PRR	Parallel Resonant Rectifier
PWM	Pulse-Width Modulation
Q_t	measure of the "quality" of the RT
rms	root mean square
R_b	resistance of the boost inductor
R_c	resistance of the RT capacitor
R_t	resistance of the RT inductor
RT	Resonant Tank
$RTBR$	Resonant Tank Boost Rectifier
S_b	boost semiconductor switch
SRC	Series Resonant Converter
SRR	Series Resonant Rectifier
THD	Total Harmonic Distortion
t_{osc}	time during which S_b is off and the RT oscillates freely
t_{pk}	time at the peak of i_b; $t_{pk} = t_1$
t_{ramp}	time during which i_b is ramping downwards to zero
t_{sw}	time at the end of the Off Period. $t_{sw} = t_4$
t_0	time at the start of the On Period; generally $t_0 = 0$
t_1	time at the peak of i_b. $t_1 = t_{pk}$
t_2	time at the end of the On Period
t_3	time at the end of the i_b ramp down when $i_b = 0$
t_4	time at the end of the Off Period. $t_4 = t_{sw}$
V_{ac}	single phase line frequency voltage
V_{br}	voltage drop across the input diode bridge
V_{db}	voltage drop across the boost diode
V_{imp}	voltage impressed across the On Period circuit
V_{in}	instantaneous value of V_{ac}
V_{ramp}	voltage impressed across the boost inductor during the Off Period
V_s	rms value of the line voltage
V_{sw}	voltage drop across and D_{sw} and S_b
v_t	voltage across C_t
V_{tp}	the peak voltage that would appear across the RT at any particular instant if all of e_t were contained in C_t
V_{tp0}	V_{tp} at time t_0

V_{tp2}	V_{tp} at time t_2
V_{tp4}	V_{tp} at time t_4
v_{t0}	v_t at the start of the the On Period
v_{t2}	v_t at the end of the the On Period
V_1	fundamental component of the single phase line frequency voltage
$\mathbf{x}$	On Period circuit variables in matrix form
$\mathbf{x(0)}$	On Period circuit initial conditions matrix
ZC	Zero Current
ZCS	Zero Current Switch
Z_t	impedance of the RT
ZV	Zero Voltage
ZVS	Zero Voltage Switch
β	phase of the RT
β_0	β at time t_0
β_2	β at time t_2
η_e	the energy efficiency of the RTBR during a switching period
η_p	the power efficiency of the RTBR during a switching period
θ	angle (radians) of the RT between t_0 and $t_{v_t=kV_{imp}}$
ζ	dissipation factor of the RT
ϕ_{ac}	phase displacement angle between V_1 and I_1
ϕ_V	phase of the ac input voltage waveform
ω_b	actual damped resonant frequency (radians) of the On Period circuit
ω_{bn}	undamped resonant frequency (radians) of the On Period circuit
ω_t	actual damped resonant frequency (radians) of the RT
ω_{tn}	undamped resonant frequency (radians) of the RT

Chapter 1

Introduction

A controlled ac to dc converter (rectifier) with sinusoidal input current is presented in this thesis. This resonant tank boost rectifier (RTBR) is designed to meet an increasing need for rectifiers with an input current total harmonic distortion (THD) of less than 5 %. This is achieved using a current feedback controller which forces the input current to follow a sinusoid in phase with the input ac line frequency. The RTBR contains only small component values of inductance and capacitance, resulting in a converter with a relatively high power density. The power factor (PF) achieved by the RTBR is comparable to other switch-mode rectifiers, and substantially greater than that achievable with the conventional diode-bridge capacitor rectifier.

In the following sections, the problems associated with current and voltage harmonics on the utility power system are described. The contribution of rectifiers to this problem is then explained. Finally, the need for actively switched rectifiers with low input current distortion is presented.

1.1 Performance Parameters

The effect of harmonics on power factor is an important concept in this thesis. Therefore, these parameters will be defined explicitly.

1.1.1 Power Factor

The term "power factor" is defined as the ratio of average usable (delivered) power to the apparent (distributed) power [1, pp. 30]. The usable power is the actual wattage that can be used by the load for useful work. This can be expressed as the product of the fundamental component of the voltage at the load and the portion of the fundamental current in phase with the voltage. The apparent power is a measure of the power delivery requirements of the power distribution system

feeding the load. This can be expressed as the product of the voltage and the full rms value of the current drawn by the load.

$$PF = \frac{V_1 I_1 \cos(\phi_{ac})}{V_{ac} I_s} \tag{1.1}$$

The voltages in this expression can be factored out if sinusoidal and free of distortion. The power factor actually has two components, the displacement power factor (DPF) and a current harmonic factor (CHF, which has also been called a purity factor [1]). Traditionally, power factor referred only to the DPF and was defined as the cosine of the phase angle between the current and voltage. This is a sufficient definition only for loads, such as induction motors, which draw predominately sinusoidal currents. For loads with significant currents at frequencies other than the fundamental, the power factor must be expanded to include the CHF.

$$CHF = \frac{I_1}{I_s} \tag{1.2}$$

$$DPF = \cos(\phi_{ac}) \tag{1.3}$$

$$PF = CHF \times DPF = \frac{I_1}{I_s} \cos(\phi_{ac}) \tag{1.4}$$

1.1.2 Total Harmonic Distortion

The harmonic content of the current waveform is often expressed in terms of the total harmonic distortion (THD). This is defined as the ratio of I_{dis}, the rms value of the harmonic currents, over I_1, the rms value of the fundamental current.

$$I_{dis} = \sqrt{\sum_{n=2}^{\infty} I_n^2} \tag{1.5}$$

$$THD = \frac{I_{dis}}{I_1} \tag{1.6}$$

The THD and CHF are related as shown:

$$CHF = \frac{1}{\sqrt{1 + THD^2}} \tag{1.7}$$

1.2 Utility Harmonics

The purpose of utility ac power distribution systems is to distribute power as efficiently as is feasible. Ideal power transfer is achieved when the current drawn by a load on the utility system exactly matches the input voltage in frequency and phase, as is the case with a purely resistive load. Any current at frequencies above the fundamental will result in a net power flow of zero when averaged over enough line cycles. Only the portion of the fundamental current in phase with the voltage results in real power flow in one direction.

1.2.1 Sources of Harmonics

Real power systems are somewhat less than ideal. Many loads draw currents that are rich in harmonics (and occasionally sub-harmonics) of the fundamental frequency. These harmonics contribute to the rms value of the current and therefore contribute to the I^2R losses in the power distribution system. Distribution wiring feeding these loads must be capable of carrying the full rms current, not just the in-phase fundamental that delivers usable power. If a load draws current with more predominant harmonics, the ratio of average usable (delivered) power to apparent (distributed) power is lowered. This ratio is the PF, and is lowered in much the same way as a lagging or leading current lowers PF. This lower PF results in a lower utilization of the power distribution system.

Harmonic currents, when drawn through the line impedance, result in harmonic voltages at points in the power distribution system. These harmonic voltages can then cause harmonic currents to flow in other loads on the system [2]. The magnitude of those harmonic currents will depend on the line and load impedances at the specific harmonics. Loads with particularly low impedances at certain harmonic frequencies will draw excessive currents at those frequencies. For example, capacitor banks installed to correct for a lagging displacement power factor (DPF) at 60 (50) Hz will attract harmonic currents. If the capacitor banks are sized for DPF correction only, they may not have the current carrying capacity to handle the harmonic currents.

Harmonic current sources can also excite parallel or series resonances between the power system and other loads on the power system [3]. This can result in an amplification of the harmonic currents in certain loads.

1.2.2 Effects of Harmonics

Harmonic currents have a detrimental effect on power systems. They add to the rms value of the current resulting in extra heating losses in the distribution system and in system loads. Operation at higher temperatures can lead to a shortened

life of some load components, such as transformers and capacitor banks. Excessive harmonic currents may result in damage to specific components.

Harmonics in power systems can cause telephone interference [2, 3]. Telephone equipment is often located in close proximity to power distribution wiring or loads. In many areas of the world, telephone and power cables share the same right-of-way. This proximity makes the telephone system susceptible to noise induced from harmonics in the power system. Excessive harmonics on the power system at frequencies within the telephone voice spectrum may cause serious degradation in signal quality.

Harmonics can have a detrimental effect on the power system itself, affecting the power generation equipment, control systems, and protection and metering equipment [2, 3]. Other detrimental effects on other loads include possible erroneous operation of control systems and television interference [2]. These are covered in detail in the literature.

In recent years, the sensitivity of ac power distribution systems to load generated current harmonics has increased [3]. Harmonic sensitive loads (such as computers, microprocessors, programmable controllers, and heat sensitive motors) and harmonic generating loads (such as common rectifiers, static VAR compensators, fluorescent lights, and switching power supplies) have both been increasing.

1.2.3 Harmonic Standards

Standards and regulations restricting the generation of both current and voltage harmonics have been imposed by various authorities in their respective countries throughout the world. Arrillaga et al. [3, ch. 8], provide a summary of such power system harmonic standards. These standards vary considerably due to the disparate nature of power distribution systems in different countries. Most define voltage harmonic limits at the "point of common coupling" (PCC) or "point of influence". For lower distribution voltages, most standards set a voltage THD limit of 5% from all customers combined at any particular point, with smaller limits for individual harmonics [2, 3, 4, 5, 6]. Many standards set restrictions on the size of certain converters at various voltage levels.

The "IEEE Guide for Harmonic Control and Reactive Compensation of Static Power Converters", Standard 519-1981 [2, pp. 36–37] sets a voltage THD limit on the general power system at medium voltages (2.4 to 69 kV) of 5%. A revision to this standard, expected in 1991, maintains this 5% limit on voltage distortion, and adds comprehensive limits for current distortion [6]. The limit is 20 % THD for loads where the current is less than 10^{-3} times the supply maximum short circuit current at the PCC.

Other examples of specific limits for harmonics can be found in the IEC-555 standard for currents and the CENELEC 50.006 standard for voltages [3].

A final example of restrictions set on harmonic voltage and current levels on utility power systems can be found here in Alberta where this research is being done. The two major provincial power companies, Transalta Utilities and Alberta Power, have agreed on acceptable limits of voltage distortion, current distortion, and telephone interference on their respective grids [4]. At bus voltages of 25 kV or less, their stated intent is to maintain the voltage THD below 5%. Individual customers are required to calculate the expected voltage and current distortion, and telephone interference values and satisfy the power company that they are below the specified limits.

1.3 AC to DC Power Conversion

AC to dc power converters (rectifiers) are a common source of current harmonics on ac power distribution systems. The simple diode bridge LC rectifier in Figure 1.1 is used extensively. The input current waveform for such a rectifier can vary from a 'pulse' to a 'square', each shown in Figure 1.2. A sine wave is also shown for comparison. All three waveforms have roughly the same fundamental component of 1.0 per unit (pu). In per unit notation, parameters are indicated as unitless values relative to a base value. This notation is used extensively in this thesis.

The THD and PF associated with the waveforms in Figure 1.2 are shown in Figure 1.3. With a very large smoothing inductor L_f, the current drawn is very close to the square wave. This has a THD of 48 % and a PF of 0.90.

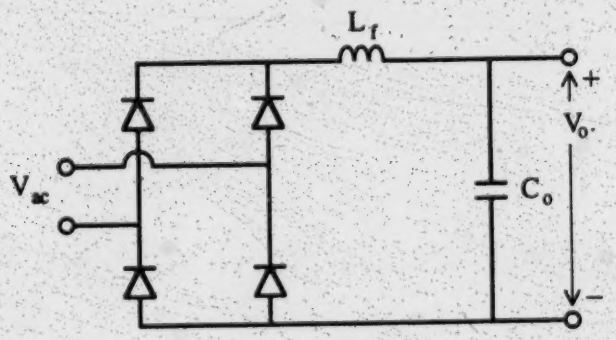

Figure 1.1: Diode Bridge LC Rectifier

Often L_f is omitted, although the line impedance contributes some inductance to the circuit. The result is an inexpensive rectifier with the 'pulse' input current waveform seen in Figure 1.2. With L_f small, this rectifier generates excessive

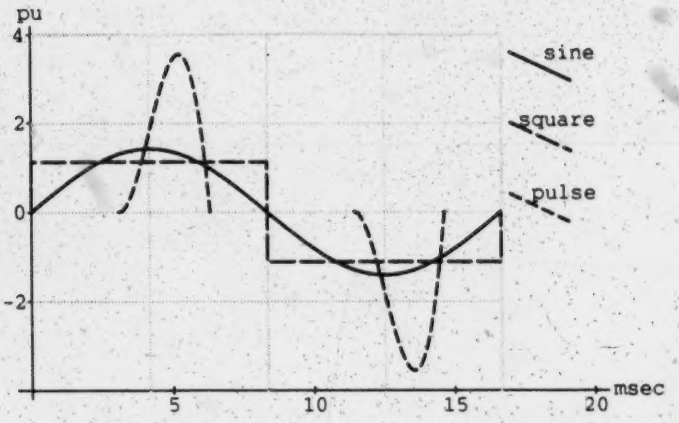

Figure 1.2: Common Rectifier Input Current Waveforms

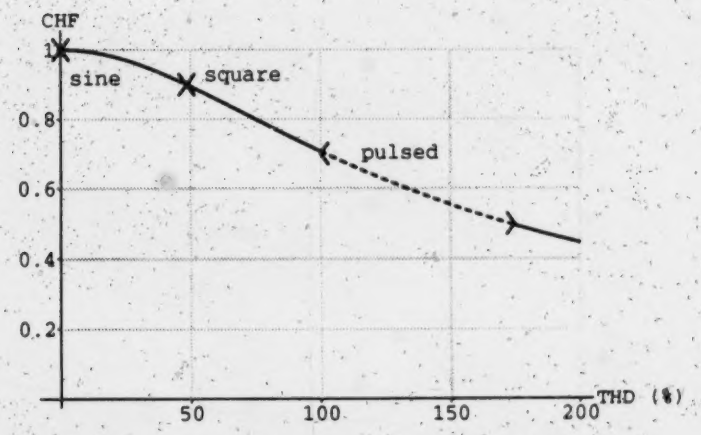

Figure 1.3: Relationship Between Distortion and Current Harmonic Factor

current harmonics. The THD varies considerably with line impedance and with the load. The THD may be as low as 100 % (PF of 0.7) with a relatively large input impedance, or 175 % (PF of 0.5) or higher for a very stiff system [7, 8].

Increasing the smoothing inductance, and thus adding to the line impedance, will generally improve the THD of the diode bridge LC rectifier [7, 8, 9, 10]. An exception to this is the region near just-continuous current where increasing the smoothing inductance actually causes an increase in the THD [8, 10]. To be effective, the impedance of this inductor must be within an order of magnitude of the load impedance. At line frequency, this is very large and therefore heavy and expensive. With a sufficiently large inductance, the optimum THD of 48 % (PF of 0.9) for this rectifier is achieved.

Other passive filtration techniques have been suggested and attempted, including resonant input filters or ferroresonant transformers [9]. Again, the components must operate at line frequency and are large.

The undesirable THD and/or component sizing of these common rectifiers, combined with increasing restrictions on the current harmonics that may be generated, has led to increased research activities on high PF rectifiers. This research is aimed at producing a circuit which emulates a resistor on the ac input side. Passive and active methods have been attempted with varying degrees of success.

While the need for higher PF rectifiers has become more apparent, advances in power electronic technology and circuit components have made new power converter topologies feasible. Much research is now concentrated on active switched rectifiers which force the current to match the sinusoidal input voltage waveform. A summary of such "hard switched" rectifier techniques is presented in the next chapter. Then, in Chapter 3, switch-mode rectifiers which utilize resonant circuits are discussed as background material to the RTBR.

The RTBR is introduced and the circuit is described in detail in Chapter 4. The theoretical operation, including the mathematical analysis, is presented and the general RTBR current control requirements are discussed. The concept of dc steady-state as it applies to the RTBR is explained. A mathematical simulation of the RTBR is then described in Chapter 5, and the results are used to show the effects of component variances on the behavior of the rectifier.

The design and construction of an 800 watt, 120 volt ac to 200 volt dc prototype RTBR is presented in Chapter 6. The specifications are discussed and design criteria explained. Simulation results are used to optimize the prototype design. The actual design of the control system for the RTBR is also covered. Then laboratory test results of the prototype are presented, indicating the extent to which unity PF has been achieved. Current waveforms, harmonic spectra, and converter efficiency are presented.

Chapter 2

Switch-mode Rectifiers

Switch-mode rectifiers (SMR) are a family of ac to dc converters which shape the input current so as to minimize the THD. The resonant switch-mode rectifiers described in Chapter 3, and the resonant tank boost rectifier (RTBR) described in this thesis, are derived from SMR's. Many concepts used in the RTBR originated in switch-mode rectifiers and are more easily explained when referenced to the original simpler circuit. Hence, the operation of switch-mode rectifiers will be explained in detail.

The prime objective of switch-mode rectifiers is to draw current with a low harmonic content. The optimum waveform would be a sinusoid which has no harmonics, although square-waves and rounded square-waves may be adequate for many applications.

Switch-mode rectifiers use a power conditioning section which forces the input current to follow the desired waveform. The active components in a switch-mode rectifier are the switches. These are semiconductor switches; transistors, MOSFET's, thyristors, diodes or any of a number of variations of these devices. The switches provide the control mechanism by which the input current is shaped.

Generally, current shaping is achieved by controlling the current in an inductor which is switched between two modes, the On Period and the Off Period. During the On Period, energy is transferred from the power system to the inductor and possibly to the output of the conditioning section as well. During the Off Period, energy is transferred from the inductor and possibly the power system, to the output.

The nature of energy transfer in each mode determines the type of converter; boost, buck, or buck-boost. Additional storage elements, split inductors, or isolating transformers may be added to these basic types to make converters such as the forward, flyback, Cuk or Sepic, all of which can be used as power conditioners [11, 12].

Switch-mode rectifiers are actually specific applications of Loss Free Resistors

described by Singer [13]. A loss free resistor is a power converter which draws current proportional to the voltage across its input terminals, as would a resistor. However, rather than dissipate the power resistively, the energy presented at the input to the loss free resistor is converted to a usable form somewhere else in the circuit. In the case of switch-mode rectifiers, that usable form is the dc output.

Since the current is forced to be proportional to the input voltage waveform in a unity PF rectifier, the instantaneous energy transfer varies with the square of the input voltage waveform. In each ac line cycle, this energy transfer varies cyclically from zero when the input voltage is zero to a peak at the input voltage crest. The frequency of this energy cycle is twice the line frequency.

The actual energy storage capability of the inductor is small compared to the total energy transferred in each ac line frequency cycle. Therefore, the instantaneous energy delivered to the output must also vary with the square of the input voltage waveform.

The energy versus time requirements of the load will, with specific exceptions, be significantly different from this cyclical energy delivered from the ac line. Obviously, the long term average energy flow at the input must equal the long term average energy flow at the output minus losses. Therefore, to make up the difference in instantaneous energy requirements between the input and the output, some form of energy storage must be incorporated into the switch-mode rectifier [9, 14, 15, 16]. Increased energy storage may also be required if output voltage holdup is desired for a period following loss of input power.

The rectifier must provide output voltage regulation and maintain the output ripple voltage below specific requirements. This ripple voltage requirement and the need for energy balance can be met in a number of ways. The simplest way is to have a sufficiently large capacitor on the output of the power conditioning section. Since the capacitor energy storage varies with the square of its voltage, reasonably small regulation and ripple requirements will necessitate a much larger device than energy balance requirements alone would require.

If a large output capacitance is not required for any other reason, the output voltage regulation and ripple voltage requirements can be met instead by a second dc to dc converter following the power conditioning section. While there will be greater losses associated with an extra converter, the bulk, expense, and losses of a large electrolytic capacitor would be eliminated. The second converter also gives another possible location for a high frequency isolating transformer.

Schlecht [14, 15] has proposed a tuned second harmonic filter combined with the output energy storage element to provide the required energy balancing and ripple minimization. This idea has been refined by King [17]. A switch-mode rectifier using such an energy balancing filter appears in Figure 2.13. The size of the output capacitor or inductor can be reduced significantly with this passive filter approach.

2.1 Boost Rectifier

One of the most popular active current-shaped rectifiers is the boost rectifier (sometimes referred to as a step-up flyback, boost chopper, or boost charger) [10, 18, 19, 20, 21, 22, 23, 24, 25, 26, 27]. This rectifier generally consists of a diode bridge followed by a power conditioning boost dc-dc converter, as shown in Figure 2.1. Boost converters are characterized by the necessity for the output voltage to exceed the input voltage, and by the relatively smooth input current.

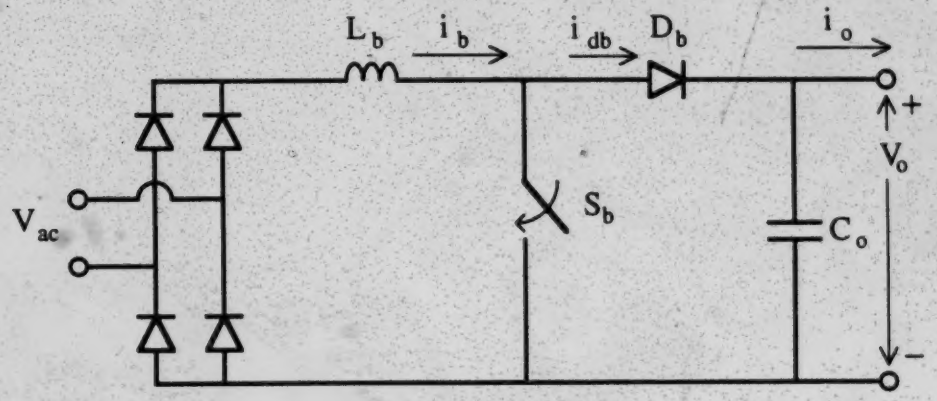

Figure 2.1: Boost Rectifier

During each switching cycle, the boost rectifier operates in one of two modes shown in Figure 2.2:

On Period The switch is on. The boost inductor L_b "charges" as energy is transferred from the power system to L_b. The current in L_b ramps upwards.

Off Period The switch is off. L_b "discharges" as energy is transferred from the power system and L_b to the output capacitor. The current in L_b ramps downwards.

2.1.1 Current Control

Control of the input current can be achieved in a number of ways. With a sufficiently large boost inductor, continuous current can be forced to flow through the inductor, with the instantaneous current being controlled by pulse-width modulating the boost switch.

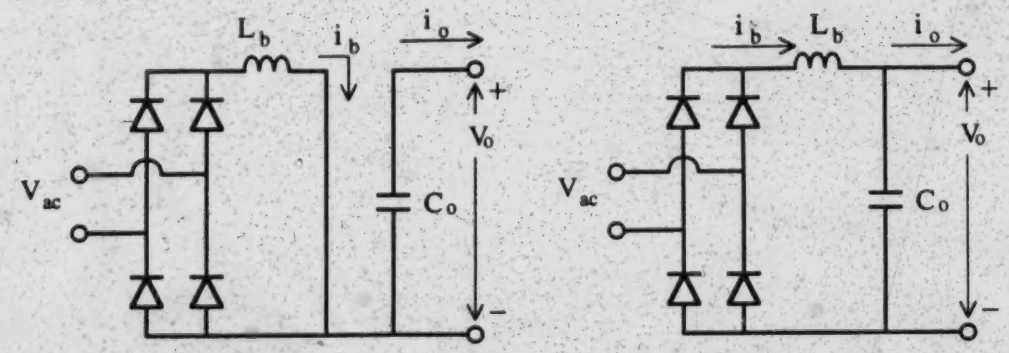

(a) On Period (b) Off Period

Figure 2.2: Boost Rectifier Modes of Operation

This closed loop current control generally contains two loops: an inner loop provides duty-cycle modulation to produce the desired average current during each switching period and a long time constant outer loop provides output voltage control [28]. The voltage error signal from the outer loop is combined with information on the desired current waveform to produce a current reference signal for the inner loop. For resistor emulation, unity PF operation, the desired current reference signal is the rectified voltage sine wave.

Control methods which can be utilized in the current control loop are listed below. The first five methods are presented by Redl et al. [29] and provide a good summary of methods used for controlling the inductor current in dc to dc boost, buck, and buck-boost converters. Since the inductor current is the input current for the boost rectifier, these methods are applicable to boost rectifier current control. The last three methods were developed specifically for boost rectifiers.

Hysteretic (bang bang) The switch is turned on when a lower current is reached and turned off when an upper current limit is reached. The desired current waveform is the average of the upper and lower limits.

Constant Off-time The switch is turned off when an upper current limit is reached and turned on when a constant off time expires.

Turn-on at Clock Time The switching period (On Period plus Off Period) is maintained constant. The switch is turned off when the sum of the inductor current and a compensating waveform reaches an upper limit, and is turned on when the switching period expires. The compensating waveform is required to ensure stability.

Constant On-time The switch is turned on when a lower current limit is reached and turned off when a constant off time expires.

Turn off at Clock Time The switching period is maintained constant. The switch is turned on when the sum of the inductor current and a compensating waveform reaches a lower limit, and is turned off when the switching period expires. Again, the compensating waveform is required to ensure stability.

Predictive Current Control This constant frequency current control method predicts the inductor current in each switching cycle from the current in the previous cycle, the reference current, and the circuit parameters [30]. The duty cycle is then determined for the next switching cycle.

Integral Control This involves choosing only one mode of operation (On or Off) for each switching period based on whether the inductor current is above or below the reference at the start of that period [28]. This is similar to the hysteretic method but with an added restriction that duration of each On Period and Off Period be multiples of the "switching period". The actual switching period will not be constant and will be larger by at least a factor of two than this so-called "switching period".

Constant Frequency Hysteresis Window This method is an simple adaptation of the hysteretic method above [31]. The upper and lower limits are replaced by a triangular waveform centered around the reference waveform. This forces the switching to occur at constant intervals, producing a constant switching frequency.

For optimum performance the current feedback would be a measured signal. However, Kazerani et al. [30] have used a current estimator (predictor) circuit which uses the voltage across the boost inductor to determine the input current. The result is only a very slight degradation in input current harmonics. The idea of estimating the current rather than measuring it has been implemented in the RTBR, as will be described in Chapter 4.

A constant current reference signal can be used, giving a square wave input current with a THD of 48 % and a PF of 0.90 (in reality, line impedances and the finite size of the boost inductor will result in rounding of the edges of the square wave and a PF slightly higher than 0.90). This will decrease the size of output capacitor required to maintain any given level of ripple voltage.

The output voltage control loop gives a current reference signal output which should be relatively constant between switching cycles. Since the rate of energy

transfer in the rectifier varies with the square of the input voltage, the instantaneous response of the rectifier to load changes or disturbances will vary significantly depending on the instantaneous input voltage. The addition of an appropriate feedforward signal into the voltage control loop can be used to compensate for fluctuations in the input voltage, as described by Carsten [32]. The second harmonic component of the output voltage ripple may need to be filtered from the feedback loop, possibly by using a sample and hold every half cycle [33].

With a smaller value of boost inductor, open loop current control can be achieved by operating the boost rectifier in discontinuous conduction, voltage follower, mode [32, 34, 35, 36, 37]. By keeping the on-time of the boost switch constant throughout each line frequency cycle, the peak input current in each switching cycle will inherently follow the input voltage waveform. If the ratio $\alpha = \frac{V_{in_{peak}}}{V_o}$ was less than 0.8, the average input current would follow a distorted sinewave with a power factor of better than 0.95 [36]. As alpha is decreased, the harmonic content of the input current is decreased. A high frequency input filter capacitor is required to remove the switching frequency component of the current waveform.

2.1.2 Variations

Variations of the boost rectifier have been developed which operate with the two modes as expressed above, but with additional components [16, 38, 39, 40]. The circuit of Latos and Bosack [38] in Figure 2.3 includes a low-pass LC filter between the diode bridge and the boost inductor and an isolation transformer between the boost diode and the output capacitor. Two additional switches are required to toggle the transformer input and two additional diodes are required to rectify the transformer output. A similar boost rectifier [38] uses the two transformer toggling switches as the boost switch, thus reducing the number of switches to two.

The idea of combining a second harmonic tuned LC filter with the output capacitor, as mentioned at the start of this chapter, has been applied to a boost rectifier by Schlecht [15]. This significantly reduces the size of capacitor required to achieve a given ripple requirement. This, in turn, greatly increases the speed of response of the rectifier to disturbances.

Schlecht [16] also presents a boost converter with the output capacitor split and the boost switch feeding the midpoint of the split capacitor, as shown in Figure 2.4. In essence, the first mode of operation of the boost converter is altered so that energy is not only transferred from the power system to the boost inductor, but also to half the output capacitor. This results in lower voltage stresses on the boost switch, but makes it necessary to add a smaller charge removal converter from the lower capacitor to the upper capacitor. Also, current can only be drawn from the input when the input voltage exceeds the voltage on the lower capacitor.

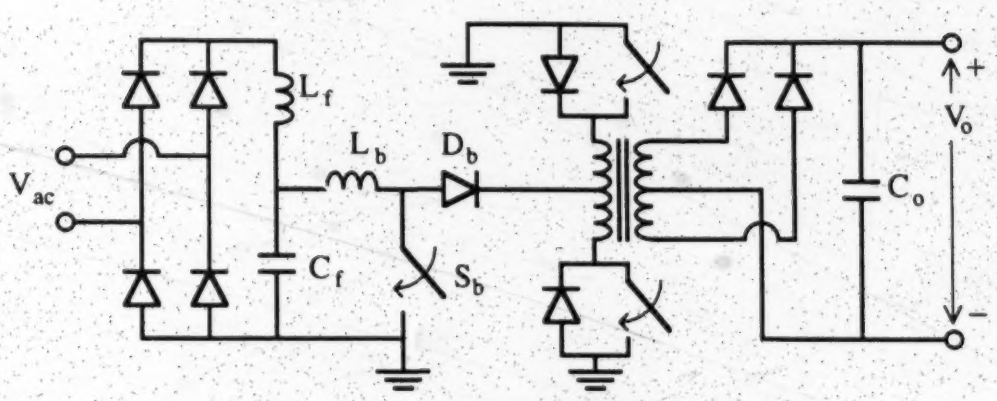

Figure 2.3: Latos and Bosack Boost Rectifier

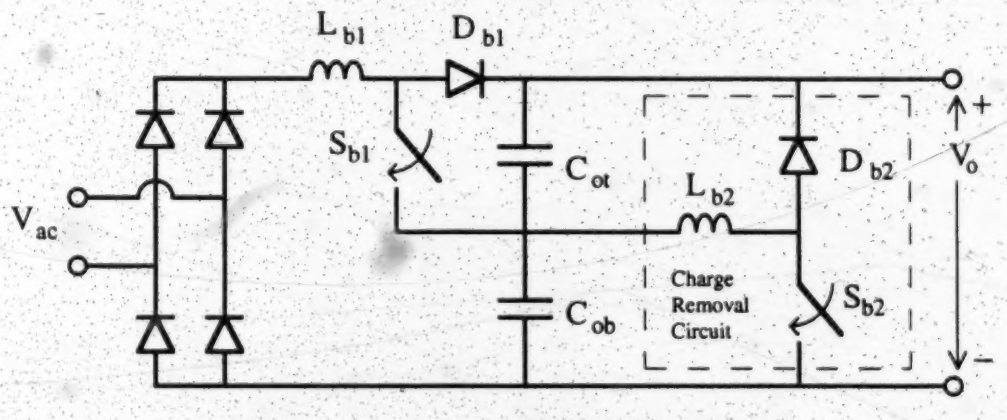

Figure 2.4: Split Capacitor Boost Rectifier

Hence, there is no current drawn near the cusps of the rectified line voltage, and unity PF is not possible.

Manias and Ziogas [39] present a transformer between the boost inductor and the output capacitor, with a full bridge input to the transformer, as shown in Figure 2.5. During each On Period, one diagonal set of switches in the bridge is on. In the subsequent On Period, the alternate diagonal set is on. The input to the transformer consists of alternating positive and negative current pulses at the switching frequency. The output of the transformer is rectified with diodes. This circuit gives the boost rectifier isolation, with improved output filtering.

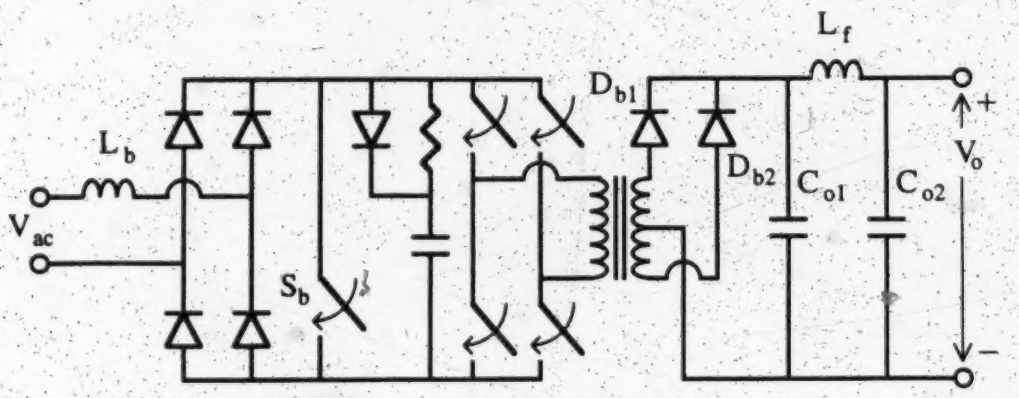

Figure 2.5: Switch-Mode Rectifier

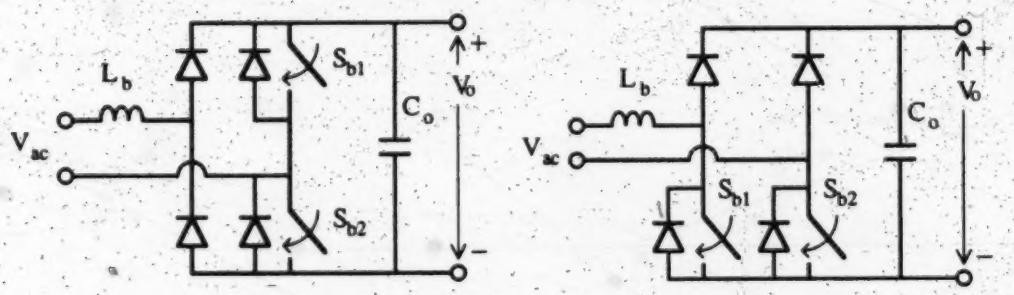

(a) Circuit A (b) Circuit B

Figure 2.6: Half-Bridge Boost Rectifier

Two papers, Itoh and Ishizaka [40] and Kagotani et al. [41], present a circuit with the boost inductor moved to the line side of the diode bridge and two of the bridge diodes replaced with switches. The rectifiers shown in Figure 2.6 operate as boost rectifiers since the two operational modes are identical to those of diode bridge boost rectifiers. Circuit A and B are identical in operation. The advantage of these circuits is that there is one less diode in each circuit mode, resulting in reduced losses. The disadvantages are that two active switches are required and that, if MOSFET's are used as the switches, the reverse diodes will not be as fast as the lone diode (normally an ultrafast diode) in the basic boost converter.

Chibani and Nakaoba [42] present a boost rectifier similar to that of Manias and

Ziogas, but without a separate boost switch, shorting two bridge switches during the On Period instead. While this reduces the switch count, it would double the On Period switch voltage drop, resulting in increased losses.

El-Hamamsy [43] presents a coupled-inductor boost rectifier which eliminates the diode bridge, but uses three switches, as shown in Figure 2.7. Switches S_{b1} and S_{b2} are used to select the polarity of the input voltage impressed across the inductor for charging. This is necessary to replace the polarity selecting characteristic of the diode bridge. S_{db} is switched on for discharging. It appears that there is no way to reverse the polarity of the input voltage during discharging, as was performed by the diode bridge in a standard boost rectifier. This rectifier would not be symmetrical through normal ac positive and negative input cycling, a problem not addressed by El-Hamamsy.

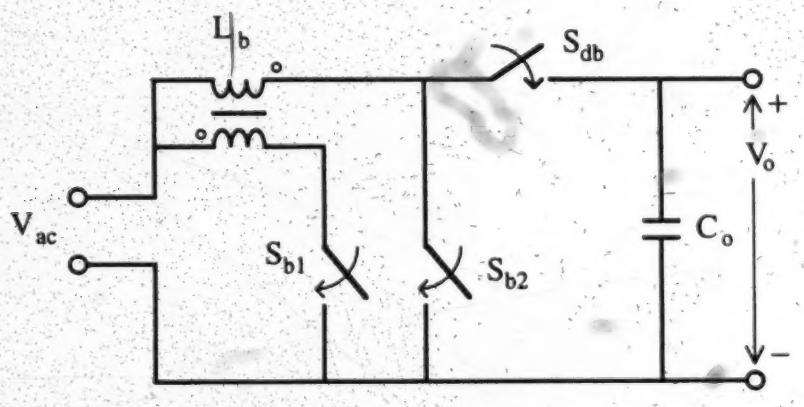

Figure 2.7: Coupled-Inductor Boost Rectifier

2.2 Buck Rectifier

Buck rectifiers are suitable for applications where a constant output current and low output voltage are desirable or at least acceptable. In its basic form, as shown in Figure 2.8, the buck rectifier consists of a diode bridge followed by a buck dc to dc converter [9, 44]. This rectifier is often used in high power applications at low switching frequencies. Buck converters are characterized by the necessity for the input voltage to exceed the output voltage, and the relatively smooth output current.

During each switching cycle, the buck rectifier operates in two modes shown in Figure 2.9:

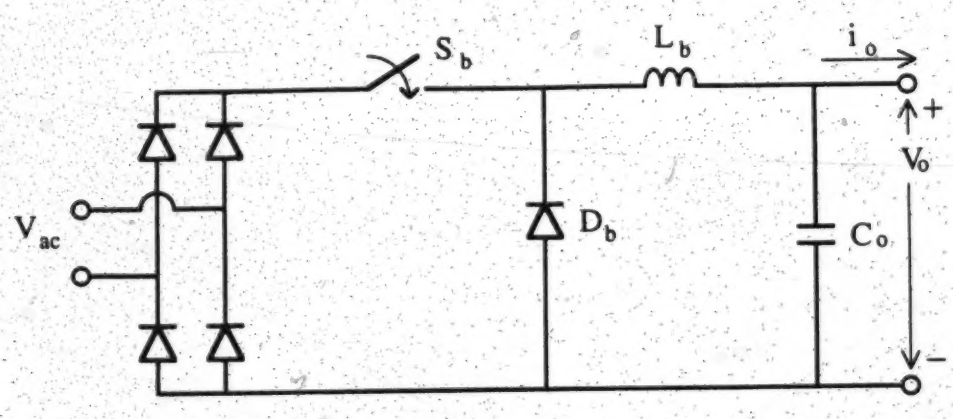

Figure 2.8: Buck Rectifier

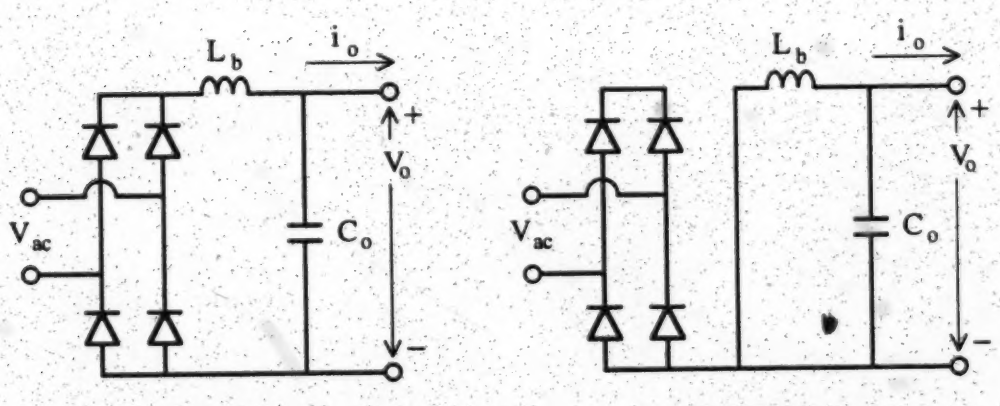

(a) On Period (b) Off Period

Figure 2.9: Buck Rectifier Modes of Operation

On Period The switch is on. The buck inductor L_b "charges" as energy is transferred from the power system to L_b and the output capacitor. The current in L_b ramps upwards.

Off Period The switch is off. L_b "discharges" as energy is transferred from L_b to the output capacitor. The current in L_b ramps downwards.

The buck switch, located on the input to the buck converter, can be incorporated into the diode bridge by replacing two or four of the diodes with gate turn-off

thyristors (GTO), as shown in Figure 2.10. As with the boost rectifier, the input current is controlled by pulse-width modulation of the GTO switches. Perfect unity PF is not achievable with the buck converter since current control can only occur when the input voltage is above the output. However, with sufficiently small output voltage and higher switching frequencies, near unity PF is possible.

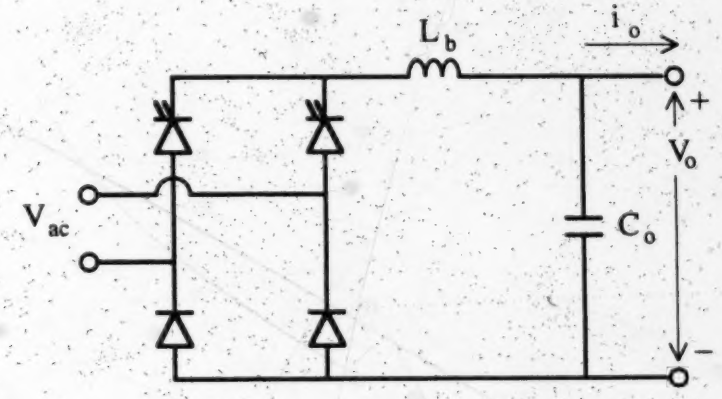

Figure 2.10: Simplified Buck Rectifier

2.2.1 Current Control

Input current control is achieved in similar ways to the boost rectifier, with an inner current control loop and an outer voltage control loop. With the buck rectifier, the input current is not the same as the inductor current, the input current is the current in the inductor during the On Period only. Assuming that the inductor current is maintained relatively constant in any given switching cycle, the average input current for that cycle will be the product of the inductor current and the on duty cycle. If the output current of the buck rectifier is maintained constant by a large buck inductor (as is normally the case since the buck inductor generally provides input to output energy balancing), then the input current waveform will be a symmetrical PWM waveform similar to the voltage waveform on the output of PWM inverters.

The discontinuous nature of the buck rectifier input current means that there is a much more significant current at the switching frequency and at harmonics of the switching frequency. Hence, an input low pass filter is required in all buck rectifiers. This results in a slightly lagging phase shift in the input current which, if not compensated for, will result in a slight deterioration in the displacement

power factor (DPF). This effect will decrease as the switching frequency increases and the size of the filter decreases.

2.2.2 Variations

Variations of the buck rectifier have been developed. An early version is the Pulse-Width Controlled Ac-to-Dc Converter described by Kataoka et al. [45] and shown in Figure 2.11. This is a thyristor controlled rectifier with additional commutation circuitry to allow multiple switchings in each line cycle for pulse-width-modulation operation. With the exception of the operation during switching (which is a very short period in each switching cycle), the operation of this rectifier follows the buck rectifier operation. There are, however, two thyristors and a diode in the current path for both modes of operation, resulting in increased losses.

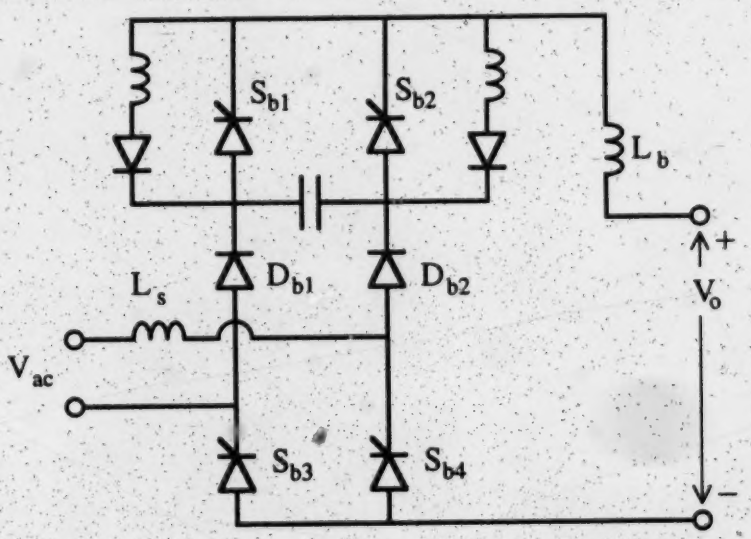

Figure 2.11: Pulse-Width Controlled AC to DC Converter

Another variation is the coupled-inductor buck rectifier which is described by El-Hamamsy [43] and shown in Figure 2.12. As with the coupled-inductor boost rectifier, the buck version does not offer symmetrical operation for normal ac positive and negative input cycling.

Schlecht [14, 15] and King [17] separately describe buck rectifiers with a second harmonic tuned LC filter combined with the buck inductor, shown in Figure 2.13. This significantly reduces the size of inductor required to achieve a given ripple

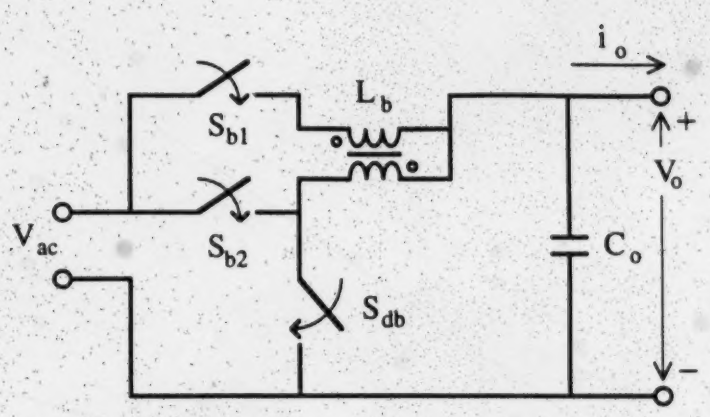

Figure 2.12: Coupled-Inductor Buck Rectifier

requirement. This, in turn, greatly increases the speed of response of the rectifier to disturbances. Schlecht also includes an input filter to remove the high switching frequency component from the buck input current waveform.

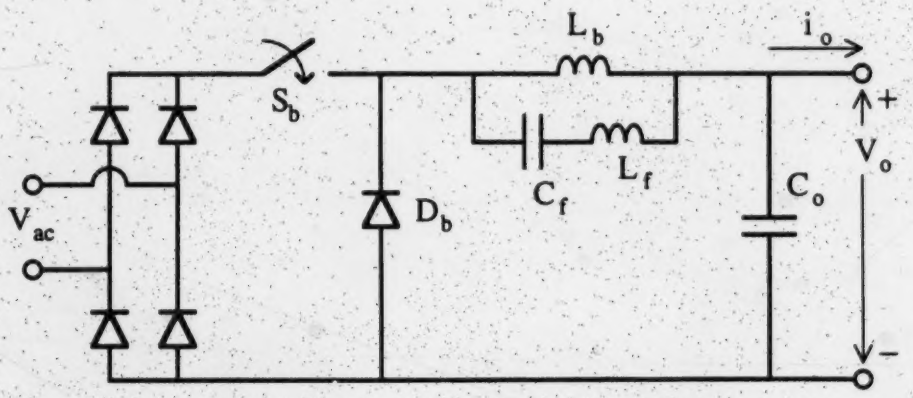

Figure 2.13: Buck Rectifier with Energy-Balancing Filter

2.3 Buck-Boost Rectifier

A third type of switch-mode rectifier is the buck-boost, or step-up/down flyback [46, 47, 48]. In its basic form, as shown in Figure 2.14, it would consist of a diode bridge followed by a buck-boost dc to dc converter. Buck-boost converters are characterized by an output voltage which can be above or below the input voltage, but with chopped current at both the input and the output.

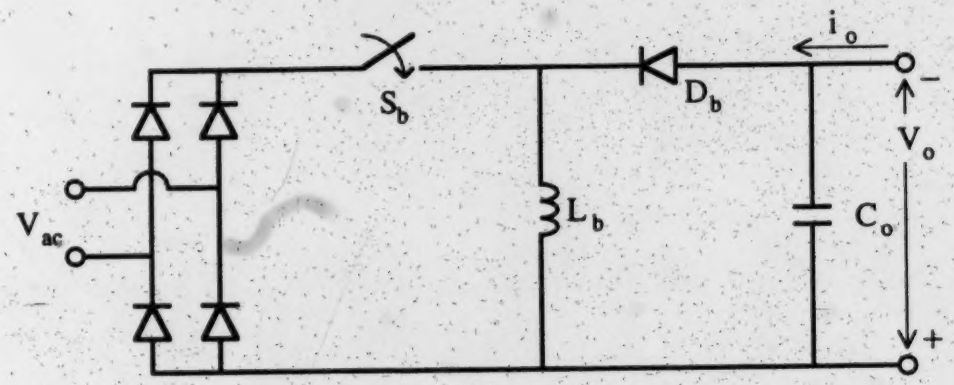

Figure 2.14: Buck-Boost Rectifier

During each switching cycle, the buck-boost rectifier operates in two modes shown in Figure 2.15:

On Period The switch is on. The buck-boost inductor L_b "charges" as energy is transferred from the power system to L_b. The current in L_b ramps upwards.

Off Period The switch is off. L_b "discharges" as energy is transferred from L_b to the output capacitor. The current in L_b ramps downwards.

As with the buck converter, the switch is located at the input to the converter and can be incorporated into the diode bridge. The input current is controlled by pulse-width modulation of the switches.

As with the boost rectifier, with a sufficiently small inductor, the buck-boost rectifier could also be operated in discontinuous (inductor) conduction mode, although an example of this has not been found in the literature. By keeping the on-time and duty-cycle of the buck-boost switch constant throughout each line frequency cycle, the per-switching-cycle average input current should inherently follow the input voltage waveform. A high frequency filter capacitor would be

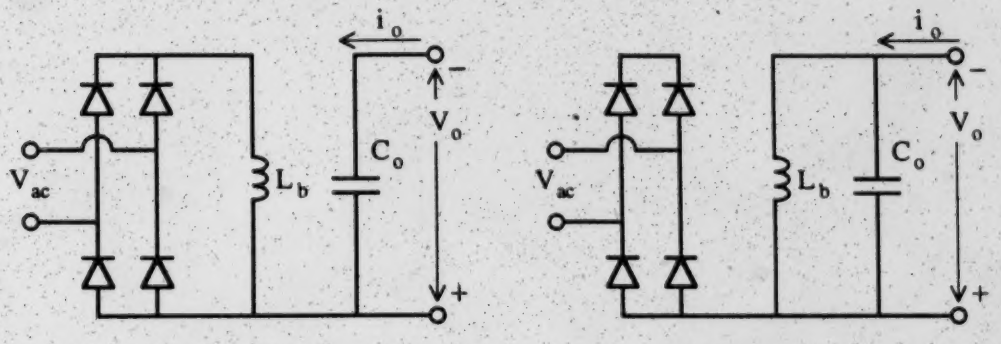

(a) On Period (b) Off Period

Figure 2.15: Buck-Boost Rectifier Modes of Operation

required at the input to the buck-boost rectifier to remove the switching frequency component of the current waveform. The result would be an in-phase, near sinusoidal, input current from open loop current control.

2.3.1 Current Control

Input current control is achieved in similar ways to the boost and buck rectifiers, with an inner current control loop and an outer voltage control loop. As with the buck rectifier, the input current is not the same as the inductor current; the input current is the current in the inductor during the On Period only. Assuming that the inductor current is maintained relatively constant in any given switching cycle, the average input current for that cycle will be the product of the inductor current and the on duty cycle. If the inductor current of the buck-boost rectifier is maintained constant by a large inductor, then the input current waveform will be a symmetrical PWM waveform.

As with the buck rectifier, the discontinuous nature of the buck-boost rectifier input current means that an input low pass filter is required, with the same effects on PF.

2.3.2 Variations

The only variation of the buck-boost rectifier found in the literature is the coupled-inductor buck-boost rectifier shown in Figure 2.16 described by El-Hamamsy [43]. Since the input and output of a buck-boost converter are never connected simultaneously to the inductor, the problem of reverse polarity of the input during the Off

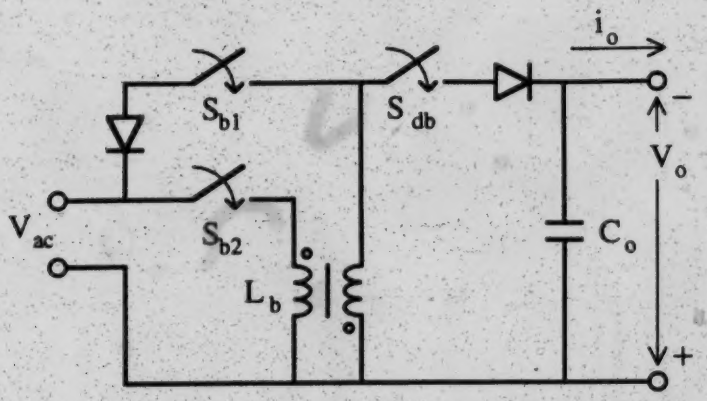

Figure 2.16: Coupled-Inductor Buck-Boost Rectifier

Period does not manifest itself in this rectifier. The single-phase coupled-inductor buck-boost rectifier appears fully feasible.

2.4 Three Switched-Network Rectifiers

Three switched-network rectifiers are boost or buck type rectifiers, with an intermediate energy storage element (capacitor or inductor) and a second switch on the output [9, 49, 50]. The input portion is identical to the boost or buck inputs with a switch used to control the input current waveshape. The energy storage element and second switch provide output voltage regulation and input to output energy balancing. The name of this converter refers to the three networks, or circuit modes, that the converter can be operated in. One such three switched-network rectifier is the modified Cuk shown in Figure 2.17.

This type of rectifier is actually two converters in one; a switch-mode rectifier for high PF, followed by a dc to dc converter for voltage regulation and ripple control (as discussed in the introduction of this Chapter). The two sections, however, are not completely independent, since the intermediate energy storage element can not be connected to both the input and the output at the same time.

2.5 Controlled Bridge Rectifiers

The controlled bridge rectifier is a boost type rectifier with reversible power flow capability. It has a boost inductance, which may be no more than the line reac-

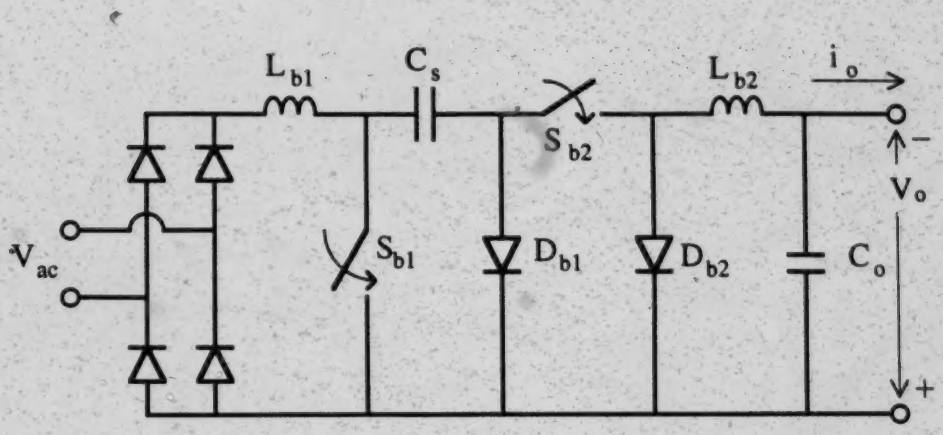

Figure 2.17: Modified Cuk Three Switched-Network Rectifier

tance, at the input to the ac line and is similar to the boost rectifier in operation. The main difference is the ability of the bridge to place all or half of the inverted output capacitance into the boost inductor charging circuit during the On Period. This provides a greater charging voltage reducing the duration of the On Period. The Off Period remains the same as with a boost rectifier. Since the Off Period is significantly longer than the On Period, the net power flow is from input to output.

2.5.1 Half Bridge Rectifiers

The half bridge rectifier in Figure 2.18 has a split output capacitor with one side of the line input tied to the midpoint, in much the same manner as a voltage doubling diode rectifier. For proper operation, the output voltage must be at least twice the input voltage. This rectifier has been called a Synchronous Front-End Rectifier (SFER) by Manias et al. [51] and a voltage-sourced reversible rectifier by Boys and Green [52].

During each switching cycle, while operating as a rectifier, the two modes of operation in Figure 2.19 are:

On Period The appropriate switch is on. The inductor L_b "charges" as energy is transferred from the power system and half of the output capacitance to L_b. The current in L_b ramps upwards.

Off Period Both switches are off. L_b "discharges" as energy is transferred from the power system and L_b to the other half of the output capacitance. The current in L_b ramps downwards.

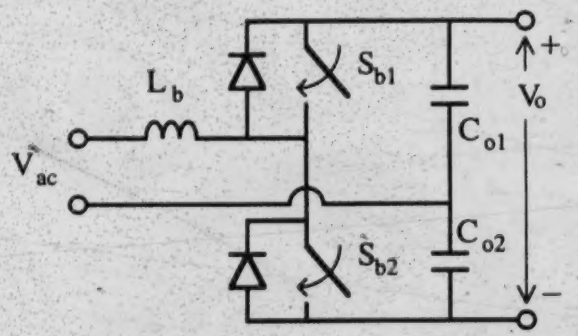

Figure 2.18: Half-Bridge Rectifier

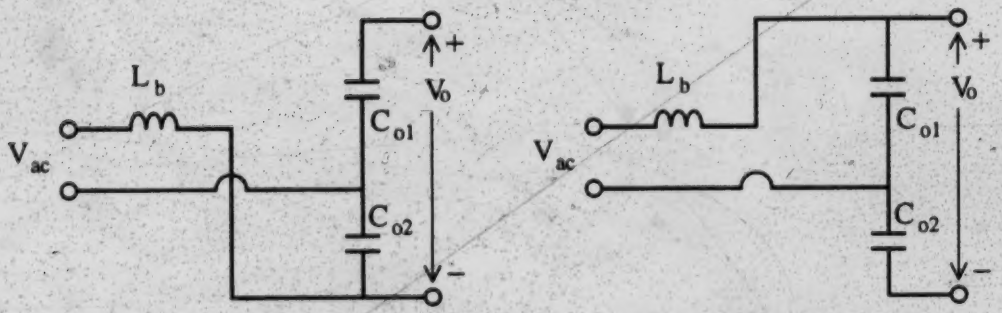

(a) On Period (b) Off Period

Figure 2.19: Half-Bridge Rectifier Modes of Operation

Only one of the two capacitors in the half-bridge rectifier is charged in each half line cycle, while the load discharges both capacitors. The On Period involves charging the inductor while discharging one capacitor. The Off Period involves discharging the inductor into the alternate capacitor. The charging and discharging capacitors are exchanged each half line cycle. As a result, the voltage at the midpoint between the capacitors must vary through the line cycle.

2.5.2 Full Bridge Rectifiers

The full bridge rectifier, shown in Figure 2.20, operates in the same manner as full bridge inverters, allowing fully controllable power flow in two directions [53, 54].

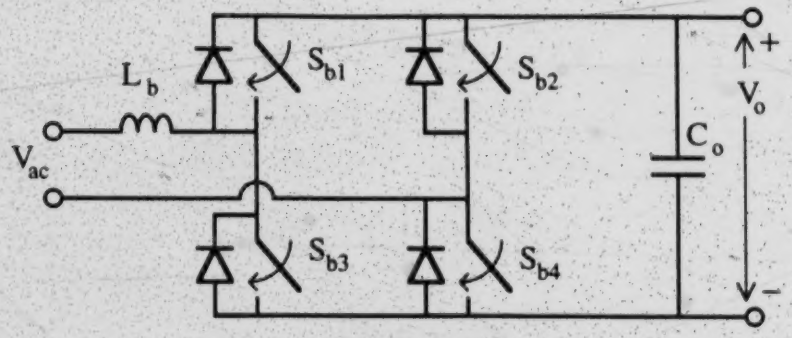

Figure 2.20: Full Bridge Rectifier

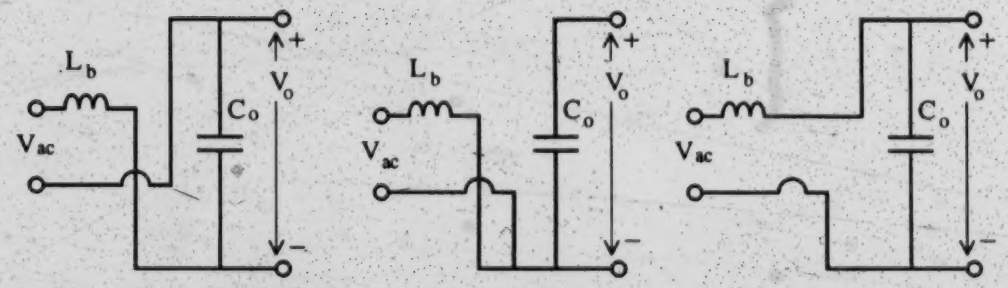

(a) Full Charging (b) Half Charging (c) Off Period

Figure 2.21: Full Bridge Rectifier Modes of Operation

While only two modes of operation of the full-bridge rectifier are apparent from the literature [53, 54], an inspection of the circuit reveals that three modes of operation are possible. These modes are shown in Figure 2.21.

Full Charging On Period The appropriate alternate switch pair is on creating a loop containing the inductor L_b, the inverted output capacitor and V_{ac}. L_b "charges" as energy is transferred from the power system and the output capacitor to L_b. The current in L_b ramps upwards.

Half Charging On Period One switch is on creating a loop containing L_b and V_{ac}. L_b "charges" as energy is transferred from the power system to L_b. The current in L_b ramps upwards.

Off Period All the switches are off. L_b "discharges" as energy is transferred from

the power system and L_b to the output capacitor. The current in L_b ramps downwards.

2.5.3 Current Control

Current control in controlled bridge rectifiers is achieved in the same manner as with the boost rectifier. The voltage at the input bridge is pulse-width-modulated to control the current in the input boost inductor. Therefore, the current control methods described in section 2.1 are all applicable.

Controlled bridge rectifiers have a distinct advantage over the boost rectifier at low input voltages. The insertion of inverted output capacitance in the inductor charging circuit provides a much larger voltage for forcing the current upwards. Therefore the rectifier is capable of full input current control at all times.

Chapter 3

Resonant Switch-Mode Rectifiers

The technology of power conversion has been advancing at a rapid pace in recent years, as new power electronic devices and new techniques for using those devices become available. The use of resonance is a technique that is proving to be useful for increasing the power density of power converters. The justification for the development of resonant switch-mode rectifiers is presented in this chapter. The operation of relevant resonant switch-mode rectifiers is described as an introduction to the subject resonant tank boost rectifier.

3.1 Switching Losses

Most switch-mode rectifiers, including those described in chapter 2, are hard-switched, which means that the active switch is:

- forced to support voltage on turn-off before the current has fully dropped to zero, and/or
- forced to conduct current on turn-on before the voltage has fully dropped to saturation levels.

Each time an active switch is turned on or off under unfavorable switching conditions, power is lost to heat during the voltage and current transition from high to low, or low to high. At turn-on, the demands of the circuit in which the switch is operating force the current through the device before the voltage has reached "on" saturation levels. The product of this current and the still present voltage is power, which is lost to heat in the device. When turning off, the power loss occurs when the current is not allowed to reach zero before the transistor is required to support a voltage across its output.

The power lost in one switching transition is normally insignificant. However, if the switching frequency of a power conversion system is increased, the switching

losses are multiplied by the increase in frequency. At some point these losses become comparable to circuit conduction losses, or other losses in the circuit. There are benefits to be gained from increasing the switching frequency, as described below, so decreasing the switching losses is important.

There are two major reasons for increasing the switching frequency. The first is to reduce the size and cost of power conversion systems by reducing the required size of transformers, inductors, and capacitors. As the frequency of operation of these devices increases, their required values and size decreases. The second is to increase the resolution of current or voltage waveforms at the fundamental frequency. Every switching period provides an opportunity for corrective action to be taken on the current waveform. Therefore, higher switching frequencies result in improvements in low frequency distortion. Also, as the switching frequency is increased, less filtering is required to remove that frequency component from the waveform.

3.2 Resonant Circuits

To achieve the benefits of the increased switching frequency without increasing the losses significantly, LC resonant circuits have been designed into power converters. These circuits provide instants of zero current (ZC) or zero voltage (ZV) in the switch in which lossless switching, or soft-switching, can occur. This can be achieved in a number of ways, as described below.

An advantage that resonance may offer over hard-switching is reduced EMI due to the smooth sinusoidal current and voltage waveforms caused by the resonant circuits. The current waveforms of hard-switches are "square" in nature, and therefore contain significant harmonics at multiples of the switching frequency.

At sufficiently high frequencies, the use of resonance circuits allows "parasitic" device capacitances and inductances to be used for energy storage and waveshaping. These device reactances, such as the drain-source capacitance of MOSFETs, and the leakage inductance of transformers, are normally considered to be sources of losses and disruptive oscillations. Resonant circuits allow them to be used constructively in the circuits.

Disadvantages of the use of resonance in power converters include high peak voltages and/or currents in devices, increased rms current values and the resulting higher conduction losses, an increased number of components required by the circuits, and an increased possibility of instability or interaction with the load in converters where the resonant circuits are not adequately decoupled from the load.

3.2.1 Resonant DC to DC Converters

The most predominant converters using resonance for soft-switching are resonant dc to dc converters. These fall into two types, series resonant converters (SRC) which use a series resonant LC circuit, and parallel resonant converters (PRC) which use a parallel resonant LC circuit. The SRC produces output dc power by rectifying the current in its resonant circuit. The PRC produces output dc power by rectifying the voltage in its resonant circuit.

A schematic diagram of a full-bridge series resonant dc to dc converter (SRC) is shown in Figure 3.1. The energy in the resonant circuit is increased when the appropriate active switches are on and is decreased when current is allowed to flow freely through the diode(s). Voltage regulation is achieved by duty cycle modulating the periods of increasing and decreasing resonant circuit energy. This energy is transferred to the load through a series transformer and a rectifier bridge with a smoothing output capacitor.

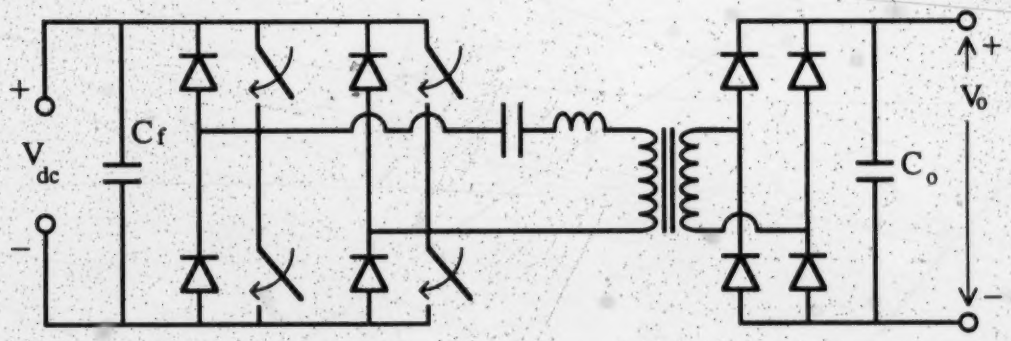

Figure 3.1: Full Bridge Series Resonant DC to DC Converter

As compared to other converter schemes, the SRC has the advantages of inherently blocking dc from the transformer and decreasing conduction losses with decreasing load. A disadvantage is that there is a high output ripple current. Also, when operated using an above resonance switching frequency for regulation, the SRC has the disadvantage of having poor low load voltage regulation.

A schematic diagram of a half-bridge parallel resonant dc to dc converter (PRC) is shown in Figure 3.2. As in the SRC, a resonating current and voltage is established in the resonant portion of the circuit. The energy in this resonant circuit is controlled by the active switches in much the same manner as with the SRC. The voltage across the resonant capacitor is fed through a parallel transformer and then rectified and filtered to give the output voltage.

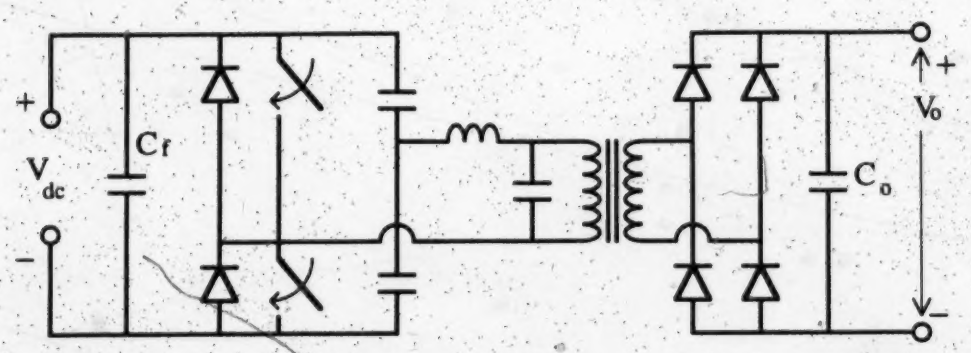

Figure 3.2: Half Bridge Parallel Resonant DC to DC Converter

The PRC has the advantages of low output ripple current and natural current limitation when the load is short-circuited. Also, when operated using an above resonance switching frequency for regulation, the PRC has good low load voltage regulation.

A disadvantage of the PRC is its increasing conduction losses with increasing output voltage, independent of load. The current in the resonant circuit is determined by the capacitor voltage which is proportional to the output voltage and not by the load current.

3.2.2 Quasi-resonant Converters

New families of quasi-resonant converters have been developed by replacing the active switches in normal switch-mode converters with resonant zero voltage switches (ZVS) or zero current switches (ZCS) shown in Figures 3.3 and 3.4 [12]. These consist of an inductance and capacitance arranged around the "switch" in such a way as to force the voltage or current respectively to a zero value at the switching instant. In essence, the energy that would have been dissipated during switching is stored by the LC tank circuit and then transferred from the input to the output.

ZCS's and ZVS's evolved from snubbers which were used to dissipate energy from the switches during switching. The use of these switches in quasi-resonant converters eliminates the need for snubbers and their associated losses.

The ZCS and ZVS techniques have certain problems associated with them. On turn-on of a MOSFET ZCS, the junction capacitance of the MOSFET is discharged as a loss. For this reason, ZCS quasi-resonant converters have not been implemented at switching frequencies above 1 MHz.

One disadvantage of the ZVS technique is that the peak voltage stress that

Figure 3.3: Zero Current Resonant Switches

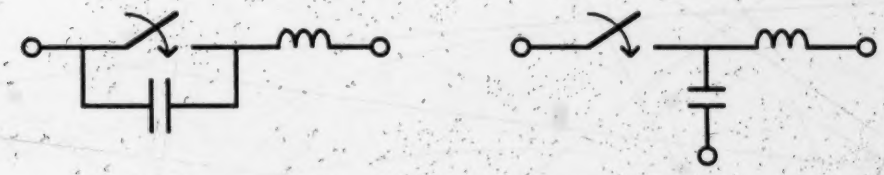

Figure 3.4: Zero Voltage Resonant Switches

the MOSFET switch experiences during the resonant pulse can be significantly greater than the same switch would see in the equivalent PWM converter. A clamped-voltage topology has been proposed which holds the switch voltage to the input voltage, thereby keeping the switch voltage rating down [55]. This, however, results in an increased peak current carrying requirement.

Another problem with the ZVS technique concerns the rectifying diode. At turn off, the junction capacitance of the diode can oscillate with the ZVS resonant inductance. If this oscillation continues undamped, the voltage gain and stability of the converter control system will be adversely affected. This can be overcome by damping the oscillation, but that will result in the power contained in the oscillation being lost to heat.

3.2.3 Resonant Rectifiers

As with switch-mode converters, resonant dc to dc converters have been applied to rectifiers as "power conditioning" sections to produce the desired input current waveform. Chambers [56] described half bridge and full bridge configurations of a series resonant rectifier (SRR), shown in Figure 3.5 and 3.6. During each line cycle, the switching frequency is kept constant and the per-switching-cycle average input current is roughly proportional to the input voltage. Line frequency sinusoidal input current is achieved through inherent open loop control. Output voltage regulation is obtained by an outer voltage control loop giving a switching frequency

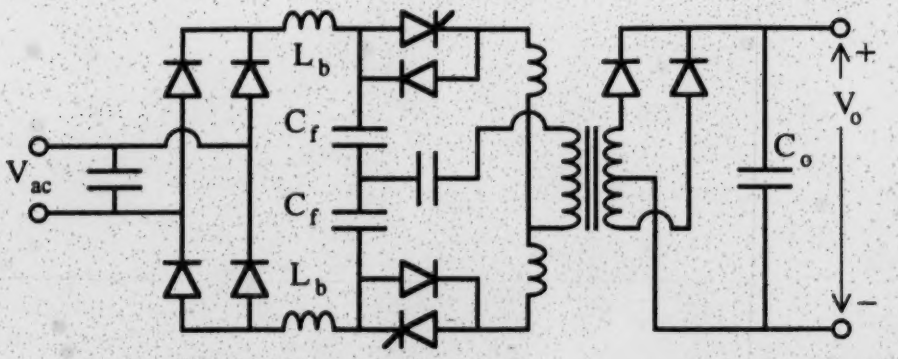

Figure 3.5: Half Bridge Series Resonant Rectifier

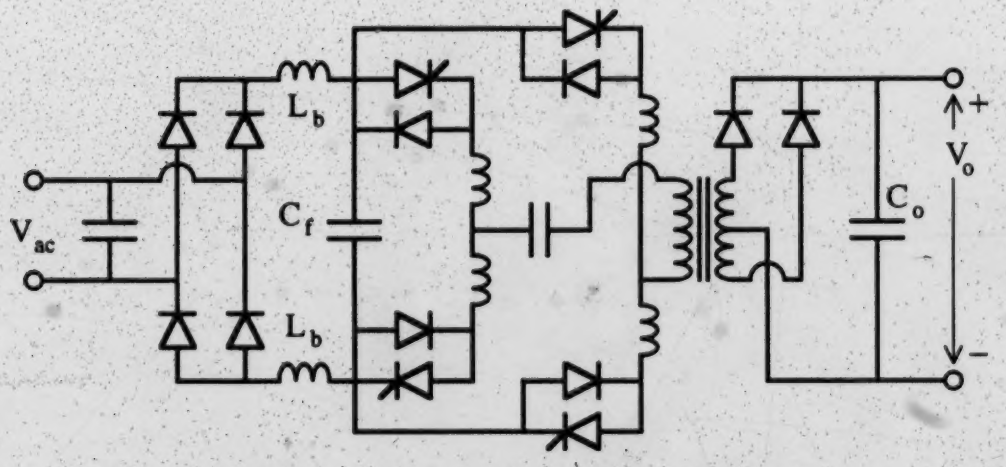

Figure 3.6: Full Bridge Series Resonant Rectifier

output as the current reference.

A high frequency (low pass) filter is placed between the diode bridge and the resonant converter to filter out the strong resonant frequency and switching frequency components of the input current waveform. This rectifier has buck characteristics in that input current cannot be drawn when the input voltage falls below the output voltage as reflected across the transformer. Also, the input current distortion will increase as the reflected output voltage is increased.

A "Tuned Class D Converter", shown in Figure 3.7, which inherently draws

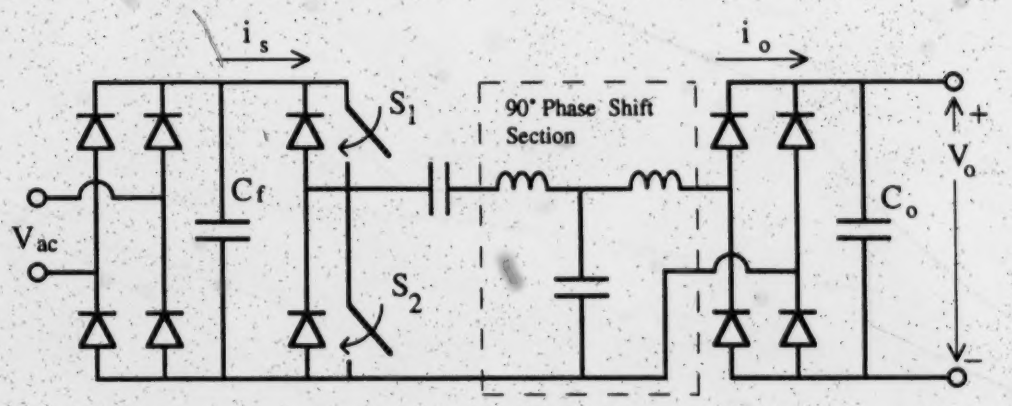

Figure 3.7: Tuned Class D Rectifier

square wave current at line frequency was described by Seidel [57]. It uses a T "90° phase shift section" which consists of passive inductance and capacitance tuned to the base switching frequency. A square wave voltage at the switching frequency is produced at the input to the phase shift section. When the phase shift section is forced by this square wave voltage, it produces a sinusoidal current source at the switching frequency at it's output. The magnitude of this current source is determined by the switching frequency. This current is rectified by the output diode bridge. The current at the input to the phase shift section is also a sinusoid at the switching frequency. Therefore, the current i_s into the switches is a half wave rectified current. The switching frequency component is removed by the filter capacitor C_f, leaving a dc current through the input diode bridge. In Seidel's converter, the filter capacitor is sufficiently large to round out the line frequency square wave current, giving a power factor of 0.93.

3.3 Resonant Boost Rectifiers

Resonance has been applied to the boost rectifier to provide soft-switching and reduce EMI problems. Nijhof [58] describes both SRR's and parallel resonant rectifiers (PRR) with single ended structures which have only one active switch and operate much like a boost rectifier, but with resonance. One of Nijhof's SRR's is shown in Figure 3.8. A number of variations of the PRR are presented. The advantages of the PRR over the SRR include reduced turn-off losses and the slightly reduced size of magnetic components. Mohan and He [59] propose the same PRR, calling it a Four-Resonant-State (FRS) converter, shown in Figure 3.9.

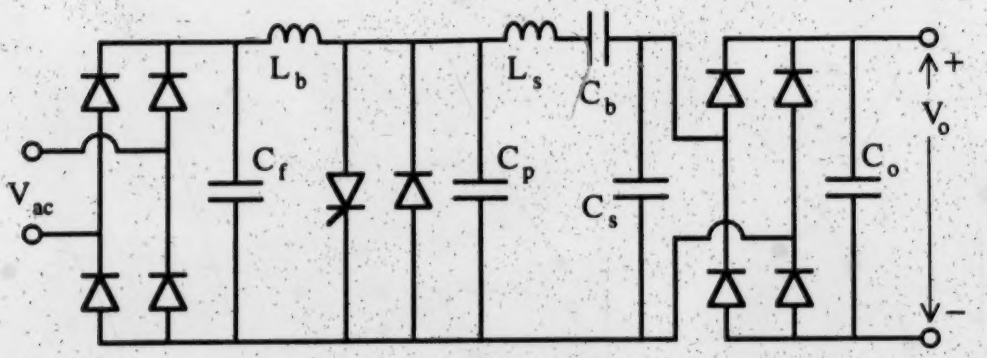

Figure 3.8: Series Resonant Rectifier

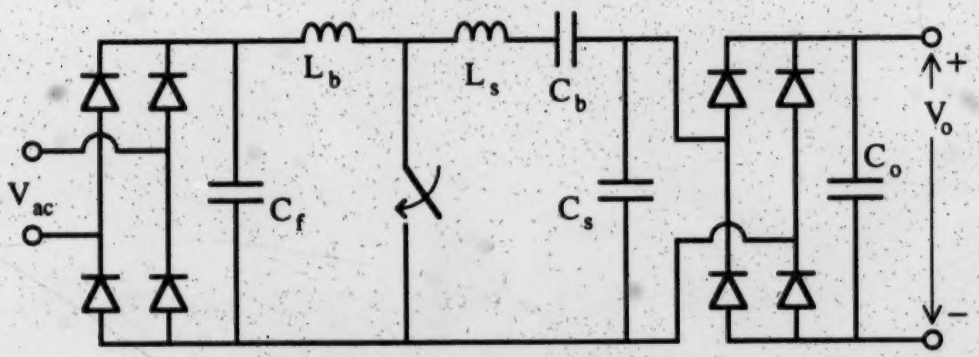

Figure 3.9: Four-Resonant-State Rectifier

The FRS converter operation is similar to that of the boost rectifier, with a "boost" inductor on the input which is alternately shorted across the input (as in On Period boost rectifier operation) and then allowed to inject current to the output circuit (as in Off Period boost rectifier operation). The output circuit, however, contains a resonant LC circuit and an output rectifying diode bridge before the output capacitance.

Energy transfer from the source to the energy storage elements in the converter is continuous. Energy transfer from those storage elements to the output occurs twice in each switching cycle, once while the active switch is on and C_s is clamped at $-V_o$ and once while the active switch is off and C_s is clamped at $+V_o$. Because the on time of the switch is determined by the circuit component values, only the

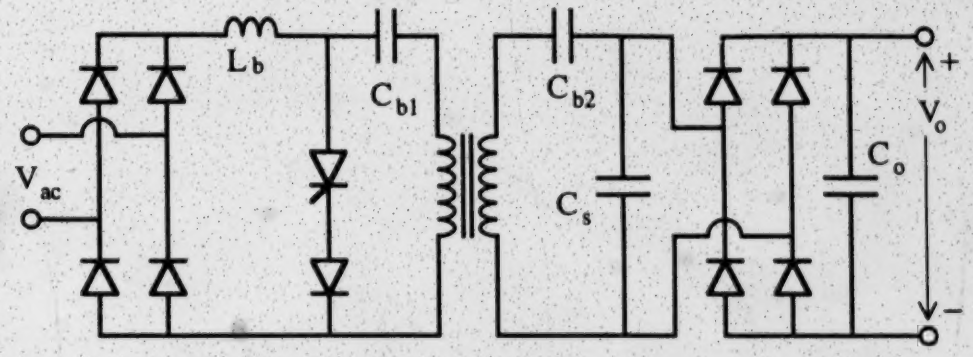

Figure 3.10: "Modified" Boost Resonant Rectifier

off time can be varied to control the input current. Input current increases with decreased off time, and therefore the switching frequency increases.

One of Nijhof's PRR's, shown in Figure 3.10, is similar to the FRS converter but with a transformer before the output diode bridge. The resonance power supply uses only a voltage control loop, with a constant current request throughout the line cycle. The line current waveform is a square wave (although rounded by a large input filter capacitor) and the power factor achieved is not as good as with the FRS converter, which uses sinusoidal current control.

De Doncker and Venkataramanan [61] analyze an Active Clamped Resonant DC Link (ACRDCL) boost rectifier, shown in Figure 3.11, which uses a voltage clamp circuit first proposed by Divan and Skibinski [62]. Put simply, it is a boost rectifier with an active clamped resonant dc link between the boost diode and the output capacitor. The resonant dc link provides regular instants of zero voltage across the boost switch at which time lossless ZV switching can occur. Therefore, the current control method is integral control, described in section 2.1.1, where the boost switch is either on or off for the duration of one dc link period. At the end of each period, at the switch ZV instant, the switch will be set on or off depending on whether the boost inductor current is above or below the reference current. Therefore, the on and off periods are multiples of the dc link resonant period. The switching frequency varies, but is always less than half the dc link resonant frequency.

The active clamp consists of a capacitor and an active switch which is controlled so as to clamp the voltage across the boost switch preventing it from exceeding a specified value, which is set at 1.6 times the output voltage in this case. This partially alleviates the problem of excessive peak switch voltage ratings generally associated with resonant converters.

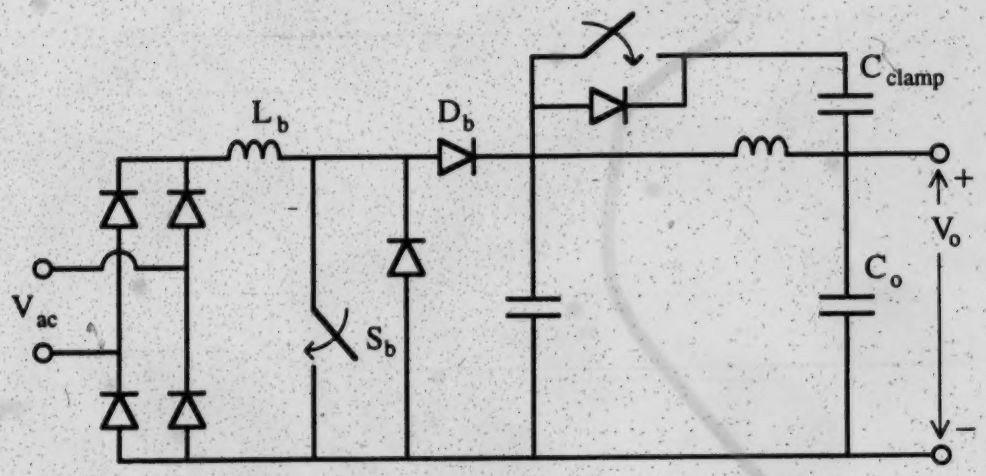

Figure 3.11: ACRDCL Boost Rectifier

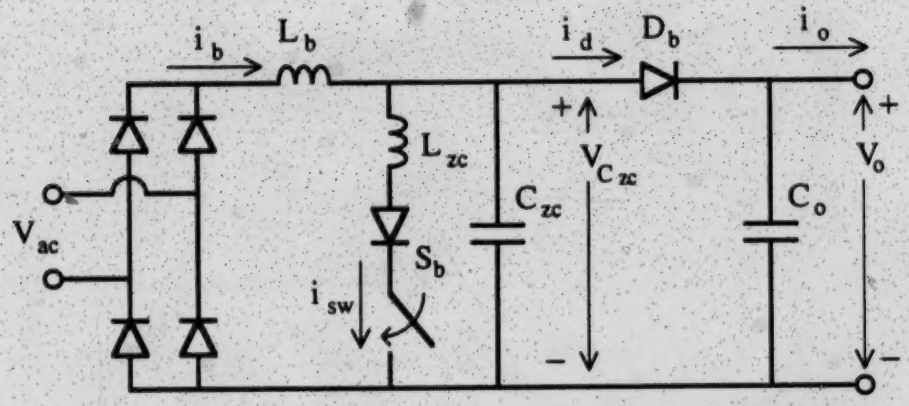

Figure 3.12: Zero-Current-Switching Quasi-Resonant Boost Rectifier

Barbi and da Silva [60] describe a Boost Zero-Current Switching Quasi-Resonant Rectifier (ZCS-QRR), shown in Figure 3.12. It consists of a standard boost rectifier with the active switch replaced by a zero current switch. At turn-on, the current in the switch is restricted from rising by the ZC inductor L_{ZC}, as shown in Figure 3.13. After turn-on, the current in the switch, which is $i_{L_{ZC}}$, rises linearly until it equals the current i_b in the boost inductor L_b at time t_1. Then the boost diode turns off and L_{ZC} combines with the ZC capacitor C_{ZC} to form a resonant circuit. $i_{L_{ZC}}$ follows a sinusoidal trajectory which rises and then resonates back to zero at time t_2 when ZC turn-off occurs. $v_{C_{ZC}}$ falls to $-V_o$, and then begins to rise just as t_2 is reached. After turn-off, $v_{C_{ZC}}$ ramps upwards as i_b flows into C_{ZC}. When $v_{C_{ZC}}$ reaches V_o, the boost diode turns on, and normal Off Period boost operation resumes.

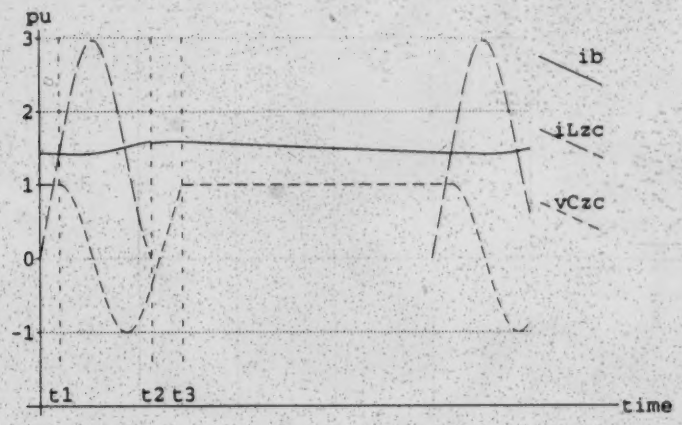

Figure 3.13: Voltage and Current Waveforms of the ZCS-Quasi-Resonant Rectifier

In this rectifier, the L_b charging period does not coincide exactly with the On Period. Energy transfer to L_b does not begin until $v_{C_{ZC}}$ drops below the input voltage, which occurs after turn-on. L_b charging ends a short time after the switch has turned off once $v_{C_{ZC}}$ has risen to reach the input voltage.

As with the FRS converter, the On Period of the ZCS-QRR is fixed by the resonant components, so control can only be achieved by varying the Off Period, which varies the switching frequency. Again, an inner current control loop and an outer voltage control loop were used. Barbi and da Silva achieved a reported power factor of 0.98 and efficiency of 92 % with their ZCS-QRR.

The topology of the ZCS-QRR is very close to that of the resonant tank boost rectifier (RTBR) which is the subject of this thesis. The RTBR topology is modified

slightly from that of the ZCS-QRR by moving the 'bottom' of C_{ZC} from the ground to the top of the boost switch, thus creating a resonant tank (RT). The effect of the RT on operation is quite significant, as will become apparent in the following Chapters. The major differences are are in how the input current is controlled, the discontinuous nature of the input current, the much smaller size of the boost inductor, and the much smaller variance in the switching frequency between full load and light load.

3.4 Disadvantages of Existing Resonant Switch-mode Rectifiers

While resonant switch-mode rectifiers have significantly lower switching losses than switch-mode rectifiers, they have a number of other disadvantages that need to be mentioned:

- The additional components in the resonant circuit and the significantly greater currents and voltages carried by those components result in increased conduction losses. These may offset the gains made in switching losses.
- Soft switching is often only achieved during one of the switching operations (either at turn-on or at turn-off), but not at both. Switching losses are not completely reduced.
- A relatively large inductance is still required to smooth the switching frequency component of the input current waveform (The boost inductance must be large enough that the current remains fairly constant through a switching cycle). While the size of this inductance is a vast improvement over the size that would be required at line frequency, further improvements would be beneficial in increasing the power density of the rectifier.
- The switching frequency in resonant switch-mode rectifiers can vary considerably, making the filtering at the switching frequency more difficult.

Chapter 4

Resonant Tank Boost Rectifier

4.1 Overview

The Resonant Tank Boost Rectifier (RTBR) is a single phase, unity power factor, soft switching, ac to dc power converter conceived by the author. It has small power circuit components and little variance in switching frequency between full load and no load. The circuit operation of the RTBR will be discussed in detail in this chapter.

The purpose of the RTBR is to convert ac power to dc power as efficiently as possible, with high power density. The RTBR topology is a boost rectifier, as described in section 2.1, with a resonant LC tank (RT), consisting of L_t and C_t, placed in the switch leg. The power circuit is shown in Figure 4.1.

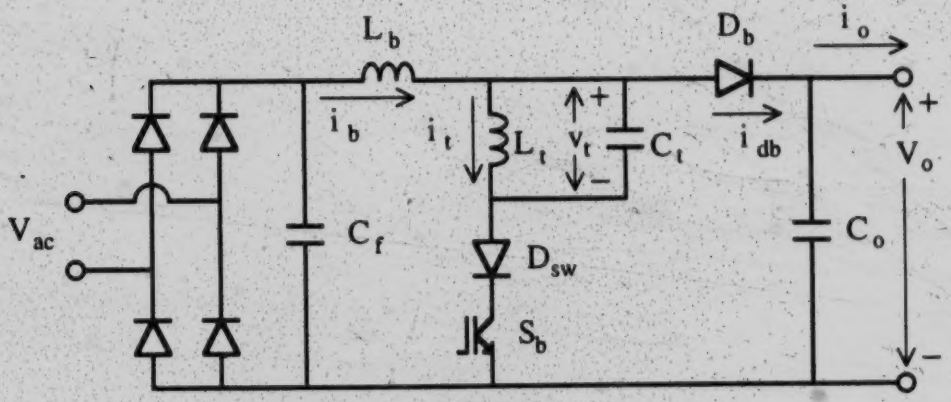

Figure 4.1: Resonant Tank Boost Rectifier

The RTBR has the following features:

- The RTBR has very low switching losses due to soft-switching. Discontinuous conduction of the boost inductor current ensures ZCS at turn-on (with a control circuit designed to keep the RTBR out of continuous conduction). The action of the RT during each current pulse results in ZVS at turn-off for all but a few low power current pulses close to the input voltage cusps.

- The input current of the RTBR is proportional to the phase of the RT at turn-on of the boost switch. Within a limited range of the RT cycle, the average input current in a switching period can be controlled by timing turn-on to occur at the appropriate phase of the RT. Since this limited range, or phase window, is open for a small fraction of the switching period, there is only a small variance in switching frequency as the rectifier load current varies.

- All components except the output capacitance are very small. The RTBR operates in discontinuous conduction mode and the boost inductor is sized accordingly. A filter capacitor, C_f, is used to filter the switching frequency component from the boost inductor current. This C_f and L_b combination provides good filtering with a small volume of components.

The input to the RTBR is a single-phase supply. The output is a variable dc load, with specified maximum power requirements and restrictions on the allowable ripple voltage. The output voltage could be variable, but must be greater than the crest of the input voltage.

4.2 Power Circuit Operation

The RTBR appears from the input to be similar to a normal boost rectifier operating in discontinuous conduction mode. The current i_b in the boost inductor L_b consists of a series of pulses at the switching frequency f_{sw}. A typical pulse, with the coincident RT voltage and current waveforms, is shown in Figure 4.2, with i_b, i_t and v_t as shown in Figure 4.1. In these waveforms, the switching occurs every second cycle of the resonant tank. All parameters are expressed in per unit quantities with V_{base} as the rated output voltage V_o, and I_{base} as the full load output current.

The switching period consists of an On Period from $t = 0$ to $t = t_2$, followed by an Off Period from $t = t_2$ to $t = t_{sw}$. The operation of the RTBR during each switching period is as follows:

On Period The switch is on. The boost inductor L_b "charges" as energy is transferred from the power system to L_b. The current in L_b resonates upwards.

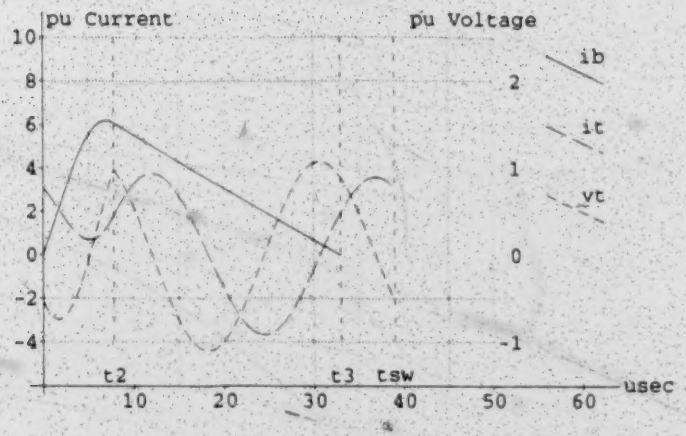

Figure 4.2: RTBR Voltage and Current Waveforms

Off Period The switch is off. L_b "discharges" as energy is transferred from the power system and L_b to the output capacitor. The current in L_b ramps downwards.

At the start of a switching cycle, the current in the boost inductor i_b is normally zero. During the switch off-to-on transition, there is no current to be commutated into the switch and current is restricted from rising by the boost inductance. Hence, ZC turn-on is achieved in the same manner as with a normal boost rectifier in discontinuous conduction mode.

The average current in each pulse is controlled so that it is proportional to the instantaneous line voltage, using a mechanism to be described in section 4.5. The pulses are smoothed by C_f. The result is a sinusoidal input line current in phase with the line voltage.

In each switching cycle, the RTBR acts as a dc to dc converter. f_{sw} is above the audible range (20 kHz) so the period of a switching cycle is more than two orders of magnitude smaller than a line cycle. Therefore, the instantaneous input voltage V_{in} will remain almost constant throughout a switching cycle. V_o is held constant by the output capacitor C_o.

Before turn-on, the voltage and current in the RT are oscillating sinusoidally at a slightly damped resonant frequency ω_t. The damping can be accommodated in the circuit by adding series resistances to L_b, L_t and C_t, as shown in Figure 4.3. While the resistances R_t and R_c must be very small for the RTBR to operate without excessive losses, the losses in the RT can be significant. ω_t is very close to

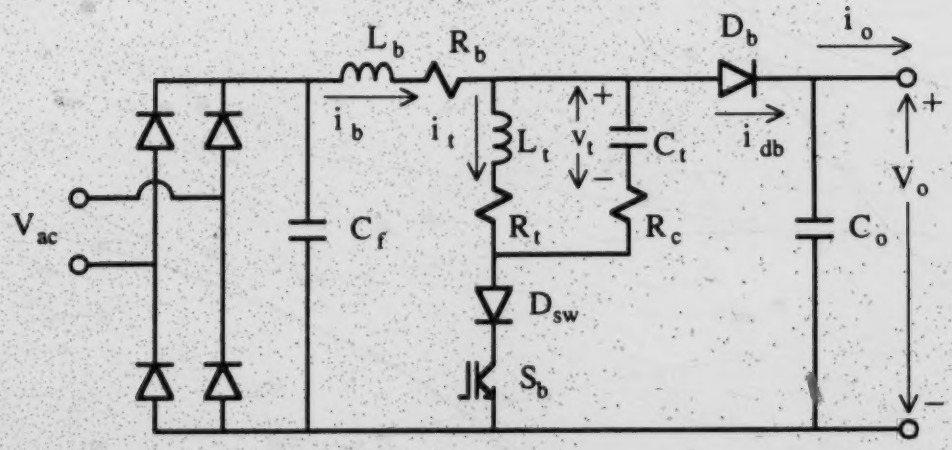

Figure 4.3: Resonant Tank Boost Rectifier with Component Resistances

the tank undamped resonant frequency ω_{tn}. These are related by the RT damping factor ζ.

$$Z_t = \sqrt{\frac{L_t}{C_t}} \tag{4.1}$$

$$\zeta = \frac{R_c + R_t}{2Z_t} \tag{4.2}$$

$$\omega_{tn} = \frac{1}{\sqrt{C_t L_t}} \tag{4.3}$$

$$\omega_t = \omega_{tn}\sqrt{1-\zeta^2} \tag{4.4}$$

4.3 On Period

At the start of the On Period, at $t_0 = 0$, a voltage V_{imp} is impressed across the boost inductor and resonant tank. V_{imp} is the instantaneous ac line input voltage V_{in}, with the effect of the diode bridge voltage drop V_{br} and the boost switch forward voltage drop V_{sw} included. V_{br} and V_{sw} are assumed to be constants in the analysis since their variance is small.

$$V_{imp} = V_{in} - V_{br} - V_{sw} \tag{4.5}$$

With V_{imp} sufficiently large, a positive voltage will be impressed across the boost inductor and the current i_b will rise. This current will be injected into the RT, causing the voltage across the tank to rise. At time t_2, the tank voltage will reach $+V_o$ and the boost diode D_b will become forward biased. D_b will begin to conduct, thus naturally commutating the boost switch off under ZV conditions.

During the On Period, the power circuit is as shown in Figure 4.4. The differential equations describing this circuit are:

$$\frac{di_b}{dt} = \frac{1}{L_b}[-(R_b + R_c)i_b + R_c i_t - v_t + V_{imp}] \tag{4.6}$$

$$\frac{di_t}{dt} = \frac{1}{L_t}[R_c i_b - (R_t + R_c)i_t + v_t] \tag{4.7}$$

$$\frac{dv_t}{dt} = \frac{1}{C_t}[i_b - i_t] \tag{4.8}$$

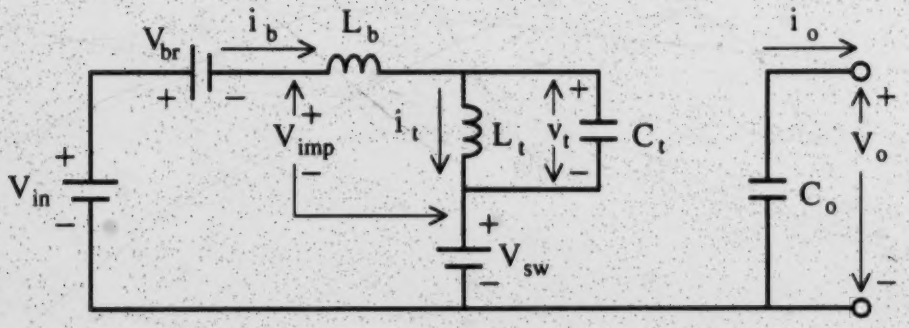

Figure 4.4: "On Period" RTBR Circuit

Differential equations (4.6), (4.7) and (4.8) can be solved using state space methods, as is done in Chapter 5 in a computer simulation program. Since the RTBR is just slightly damped, the values for R_b, R_t, and R_c will be relatively small. If these resistances are neglected, a much simplified undamped solution, which is very close to the damped solution, can be determined. Equations (4.6), (4.7) and (4.8) reduce to:

$$\frac{di_b}{dt} = \frac{1}{L_b}(v_t + V_{imp}) \tag{4.9}$$

$$\frac{di_t}{dt} = \frac{1}{L_t}v_t \tag{4.10}$$

$$\frac{dv_t}{dt} = \frac{1}{C_t}(i_b - i_t) \tag{4.11}$$

Differentiating (4.11) and then substituting for $\frac{di_b}{dt}$ and $\frac{di_t}{dt}$ gives a second order differential equation, which can be solved for v_t.

$$\frac{d^2v_t}{dt^2} - \left(\frac{L_b + L_t}{L_bL_tC_t}\right)v_t = \frac{V_{imp}}{L_bC_t} \tag{4.12}$$

In normal operation, the current and voltage in the RT oscillate continuously at the tank resonant frequency. At the instant of turn-on, the RT will be found at a particular point in that oscillation, with a current i_{t0} in the inductor, and a voltage v_{t0} across the capacitor. The subscript 0 will be used to indicate an instantaneous value of a variable at turn-on when $t_0 = 0$. i_{b0}, i_{t0} and v_{t0} are the initial conditions for the tank variables and for equation (4.12). i_{t0} and v_{t0} can be conveniently expressed in terms of the phase β of the tank oscillation, and the parameter V_{tp}. β is a value between 0° and 360°, with $\beta = 0°$ when the RT voltage is at its positive peak V_{tp} and the RT current is at zero and rising, as can be seen in Figure 4.8.

V_{tp} is given by the expression:

$$V_{tp} = \sqrt{v_t^2 + Z_t^2 i_t^2} \tag{4.13}$$

While V_{tp} will vary through the switching period, it is expressed here in upper-case since the value of V_{tp} at turn-on, V_{tp0}, and the value at turn-off, V_{tp2} are used as constants in the expressions for circuit voltages and currents. V_{tp0} is given by the expression:

$$V_{tp0} = \sqrt{v_{t0}^2 + Z_t^2 i_{t0}^2} \tag{4.14}$$

V_{tp0} and β_0 are the values of V_{tp} and β respectively at turn-on. These values are determined by the operation of the RTBR in prior switching cycles and will be discussed in greater detail in section 4.6.1. i_{t0} and v_{t0} are expressed in terms of V_{tp0} and β_0 so that i_b, i_t and v_t can be expressed in terms of β_0.

$$i_{b0} = 0 \tag{4.15}$$

$$i_{t0} = \frac{V_{tp0}}{Z_t}\sin(\beta_0) \tag{4.16}$$

$$v_{t0} = V_{tp0}\cos(\beta_0) \tag{4.17}$$

$$\frac{dv_{t0}}{dt} = -\frac{1}{C_t}i_{t0} = -\omega_{tn}V_{tp0}\sin(\beta_0) \tag{4.18}$$

With these initial conditions, the solution to (4.12) is:

$$v_t = kV_{imp} + [V_{tp0}\cos(\beta_0) - kV_{imp}]\cos(\omega_{bn}t) - \sqrt{1-k}V_{tp0}\sin(\beta_0)\sin(\omega_{bn}t) \tag{4.19}$$

ω_{bn} is the boost On Period circuit undamped resonant frequency, and k is a commonly occurring ratio of circuit inductances:

$$\omega_{bn} = \sqrt{\frac{1}{C_t}\left(\frac{1}{L_b} + \frac{1}{L_t}\right)} \tag{4.20}$$

$$= \sqrt{\frac{L_b + L_t}{C_t L_b L_t}} \tag{4.21}$$

$$k = \frac{L_t}{L_b + L_t} \tag{4.22}$$

With the appropriate values of V_{imp}, V_{tp0}, and β_0, the resonant tank voltage v_t will increase during the On Period until it reaches the output voltage, at which time the On Period ends. In the expression for v_t in (4.19), the $\cos(\omega_{bn}t)$ and $\sin(\omega_{bn}t)$ terms together make a single sinusoidal term with a phase offset θ. Equation (4.19) becomes:

$$v_t = kV_{imp} + c_{vt}\sin(\omega_{bn}t - \theta) \tag{4.23}$$

where:

$$a_{vt} = V_{tp0}\cos(\beta_0) - kV_{imp} \tag{4.24}$$

$$b_{vt} = -\sqrt{1-k}V_{tp0}\sin(\beta_0) \tag{4.25}$$

$$c_{vt} = \sqrt{b_{vt}^2 + a_{vt}^2} \tag{4.26}$$

$$\theta = \pi + \arcsin\left(\frac{a_{vt}}{c_{vt}}\right) \quad for \quad \beta_0 \leq \pi \tag{4.27}$$

$$\theta = -\arcsin\left(\frac{a_{vt}}{c_{vt}}\right) \quad for \quad \beta_0 > \pi \tag{4.28}$$

The time when v_t reaches specific values can be determined by solving for t in (4.23) and substituting for θ based on the value of β_0.

$$t = \frac{1}{\omega_{bn}}\left[\arcsin\left(\frac{v_t - kV_{imp}}{c_{vt}}\right) + \theta\right] \tag{4.29}$$

The peak boost inductor current occurs when the voltage across L_b is zero, in which case $v_t = V_{imp}$. Substituting for v_t in (4.29) gives:

$$t_{pk} = \frac{1}{\omega_{bn}}\left[\arcsin\left(\frac{(1-k)V_{imp}}{c_{vt}}\right) + \theta\right] \tag{4.30}$$

The currents i_b and i_t during the On Period can be derived by substituting v_t into (4.9) and (4.10), using the initial conditions in (4.15) and (4.16), and then integrating between 0 and t.

$$i_b = \frac{V_{imp}t}{L_b + L_t} + \left[\frac{kV_{imp} - V_{tp0}\cos(\beta_0)}{\omega_{bn}L_b}\right]\sin(\omega_{bn}t)$$

$$+ \frac{V_{tp0}\sin(\beta_0)}{\omega_{tn}(L_b + L_t)}[1 - \cos(\omega_{bn}t)] \tag{4.31}$$

$$i_t = \frac{V_{imp}t}{L_b + L_t} + \frac{1}{\omega_{bn}L_t}[V_{tp0}\cos(\beta_0) - kV_{imp}]\sin(\omega_{bn}t)$$

$$- \frac{1}{\omega_{tn}L_t}V_{tp0}\sin(\beta_0)[(1-k)\cos(\omega_{bn}t) + k] \tag{4.32}$$

The boost inductor current increases to a peak value at time t_{pk} and then decreases slightly until natural commutation occurs at time t_2, when the tank voltage v_t equals $V_{t_{com}}$.

$$V_{t_{com}} = V_o + V_{db} - V_{sw} \tag{4.33}$$

$$t_2 = \frac{1}{\omega_{bn}} \left[\arcsin \left(\frac{V_{t_{com}} - kV_{imp}}{c_{vt}} \right) + \theta \right] \tag{4.34}$$

At the end of the On Period, the RT is generally left with an increased amount of energy e_{t2} and at a phase β_2 near 0°. These can be determined from the tank current i_{t2} and voltage v_{t2} at turn-off t_2.

$$V_{tp2} = \sqrt{v_{t2}^2 + Z_t^2 i_{t2}^2} \tag{4.35}$$

$$\beta_2 = \arcsin \left(\frac{i_{t2} Z_t}{v_{t2}} \right) \tag{4.36}$$

After time t_2, the On Period circuit ceases to be valid.

4.4 Off Period

The Off Period begins at time t_2 when the boost diode D_b turns on. The switch is turned off at the gate coincident with the natural commutation. The Off Period circuit is shown in Figure 4.5. The circuit actually consists of two relatively independent smaller circuits; the loop containing L_b, and the RT loop.

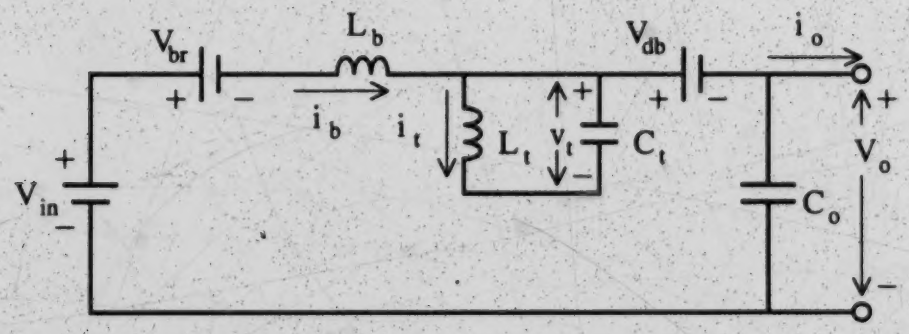

Figure 4.5: "Off Period" RTBR Circuit

Immediately after the boost diode turns on, a fixed voltage V_{ramp} is impressed across the boost inductor, causing the current i_b to ramp down almost linearly. V_{ramp} includes the effects of the diode bridge voltage drop V_{br} and the boost diode voltage drop V_{db}, which are assumed to be constants.

$$V_{ramp} = (V_{in} - V_{br}) - (V_o + V_{db}) \tag{4.37}$$

The differential equation describing the ramping boost inductor current is:

$$\frac{di_b}{dt} = \frac{1}{L_b}(V_{ramp} - R_b i_b) \tag{4.38}$$

The solution for (4.38) is a summation of the transient and forced responses for an LR circuit. The solution is simple enough without ignoring the resistance R_b, and the damping will prove significant in determining the steady-state response in section 4.6.

$$i_{b_{ramp}} = \frac{V_{ramp}}{R_b} + \left(i_{b2} - \frac{V_{ramp}}{R_b}\right) e^{-\frac{R_b}{L_b}t} \tag{4.39}$$

The time t_3 when the current in L_b reaches zero can be determined by setting $i_b = 0$ in (4.39) and solving for t.

$$t_3 = \frac{L_b}{R_b} \ln\left(1 + \frac{i_{b2} R_b}{V_{ramp}}\right) \tag{4.40}$$

While the boost inductor current is ramping downwards, the resonant tank is left to operate independently. At time t_2, the RT circuit will be left with a voltage of $+V_o$ and a small current i_{t2} in the inductor. Starting from those values, the RT voltage and current will follow a slightly damped, sinusoidal oscillation. The differential equations describing the tank oscillation are:

$$\frac{di_t}{dt} = \frac{1}{L_t}[v_t - (R_c + R_t) i_t] \tag{4.41}$$

$$\frac{dv_t}{dt} = -\frac{1}{C_t} i_t \tag{4.42}$$

Equations (4.41) and (4.42) can be combined to form a single second order differential equation in v_t.

$$L_t C_t \frac{d^2 v_t}{dt^2} + C_t(R_t + R_c)\frac{dv_t}{dt} + v_t = 0 \tag{4.43}$$

This equation is of the standard form:

$$\frac{1}{\omega_{tn}^2}\frac{d^2v_t}{dt^2} + 2\frac{\zeta}{\omega_{tn}}\frac{dv_t}{dt} + v_t = 0 \tag{4.44}$$

The initial conditions for (4.43) are i_{t2} and v_{t2}, the values of i_t and v_t at time t_2. These can be expressed in terms of V_{tp2} and β_2, given in (4.35) and (4.36). The solution to (4.44) yields:

$$v_{t_{osc}} = V_{tp2}e^{-\zeta\omega_{tn}(t-t_2)}\cos[\omega_{tn}(t-t_2)+\beta_2] \tag{4.45}$$

$$i_{t_{osc}} = \frac{V_{tp2}}{Z_t}e^{-\zeta\omega_t(t-t_2)}\sin[\omega_t(t-t_2)+\beta_2] \tag{4.46}$$

Once the current in the boost inductor has fallen to zero, the voltage at the "top" of the RT drops from V_o to V_{in}. The tank continues to oscillate at its resonant frequency until $t = t_{sw}$, at which time the switch is turned on to start the next switching cycle.

$$t_{sw} = t_2 + \frac{1}{\omega_t}[(2c-1)\pi + \beta_0 - \beta_2] \tag{4.47}$$

In (4.47), c is the number of RT cycles per switching cycle. During the free oscillation, the peak resonant tank voltage decreases sightly. V_{tp4} at the end of the Off Period is given as:

$$V_{tp4} = V_{tp2}e^{-\zeta\omega_{tn}(t_{sw}-t_2)} \tag{4.48}$$

V_{tp4} will be the value for V_{tp0} for the next switching cycle.

4.5 Control System

The ac line cycle current drawn by the RTBR is shaped by controlling the average boost inductor current $i_{b_{av}}$ in each switching period. The average current will be the ac line current after the switching frequency component has been removed by C_f. By controlling the average current in each switching cycle, the desired current waveform for an ac line cycle can be constructed.

The basic control of the RTBR must consist of an output voltage control loop and a switching period current control circuit as shown in Figure 4.6. The switching period current control circuit controls the average current in L_b in each switching cycle, using the reference signal provided by the voltage control loop.

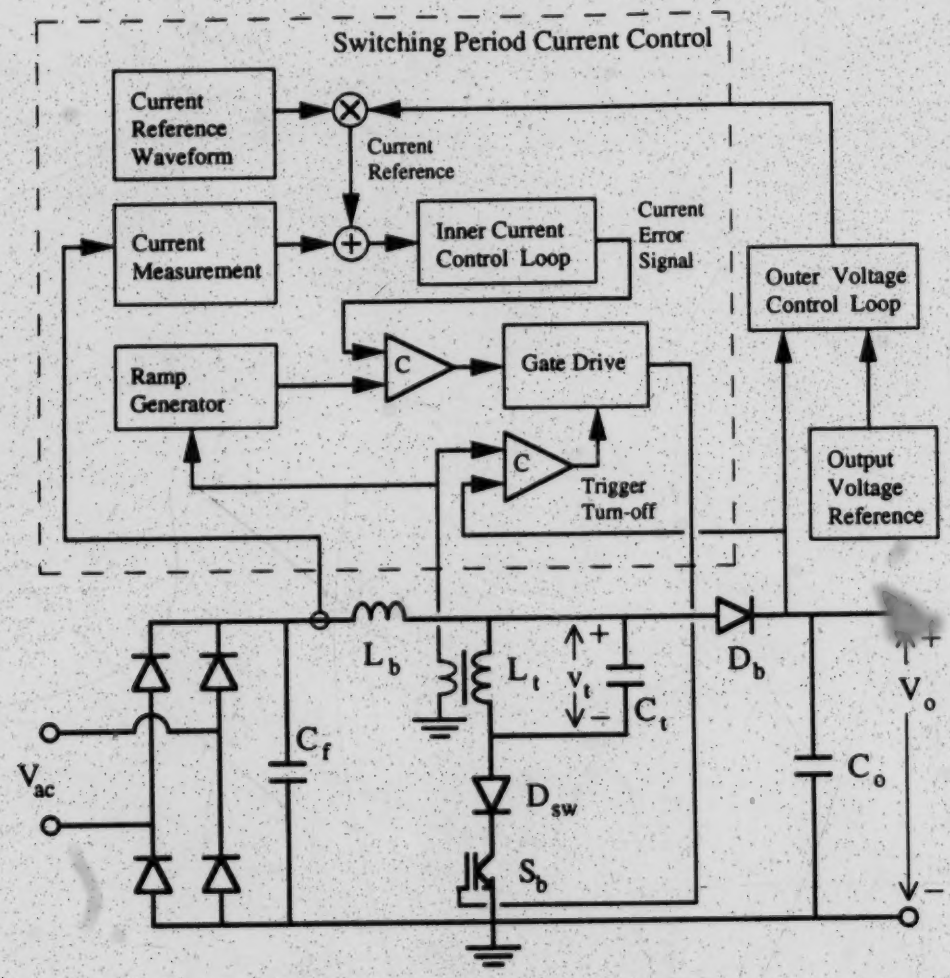

Figure 4.6: Basic Control of the RTBR

4.5.1 Tank Phase Window

The mechanism for the control of the input current is provided by the RT. The relationship between the phase β_0 of the RT at turn-on, and the resulting average current of the pulse is very close to linear at any given value of V_{in}. The simulated curves in figure 4.7 depict the average value of the pulse current for specific values of V_{in} as β_0 is varied. At any V_{in}, the desired $i_{b_{av}}$ can be obtained by turning on S_b at the appropriate RT phase.

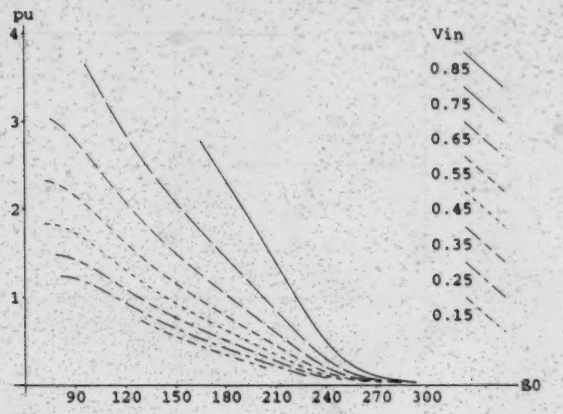

Figure 4.7: Average Input Current $i_{b_{av}}$ versus RT Phase at Turn-on

This linear relationship between $i_{b_{av}}$ and β_0 can be used in a current control system in the same manner as the current versus duty cycle relationship is used in the switch-mode rectifiers described in Chapter 2.

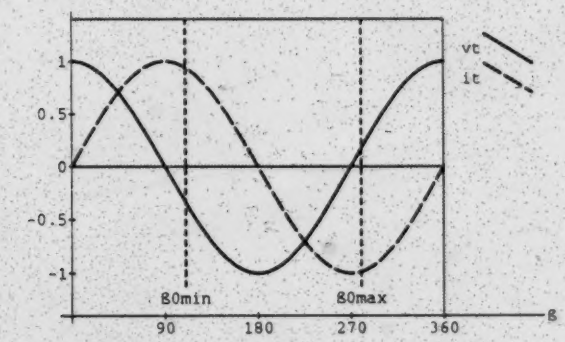

Figure 4.8: Turn-On Phase Window

To ensure stability and control, the turn-on of the switch must be restricted to a certain phase window shown in figure 4.8. Turn-on of the switch at a phase outside of that window will either result in undesirable circuit behavior, or will have no effect at all since the boost On Period circuit will not be forward biased.

At each V_{in}, there is an absolute lower limit of the phase window. This is determined by the point where i_b becomes just-continuous, or where steady-state

is no longer achievable due to insufficient On Period RT energy gain. This is discussed in detail in section 4.6.1. There is also a practical lower limit which corresponds to the lowest β_0 that would be required to achieve the desired average current. This $\beta_{0_{min}}$ is discussed in section 5.3.1.

There is also an upper limit $\beta_{0_{max}}$ at each V_{in} beyond which further increases in β_0 result in minimal decreases in average current. The value for $\beta_{0_{max}}$ is somewhat arbitrary since the different V_{in} curves end at different values of β_0. A value is chosen close to the point where the $V_{in} = 0.85$ curve ends. Zero current can only be achieved by avoiding turn-on altogether.

In summary, for input current control, turn-on is timed to occur at a time when the RT is within the turn-on phase window. Current control is achieved by varying β_0 so as to produce the desired average pulse current.

β_0 is controlled through a switch timing control circuit. This must include resonant tank phase detection, turn-on timing, commutation detection and back-up turn-off timing. Turn-on is timed to occur at the appropriate phase of the resonant tank corresponding to the current reference signal. Turn-off is timed to coincide with the natural switch turn-off as the boost diode turns on.

As V_{in} varies through the ac line cycle, β_0 is varied by the control system as it attempts to produce a sinusoidal current waveform. If the voltage error signal (discussed below) was fed directly into the switch timing circuit, β_0 would not vary significantly between ac line cycles. The result would be open loop current control as shown in Figure 4.9. The input current would not be sinusoidal, but rather would have a quasi-triangular waveform. The simulated curves in Figure 4.10 depict the average value of the pulse current for specific values of β_0 as V_{in} is varied through a line cycle. Although not sinusoidal, these waveforms represent a substantial improvement in PF over conventional diode rectifiers, as will be discussed in Chapter 6.

4.5.2 Inner Current Control Loop

More accurate input current control can be implemented with the addition of an inner current control loop, including a reference current waveform generator and a current estimator or measurement circuit. The waveform generator will generate a signal of the desired waveshape proportional in magnitude to the current reference from the voltage control loop. For unity power factor operation, the desired waveshape is a pure sinusoid at the line frequency and in phase with the line voltage.

It is possible to mathematically estimate the average pulse current that would be drawn at any given V_{in} and β_0. Using such an estimation, it would be possible to draw a sinusoidal current without current feedback. This would however require a significant amount of real time computation, or enough memory for a look-up

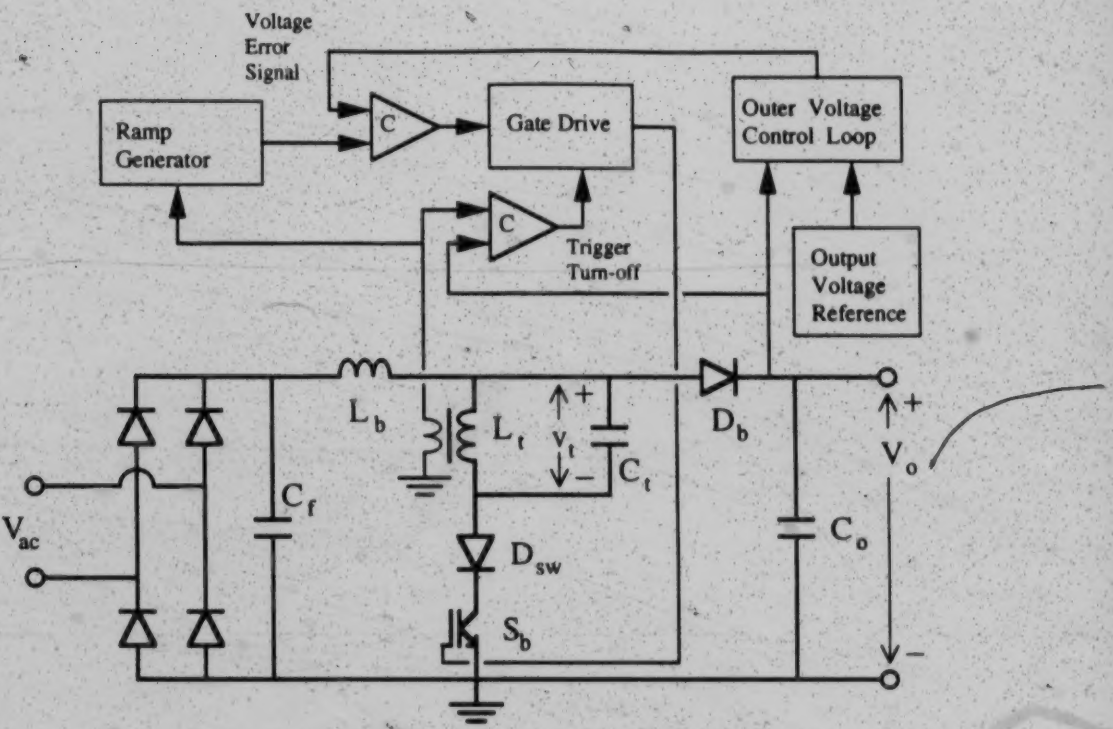

Figure 4.9: Open Loop Current Control of the RTBR

table. It would also be very dependent on actual component values, and would be adversely affected by component value drift due to temperature or other factors.

The obvious method of line cycle current control is a feedback control loop. While this would introduce a slight phase shift in the actual current response, a sinusoid with very low distortion is possible due to the high switching frequency. The actual current drawn by the RTBR is compared to the current reference signal, and an error signal is generated. β_0 is adjusted interactively so as to minimize the error. A proportional, integral, derivative (PID) control system is quite adequate to achieve an input current with very low THD.

With sinusoidal input current, the actual lower limit $\beta_{0_{min}}$ of the turn-on phase window is determined by the average pulse current required at full load. This lower limit will vary sinusoidally as V_{in} varies through a line cycle. The vertical bars on the curves in figure 4.7 show the current and corresponding β_0 required at full load at 90 % efficiency. This efficiency was chosen as a realistic minimum

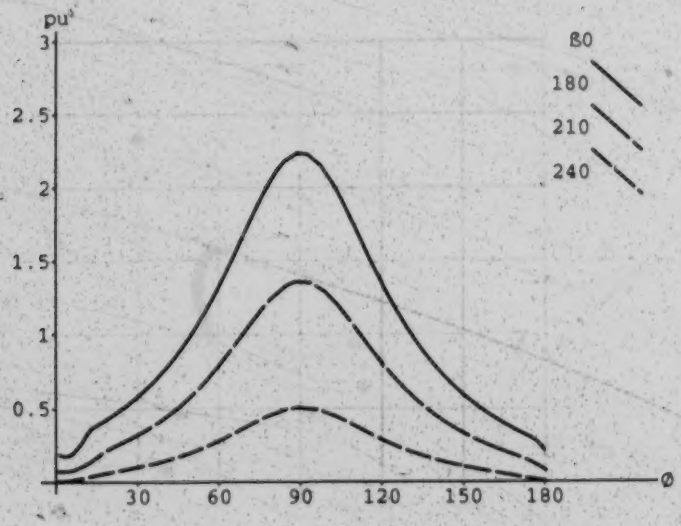

Figure 4.10: Average Input Current $i_{b_{av}}$ in a Half Line Cycle

target efficiency for the converter.

The capability of this RTBR to draw a square wave current is limited, since the current drawing capability is significantly reduced at low input voltages. However, a square wave with rounded edges is quite possible, and may offer significant advantages, such as reduced peak currents for a given load.

4.5.3 Outer Voltage Control Loop

The output voltage of the RTBR is controlled using an outer control loop which produces a voltage error signal. Generally, a proportional integral voltage control loop will be sufficient. The time constant of the output voltage control loop will be a compromise on conflicting speed of response requirements. A slow response is desirable so that the current request remains effectively constant throughout each line cycle to minimize current harmonics. A change in the current request in mid-cycle would result in a deviation of the input current waveform from the desired waveform (generally a sine wave). This requirement would dictate a time constant set at a number of line cycles.

A faster response could be desirable for a number of reasons:

- to minimize the size of the output capacitance C_o for economic reasons or physical space limitations.

- to minimize the output voltage ripple for any given value of C_o.
- to maintain the output voltage regulation under varying load conditions for any given value of C_o.

The presence or lack of a post dc to dc converter will affect the voltage ripple and voltage regulation requirements. Also, a need for a long hold-up time on loss of input power may dictate a larger C_o, minimizing or eliminating any need for a fast voltage loop response. Alternatively, the output capacitance could be significantly reduced in size and the response time significantly improved with the addition of an LC filter on the output to attenuate the large twice line frequency component [14, 15].

4.5.4 Forced Commutation

Normally, commutation is detected and turn-off is timed to coincide with the natural switch turn-off as the boost diode turns on. However, during periods of low input voltage and/or low RT energy e_t, the RT will not oscillate up to V_o after turn-on. Instead v_t will oscillate sinusoidally around a value of kV_{imp}, as can be seen in the formula for v_t. Referring to (4.23), natural commutation will not occur if $kV_{imp} + c_{vt}$ is less than the commutation voltage $V_{t_{com}}$, given by (4.33). If turn-off was left to natural commutation, the switch would remain on for an extended period and the current in the boost inductor would rise unchecked. Therefore, the switch must be turned off by forced commutation. The options for turn-off include;

Trigger: Turn-off when v_t reaches a specified value less than V_o.

Peak: Turn-off at the peak of v_t.

Time-out: Turn-off after a maximum on time has elapsed.

During this period of forced commutation, S_b will turn off and D_b will turn on under non-ZV conditions and some turn-off losses will be incurred. This loss is largely mitigated by the following conditions:

- There will still be a significant voltage across the RT and little voltage to be transferred from S_b to D_b.
- Forced commutation only occurs for small values of V_{imp}, where the average current in the pulse is controlled to be proportional to the small voltage value. Thus, only reduced currents will be force-commutated.
- Forced commutation only occurs for small values of V_{imp}, which only occurs for a small fraction of the line cycle.

The Trigger and Peak turn-off options will minimize the switching losses. The Trigger turn-off has an added advantage in that it results in an earlier turn-off. This is beneficial because the RT energy is increasing at the end of the On Period, while the energy in L_b has begun to fall. An earlier turn-off will result in more current delivered to the output and a lower tank energy in the ensuing RT oscillation. This lower tank energy corresponds to a lower V_{tp} and hence lower RT losses and voltage stresses. Of course, if turn-off is advanced too much, the switching losses will increase and may supersede the RT losses.

The turn-off time-out is generally undesirable since the voltage across the switch at turn-off would be indeterminate and could be significant. Therefore, this option is used only as a safety mechanism in case all other turn-off mechanisms have failed for some reason.

4.6 Continuous Operation

4.6.1 Steady-State Operation

If V_{in} and β_0 were held constant over a number of switching periods, dc steady-state operation of the RTBR would soon be reached. Using the formulae in section 4.2, specific input and output currents, tank losses, and efficiencies could be found for specific values of V_{in} and β_0.

Since the switching frequency f_{sw} is much greater than the line frequency, V_{in} will not change significantly between switching periods. Any given switching period within a line cycle will be preceded by switching periods at close to the same V_{in} and β_0. Therefore, the ac operation of the RTBR could be expected to be very close to dc steady-state during any given switching period. This ac operation where the switching cycle characteristics are varying from cycle to cycle, but are always close to the dc steady-state characteristics can be called ac quasi-steady-state. The closeness of the ac quasi-steady-state to the dc steady-state is verified in the simulation in Chapter 5 and in the results in Chapter 6.

In dc steady-state, the value of V_{tp0} for every switching cycle must be the same. Since the value V_{tp4} at the end of one switching cycle is the value V_{tp0} for the next switching cycle, V_{tp0} must equal V_{tp4} in each switching cycle. This can also be expressed in terms of the tank energy e_t. The energy e_{t0} at the start of each switching cycle must equal the energy e_{t4} at the end of the switching cycle. Then the e_{t0} of each switching cycle will be the same and steady-state will be achieved. The energy in the tank is given by the expression:

$$e_t = \frac{1}{2}(L_t i_t^2 + C_t v_t^2) \tag{4.49}$$

V_{tp} can be defined as the voltage that would appear across C_t at any instant if all the tank energy at that instant were contained within C_t. V_{tp} is an actual voltage only when i_t is zero, which happens twice per resonant cycle of the tank. V_{tp} and e_t are related by the expression:

$$V_{tp} = \sqrt{\frac{2e_t}{C_t}} \tag{4.50}$$

For e_{t4} to equal e_{t0}, the energy added to the tank during the On Period must exactly match the energy lost during the tank oscillation in the Off Period.

$$e_{t2} - e_{t0} = e_{t2} - e_{t4} \tag{4.51}$$

The steady-state e_t of the RTBR is very dependant on the quality Q_t and impedance Z_t of the RT, and on the actual turn-off timing should it differ from the time of natural commutation.

$$Q_t = \frac{Z_t}{R_t + R_c} = \frac{1}{2\zeta} \tag{4.52}$$

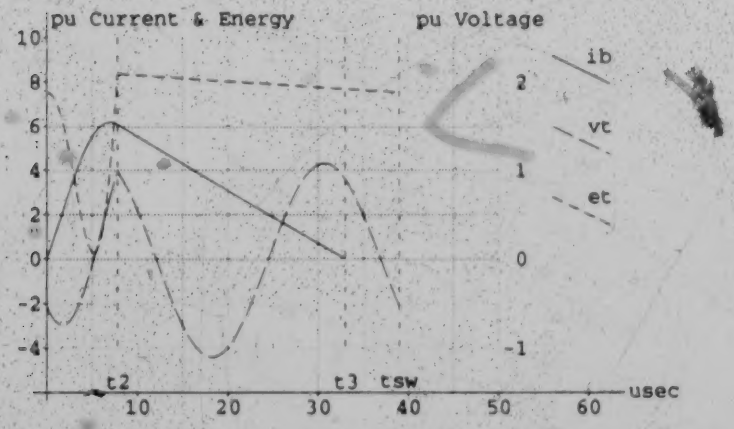

Figure 4.11: RTBR Voltage, Current, and Energy Waveforms

Figure 4.11 shows a typical curve of tank energy as it varies through a switching cycle. Again, all parameters are expressed in per unit quantities, with V_{base} as the rated output voltage V_o, and I_{base} as the full load output current. e_{base} is derived:

$$e_{base} = V_{base} I_{base} t_{base} \tag{4.53}$$

The energy gain of the tank during the On Period is dependent on V_{tp0}, V_{in} and β_0. Assuming V_{in} and β_0 to be invariant, the effects of varying the tank energy can be explored. An increase in V_{tp0} above steady-state values will result in an increased gain in e_t and a resulting higher V_{tp2}. This will in turn result in a higher current $i_{t_{osc}}$ during the Off Period and therefore higher Off Period tank losses. The end result will be an energy gain and loss through the switching period that are nearly offsetting, but not quite. The energy loss will actually be larger, and V_{tp4} will be slightly less than V_{tp0}, tending to pull the RTBR back to steady-state conditions. The opposite would occur if the RTBR were perturbed with a lower V_{tp0}.

Since the steady-state values are so dependent on a balancing of energy gain with energy loss, any circuit changes affecting the On Period gain differently than the Off Period loss will have a significant effect on the steady-state operation of the circuit. Q_t, Z_t, and the turn-off timing are three such parameters.

Decreasing Q_t will increase the slope of the energy curve in figure 4.11 during the Off Period, while having a minimal effect on the energy gain during the On Period. This will produce a lower steady-state V_{tp}, resulting in lower voltage stresses on the components. It will also produce higher tank losses in spite of the lower V_{tp}, as will be verified in the simulation in Chapter 5.

An earlier turn-off in figure 4.11 would result in a decrease in the tank energy gain during the On Period, while not affecting the damping constant of the RT. This will produce a lower steady-state V_{tp}. Assuming Q_t is constant, this would also decrease the tank losses. The disadvantage of this is that the switch turn-off would no longer be ZV, and switching losses would increase.

The energy balance of the RTBR is affected by the relationship between Q_t, Z_t, and the RT losses, which can be approximated as I^2R losses. If $i_{tp} = \frac{V_{tp}}{Z_t}$, a simple expression for the RT losses can be derived using (4.52). Equation (4.54) confirms that decreasing the Q of the RT results in higher RT losses.

$$P_t \propto (R_t + R_c) i_{tp}^2 \propto \frac{V_{tp}^2}{Q_t Z_t} \tag{4.54}$$

Chapter 5

Simulation of the RTBR

Mathematical simulations of the RTBR were developed to clarify the operation and parameter sensitivity of the circuit and to optimize the design of the prototype circuit. At the heart of the simulations is the calculation of the switching period behavior of a RTBR with specific circuit components. The circuit behavior is dependent on the input and output voltages and the RT phase at turn-on. Using these as independent input variables, circuit parameters for the switching period are determined. Then overall RTBR characteristics were found over a number of switching periods with one of the independent inputs varying.

Two simulation programs were developed; **DCSteadyState** to find the dc steady-state operation of an RTBR, and **ACLineCycle** to simulate the operation through an ac line cycle. Voltages, currents, and time-periods are expressed in per unit quantities so that the results are easily transferrable to different voltage, power, and time frames.

The accuracy of the simulation results are verified in Chapter 6 where the experimental behavior of the RTBR is compared with the simulated behavior. Program listings for **DCSteadyState** and **ACLineCycle** are shown in Appendices A and B.

5.1 DCSteadyState

This program was developed to determine the dc steady-state operating characteristics of the RTBR. This was required so that component values could be accurately found and control system parameters (such as the choice of turn-on phase window of the RT) determined.

5.1.1 Program Description

DCSteadyState generates data for switching period characteristic curves for an RTBR with specific circuit values (L_b, L_t, C_t, R_b, R_t, R_c, V_{out}, V_{br}, V_{sw}, V_{db}, and Q_t). Each curve is determined at a specific V_{in}, with β_0 as the independent variable. Each "point" on a curve represents one switching period pulse at a specific β_0.

Only discontinuous conduction steady-state operation with natural turn-off was considered. Natural turn-off could be due to natural commutation at zero voltage or due to turn-off at zero current. Natural commutation occurs when the RT voltage v_t reaches the output voltage, naturally switching on the boost diode. Turn-off at zero current occurs when the input current pulse falls back to zero and the boost diode does not turn-on. In this latter case, all of the input power is lost to heat and/or to charging the RT.

The flowchart for **DCSteadyState** is shown in Figure 5.1. The program finds the steady-state peak tank voltage V_{tp0} for a switching period. At this V_{tp0}, the increase in tank energy during the On Period equals the decrease during the Off Period, as discussed in detail in subsection 4.6.1. An initial guess of V_{tp0} for the switching period is extrapolated from the V_{tp0}'s for previous points on the curve. Starting with the initial guess, parameters for the switching period are calculated, and V_{tp4} is determined. If V_{tp4} is not sufficiently close to the V_{tp0} used, the program extrapolates a new guess for V_{tp0}, and re-calculates the switching period parameters with that V_{tp0}. This iterative process is continued until V_{tp0} equals V_{tp4}, at which time steady-state has been found.

The curves of dc steady-state characteristics for a particular V_{in} only exist over a limited range of the tank phase β_0. At any specific input voltage and tank phase, there is a maximum V_{tp0} above which the boost inductor would not be forward biased, and a minimum V_{tp0} below which v_t would not oscillate high enough to allow commutation to occur. If the starting V_{tp0} is above the maximum or below the minimum, it is lowered or raised before the iterations begin. The point in the curve where steady-state can no longer be achieved is found where the maximum V_{tp0} falls below the minimum V_{tp0}, or where continuous conduction begins.

Once the steady-state V_{tp} is found, the corresponding input pulse average and peak current, RT losses, pulse efficiency, circuit time periods, RT phase at turn-off β_2, and the switching period for the pulse are all determined.

The development of this program was based on the premise that the dc steady-state behavior of the RTBR at any particular V_{in} and β_0 would be very close to the ac behavior at the same input voltage within an ac line cycle. This was considered to be a reasonable premise since the line cycle input voltage has little variance between switching periods and the predominate determinant of the pulse characteristics is V_{in} and β_0. The V_{tp} of successive pulses with line cycle V_{in} could be expected to be fairly close. This is confirmed in section 5.3.1.

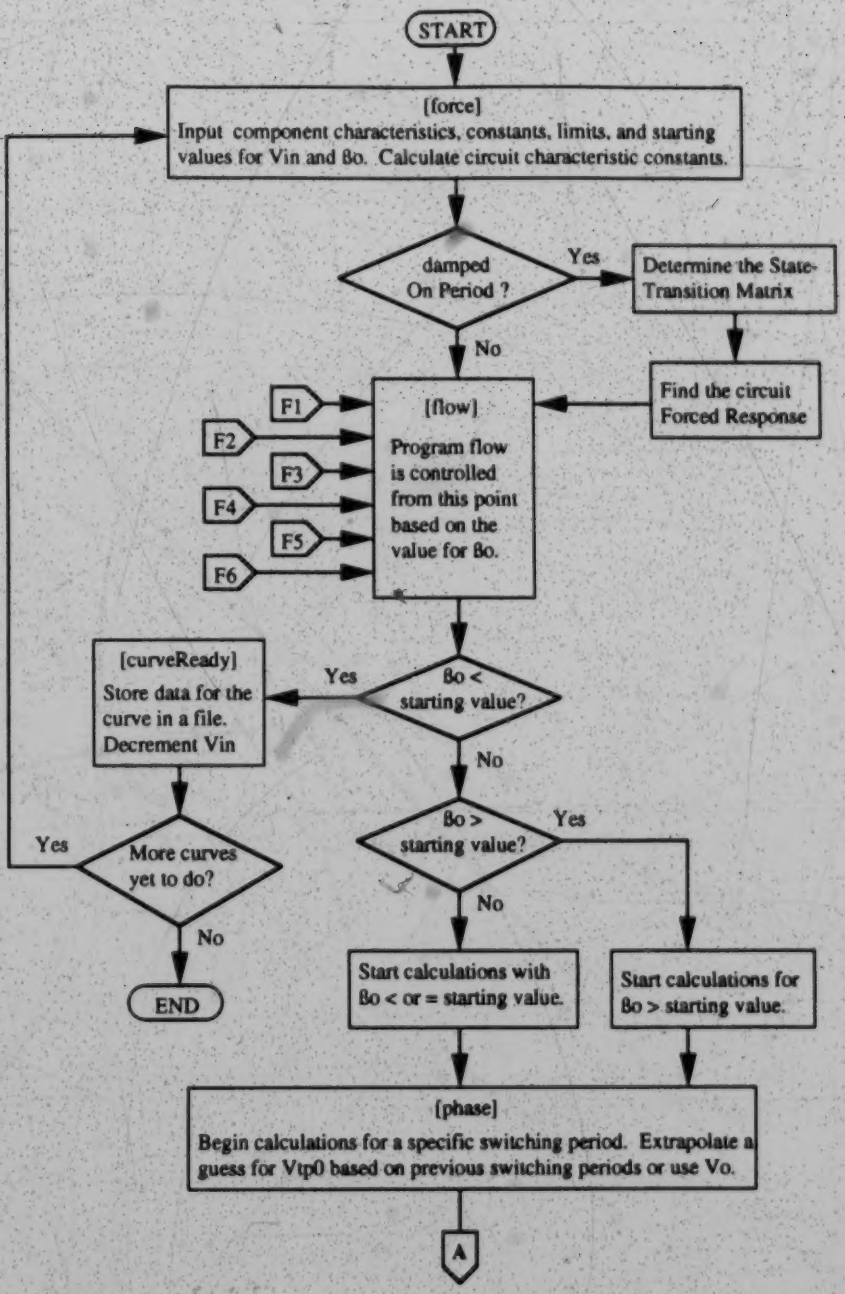

Figure 5.1: **DCSteadyState** Simulation Flowchart, sheet 1.

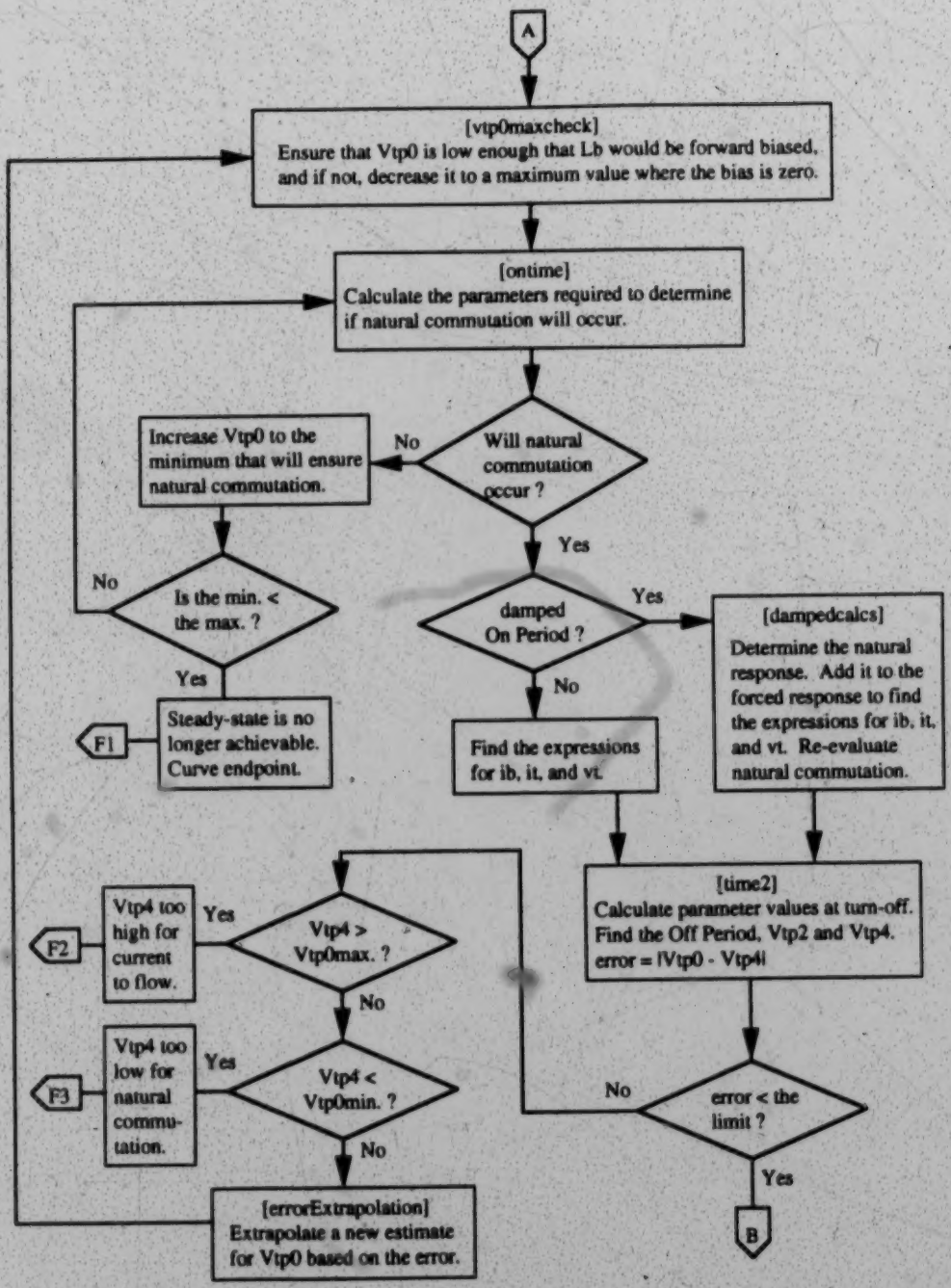

Figure 5.1: **DCSteadyState** Simulation Flowchart, sheet 2.

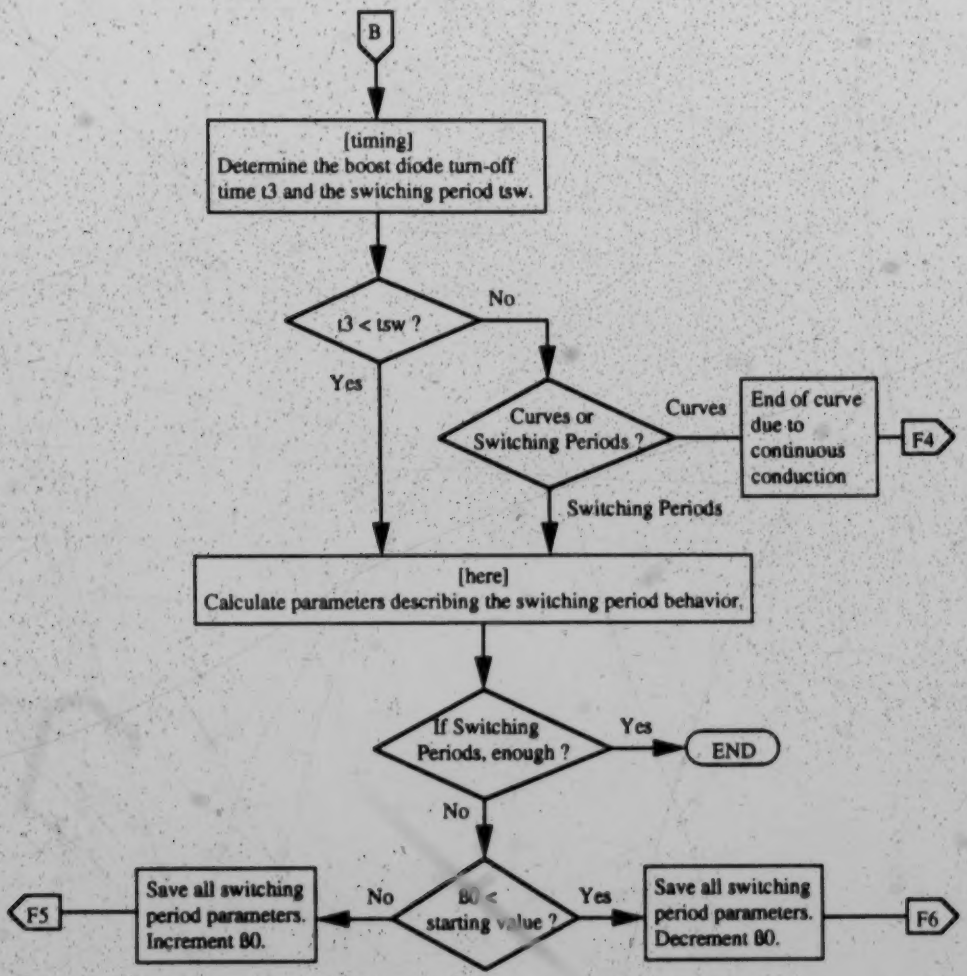

Figure 5.1: **DCSteadyState** Simulation Flowchart, sheet 3.

Both simulation programs were written with the capability of performing calculations for a specific number of pulses without calculating a full curve of data.

5.1.2 Circuit Variable Formulae

DCSteadyState was adapted for two On Period cases; the "damped" case and the "undamped" case. The damped case accounts for component losses in the determination of circuit voltages and currents during the On Period. The undamped case assumes non-resistive components in finding the expressions for voltages and currents, but during the On Period only. Once the formulae for the currents have been determined, the formulae can then be used in expressions which include the losses, with little loss of accuracy. The two On Period cases were required due to the significant length of time it took to calculate the damped case for each pulse. The undamped case was used to give relatively quick indications of performance, while the damped case was used when greater accuracy was desired. The actual difference in output between the two was roughly 5%. Both cases use component losses during the Off Period in the expressions for voltages and currents.

This program includes a choice of formulae to use in the calculations of i_b, i_t and v_t during the On Period. If the undamped case is chosen, the formulae determined in the mathematical solutions of section 4.3 are used. Calculations of the Off Period parameters were done using the mathematical solutions of section 4.4, which did include losses. The overall error of this case is very small since the On Period is only roughly 15 % of t_{sw} and semiconductor voltage drops are included throughout.

If the damped case is chosen, the formulae for i_b, i_t and v_t during the On Period are derived from the naturally damped mathematical solutions of (4.6), (4.7) and (4.8). The solutions to these equations are determined in **DCSteadyState** as described below. Since this case includes all component losses, as well as the semiconductor voltage drops, it is more accurate than the undamped case.

State space methods were used to determine the mathematical expressions. Matrices **A**, **Bu** and **x(0)** are the characteristic matrix, the input matrix, and the initial conditions matrix respectively for the On Period circuit.

$$\mathbf{A} = \begin{bmatrix} -\left(\frac{R_b+R_c}{L_b}\right) & \frac{R_c}{L_b} & -\frac{1}{L_b} \\ \frac{R_c}{L_t} & -\left(\frac{R_t+R_c}{L_t}\right) & \frac{1}{L_t} \\ \frac{1}{C_t} & -\frac{1}{C_t} & 0 \end{bmatrix}$$

$$\mathbf{Bu} = \begin{bmatrix} \frac{V_{imp}}{L_b} \\ 0 \\ 0 \end{bmatrix}$$

$$\mathbf{x(0)} = \begin{bmatrix} 0 \\ i_{t0} \\ v_{t0} \end{bmatrix}$$

Equations (4.6), (4.7) and (4.8) reduce to a single equation in state-space notation:

$$\dot{\mathbf{x}} = \mathbf{Ax} + \mathbf{Bu} \tag{5.1}$$

The solution to (5.1) has two components, the natural or transient response $x_t(t)$ and the forced response $x_f(t)$. The transient response is given by a simple matrix multiplication of the state-transition matrix $e^{\mathbf{A}t}$ and the circuit initial conditions matrix. The forced response is given by the convolution of the state-transition matrix and the input matrix. Together, they form the total response, $x(t)$. Setting $t_0 = 0$:

$$x(t) = x_t(t) + x_f(t) = e^{\mathbf{A}t}\mathbf{x(0)} + \int_0^t e^{\mathbf{A}(t-\lambda)}\mathbf{B}u d\lambda \tag{5.2}$$

DCSteadyState was written in a mathematical language which could perform the matrix calculations in (5.2) directly. While the integration could be performed symbolically, numerical solutions were found so as to minimize the calculation time. The final results using the numerical solution were found to be the same as those using the symbolical solution.

5.1.3 Switching Period Calculations

Parameters determined for each switching period and the formulae used are listed in this section. The following parameters were found using numerical integration:

The average input current:

$$i_{b_{av}} = \frac{1}{t_{sw}}\left(\int_0^{t_2} i_b dt + \int_{t_2}^{t_3} i_{b_{ramp}} dt\right) \tag{5.3}$$

The average output current:

$$i_{D_{av}} = \frac{1}{t_{sw}}\int_{t_2}^{t_3} i_{b_{ramp}} dt \tag{5.4}$$

The RT power loss:

$$P_t = \frac{(R_c + R_t)}{t_{sw}} \left(\int_0^{t_2} i_t^2 dt + \int_{t_2}^{t_{sw}} i_{t_{osc}}^2 dt \right) \tag{5.5}$$

This method of calculating the RT power loss was used for both the damped and undamped On Period cases.

The efficiency of each pulse could be used to indicate areas of operation to be avoided. The pulse efficiency η_p was determined in **DCSteadyState** using power since the RT energy e_t is the same at the start of the switching period as it is at the end.

$$\eta_p = \frac{P_{out}}{P_{in}} = \frac{V_{in} i_{b_{av}}}{V_{out} i_{D_{av}}} \tag{5.6}$$

5.2 ACLineCycle

The ac steady-state program **ACLineCycle** was developed to determine the ac steady-state operating characteristics of the RTBR. This was required to verify that the characteristics determined in **DCSteadyState** were indeed representative of the actual ac operation, and to show how circuit parameters would behave near the cusps of the rectified line voltage where the voltage was too low for dc steady-state to be achieved. **ACLineCycle** was also beneficial in determining circuit component values and control system parameters.

5.2.1 Program Description

ACLineCycle generates data for pulse characteristic curves at a specific β_0, with the RTBR operating through $\frac{5}{8}$ of a line cycle, from the phase of the input voltage, $\phi_V = -45°$ to $180°$. AC steady-state can be expected to be reached before ϕ_V reaches zero. Each "point" on the curves represents one switching period pulse. As would happen in the actual RTBR, the program uses the RT peak voltage V_{tp1} at the end of a previous switching period as the V_{tp0} for the next pulse. For each pulse, it determines the corresponding input pulse average and peak current, RT losses, pulse energy efficiency, circuit time periods, RT phase at turn-off β_2, and the switching period for the pulse.

In each switching period, a check is made to ensure that V_{in} is larger than v_{t0} so that L_b will be forward biased and positive current would flow. If v_{t0} is found to be too large, actual switch turn-on will be delayed until v_t falls below V_{in}. This delay is determined and calculations performed accordingly.

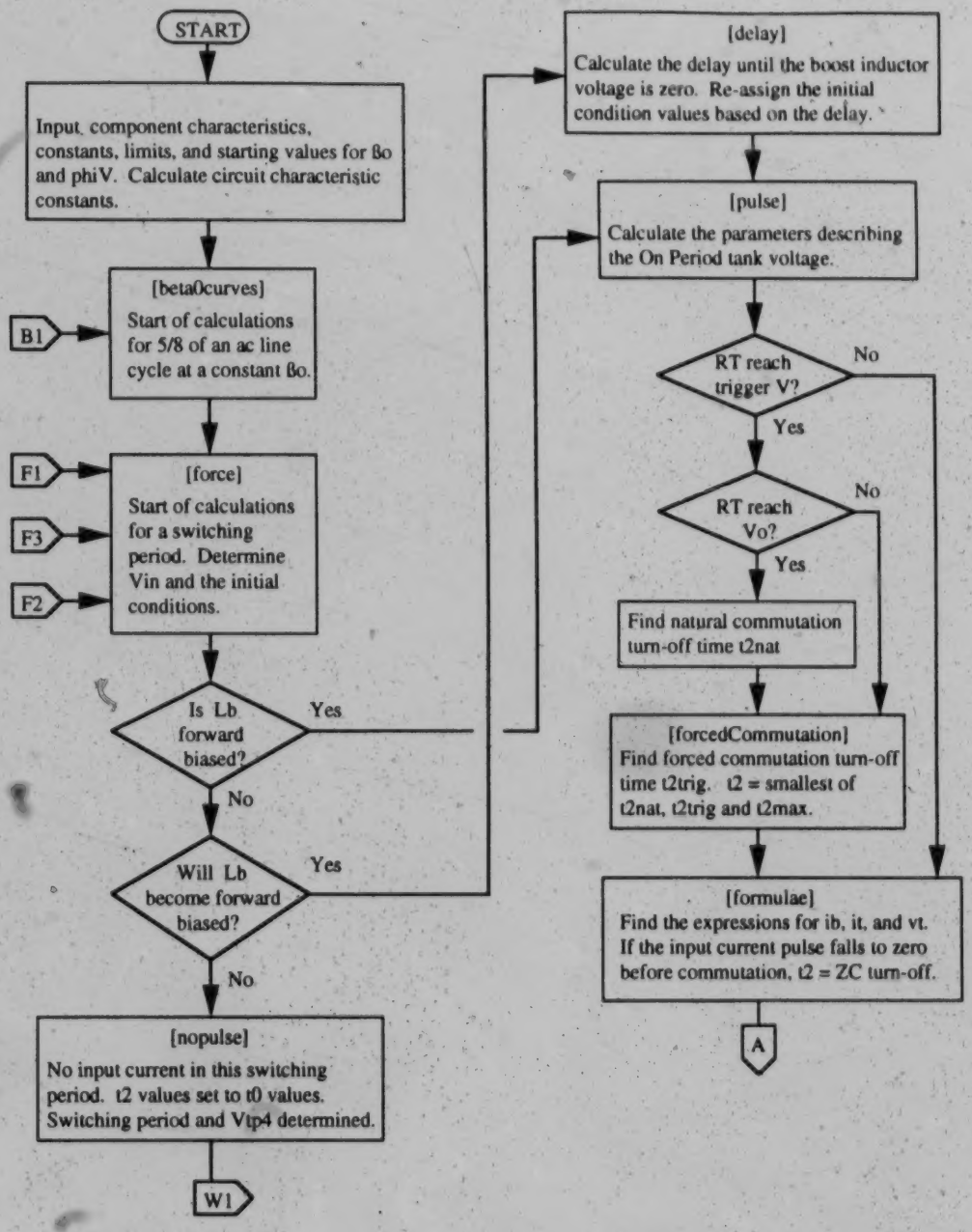
START
Input component characteristics, constants, limits, and starting values for ßo and phiV. Calculate circuit characteristic constants.
[beta0curves]
Start of calculations for 5/8 of an ac line cycle at a constant ßo.
B1
[force]
Start of calculations for a switching period. Determine Vin and the initial conditions.
F1
F3
F2
Is Lb forward biased?
Yes
No
Will Lb become forward biased?
Yes
No
[nopulse]
No input current in this switching period. t2 values set to t0 values. Switching period and Vtp4 determined.
W1
[delay]
Calculate the delay until the boost inductor voltage is zero. Re-assign the initial condition values based on the delay.
[pulse]
Calculate the parameters describing the On Period tank voltage.
RT reach trigger V?
No
Yes
RT reach Vo?
No
Yes
Find natural commutation turn-off time t2nat
[forcedCommutation]
Find forced commutation turn-off time t2trig. t2 = smallest of t2nat, t2trig and t2max.
[formulae]
Find the expressions for ib, it, and vt. If the input current pulse falls to zero before commutation, t2 = ZC turn-off.
A

Figure 5.2: **ACLineCycle** Simulation Flowchart, sheet 1.

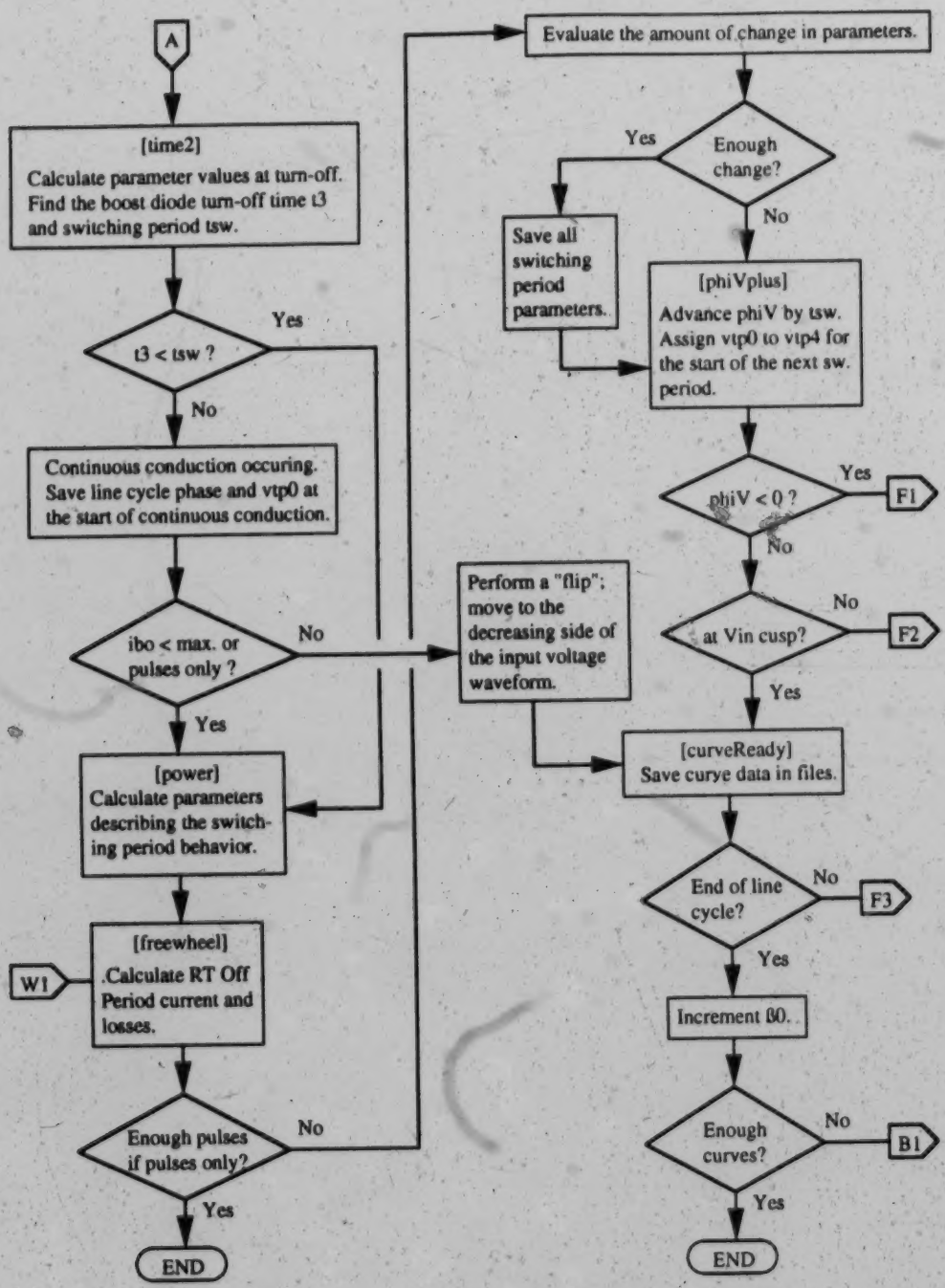

Figure 5.2: **ACLineCycle** Simulation Flowchart, sheet 2.

In the actual RTBR, four mechanisms exist for turn-off; two are natural and two are forced by the control circuit to ensure stable operation. These mechanisms are simulated in **ACLineCycle** in the following manner:

Natural Commutation. v_t is compared to v_{tcom} to determine when natural commutation from the switch to the boost diode will occur.

Trigger Commutation. v_t is compared to a trigger voltage v_{trig} to determine whether forced commutation will occur. If it does, turn-off occurs a short time after v_t reaches v_{trig}. The time delay is introduced by the turn-off control circuit and is beneficial in preventing the pre-emption of natural commutation.

Turn-off on Time-Out. If v_t does not reach v_{trig}, the switch is forced off after a time-out period, t_{2max}.

Turn-off at Zero Current. i_b is checked and turn-off at zero current occurs when the input current pulse falls back to zero before any of the above three mechanisms has worked. In this case, the boost diode does not turn-on.

5.2.2 Circuit Variable Formulae

ACLineCycle was only developed for the undamped case, which ignores component losses during the On Period when determining the circuit voltages and currents. This was done to cut down on calculation time since the error in omitting those losses was not considered great. The ac simulation is identical to the undamped dc simulation in the mathematical description of the RTBR behavior. The formulae determined in the mathematical solutions of sections 4.3 and 4.4 are used.

5.2.3 Switching Period Calculations

Parameters determined for each switching period in **ACLineCycle** were largely the same as those used in **DCSteadyState** as described above. However, the pulse efficiency η_e was determined using energy rather than power since the RT energy e_t could vary significantly between successive switching periods. If $\frac{P_{out}}{P_{in}}$ alone was used, unreplaced energy drawn out of the RT during a switching cycle could give efficiencies greater than 1. Including e_{t0} and e_{t4} in the efficiency calculation gives a more accurate representation of the efficiency.

$$\eta_e = \frac{E_{end}}{E_{start}} = \frac{(P_{out}t_{sw} + e_{t4})}{(P_{in}t_{sw} + e_{t0})} \tag{5.7}$$

5.3 Simulation Results

Simulations were performed repetitively in studying the behavior of the RTBR, and in determining the final values of components. The general trends observed in these simulations are shown in this section. A base case simulation was chosen that was considered to be representative of a desirable circuit. Compared with the prototype RTBR to be discussed in Chapter 6, the simulation base case has a higher Q_t and no commutation time. The prototype was constructed from materials available in the lab that were not always optimum. A base case with an improved Q_t was considered to be closer to a manufacturable product. Variances from the base case were then simulated to indicate how circuit design variables affected the RTBR behavior.

While the simulation results are intended to be applicable regardless of the per unit base values, it helps to give representative values. The base values applicable to a RTBR of the same size (800 watts) as the prototype are given in Table 5.1 so that representative actual component values can be given in Table 5.2.

Z_t and Q_t are derived from the component values:

$$Q_t = \frac{Z_t}{R_t + R_c} = 136$$

$$Z_t = \sqrt{\frac{L_t}{C_t}} = 0.298\ pu$$

In this section, **DCSteadyState** simulation results using the damped On Period case are presented as the base case. **ACLineCycle** simulation results are also presented when pertinent information on the RTBR behavior can be revealed. Then other **DCSteadyState** simulation cases are presented where applicable to illustrate certain characteristics of the RTBR behavior. These other cases include:

- Undamped On Period.
- Simulation with R_t increased to 0.0028, resulting in a reduced Q_t of 100.
- Simulation with Z_t reduced to 0.159, but with Q_t maintained at 136. In this case, some component values change from the base case, and are given in Table 5.3.
- Simulation with time t_2 at the end of the On Period delayed for 0.25 μseconds after normal commutation would have occurred. This simulation gives an rough indication of the effects of the finite time it takes for the current to commutate from the switch path to the diode path. In an actual RTBR during this commutation time, the S_b current ramps down to zero, and the

Table 5.1: Simulation and Prototype Per Unit Base Parameters

Parameter	*Formula*	*Value*
V_{base}	V_o	200 V
I_{base}	I_o	4 A
t_{base}		1 μsec.
L_{base}	$\frac{V_{base}t_{base}}{I_{base}}$	50 μH
C_{base}	$\frac{I_{base}t_{base}}{V_{base}}$	20 nF
R_{base}	$\frac{V_{base}}{I_{base}}$	50 Ω
E_{base}	$V_{base}I_{base}t_{base}$	800 μJ

Table 5.2: Simulation Base Case Component Values

Parameter	*Per Unit Value*	*Actual Value*
L_b	1.18	59 μH
L_t	1.18	59 μH
C_t	13.3	266 nF
R_b	0.0040	0.20 Ω
R_t	0.0020	0.10 Ω
R_c	0.000188	0.0094 Ω
V_{br}	0.0100	2.0 V
V_{sw}	0.0185	3.7 V
V_{db}	0.0050	1.0 V

Table 5.3: Component Values Changed from the Base Case for $Z_t = 0.159$

Parameter	*Per Unit Value*	*Actual Value*
L_b	1.3	65 μH
L_t	0.63	31.5 μH
C_t	25.0	500 nF
R_t	0.00107	0.0535 Ω
R_c	0.00010	0.0050 Ω
Z_t	0.159	7.95 Ω

D_b current ramps up until it reaches i_b. As an approximation to this behavior, half the expected commutation time of 0.5 μseconds is added to the On Period for determining t_2 parameters. Then, the rest of the commutation time is left as part of the Off Period.

5.3.1 Average Input Pulse Current

The graph in Figure 5.3(a) shows the linearity of the relationship between $i_{b_{av}}$ and β_0. The current at the left edge of the $V_{in} = 0.85$ curve is the peak current that can be drawn at the crest of V_{in} by this particular RTBR without entering continuous conduction.

The vertical bars on the curves show the current and corresponding β_0 required for sinusoidal input current at full load at 90 % efficiency. A horizontal line at constant $i_{b_{av}}$ would indicate the limit of $\beta_{0_{min}}$ required for a square wave input current. A vertical bar at $\beta_0 \approx 165^o$ would indicate the current limit achievable from an RTBR with open loop current control (i.e. at a constant β_0). Open loop operation at lower β_0's would result in continuous conduction, and a loss in the $i_{b_{av}}$ versus β_0 linearity.

The curves for $V_{in} = 0.75$ and 0.65 show that significantly higher currents are possible when the input voltage is less than 0.85. With lower input voltages, the voltage across L_b is greater during the ramp down, resulting in a greater $\frac{di}{dt}$. Continuous conduction can then be achieved with greater peak currents and therefore greater average currents.

Simulation results from **DCSteadyState** using the undamped On Period case are similar to the damped results. The graph of $i_{b_{av}}$ versus β_0 in Figure 5.3(b) shows curves just slightly elevated from those in Figure 5.3(a). The elevation is due to the slightly greater currents attainable when losses are ignored. Since the error is less than 5 %, simulations using the undamped On Period case can be useful in indicating trends.

ACLineCycle results for $i_{b_{av}}$ are shown in Figure 5.4. The graph of $i_{b_{av}}$ versus ϕ_V shows the quasi-triangular current waveform drawn by the RTBR at a constant β_0. The gaps in the curves for $\beta_0 = 90^o$, 120^o and 150^o near the crest of the input voltage represent times of continuous conduction. Since the RTBR is not intended to be operated in continuous conduction, that range of operation was not simulated. In an RTBR with sinusoidal input current, β_0 would be increased near the input voltage crest and the RTBR would be kept out of continuous conduction. The current near the cusps of the input voltage (near $\phi_V = n\pi$) falls off rapidly for low β_0's. This is due to the effect of forced commutation at $t_{2_{max}}$.

The agreement between dc steady-state and ac line cycle characteristics can be verified by observing Figures 5.3(b) and 5.4. Points at the same V_{in} and β_0

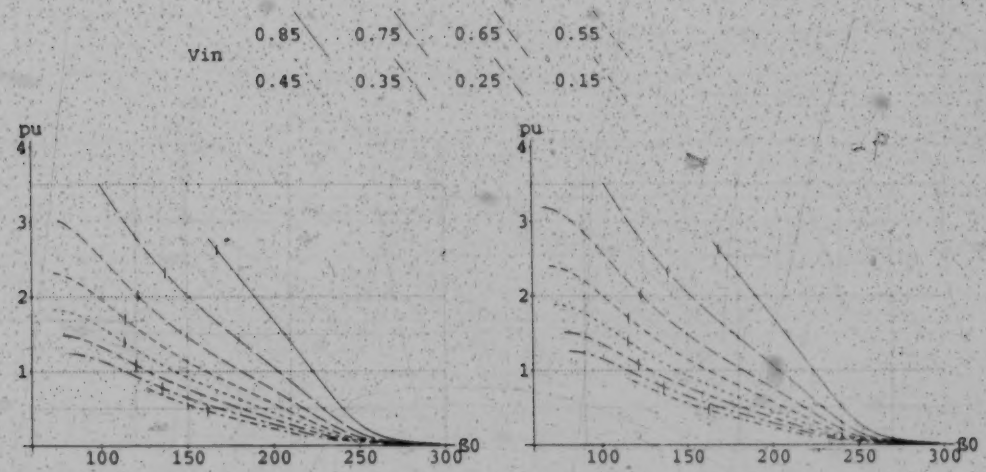

(a) Base Case with Damped On Period (b) Undamped On Period

Figure 5.3: DCSteadyState: Pulse Average Current $i_{b_{av}}$ versus RT Phase at Turn-on

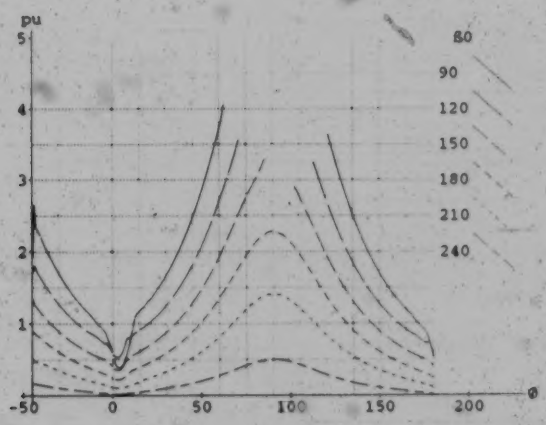

Figure 5.4: ACLineCycle: Pulse Average Current $i_{b_{av}}$ versus Phase ϕ_V of V_{ac}

Table 5.4: Comparison of Average Input Currents Determined in **DCSteadyState** and **ACLineCycle**

V_{in} (*pu*)	ϕ_V (*degrees*)	β_0 (*degrees*)	*Average Input Current* $i_{b_{av}}$	
			DCSteadyState (*pu*)	*ACLineCycle* (*pu*)
0.25	17.1	150	0.65	0.64
0.25	17.1	210	0.23	0.22
0.55	40.4	120	1.62	1.59
0.55	40.4	180	0.79	0.79
0.55	40.4	240	0.15	0.14
0.85	90.0	180	2.30	2.28
0.85	90.0	240	0.51	0.50
0.65	130.0	120	2.09	2.12
0.65	130.0	180	1.03	1.04
0.65	130.0	240	0.21	0.21
0.35	155.6	150	0.75	0.78
0.35	155.6	210	0.29	0.29

show values of $i_{b_{av}}$ that are very close. Of course, this only holds true where a dc steady-state characteristic could be determined. A numerical comparison of a few sample points is shown in Table 5.4.

The effect of a lower Q_t is shown in Figure 5.5(b). With $Q_t = 100$, the $i_{b_{av}}$ curves are almost identical to those generated in the base case. Changing Q_t has very little effect on the current drawn by the RTBR. This is significant because it means that variances in Q_t, which are sure to occur, will not affect the power rating of the RTBR.

The effect of a lower Z_t on the $i_{b_{av}}$ curves is pronounced. In Figure 5.5(c), the $i_{b_{av}}$ curves are shifted in a clockwise direction from the base case. $\beta_{0_{min}}$ is roughly 30° higher, giving a shortened turn-on phase window. Z_t is a design variable with implications that will become more apparent in the discussion of RT losses and RTBR efficiency.

Adding the approximation of commutation time to the RTBR simulation produces a slightly smaller $\beta_{0_{min}}$ while increasing the β_0 required at the crest of the input voltage, as shown in Figure 5.5(d). This increased separation between the $i_{b_{av}}$ curves has the effect of increasing the variance in overall current control loop gain between low and high input voltages.

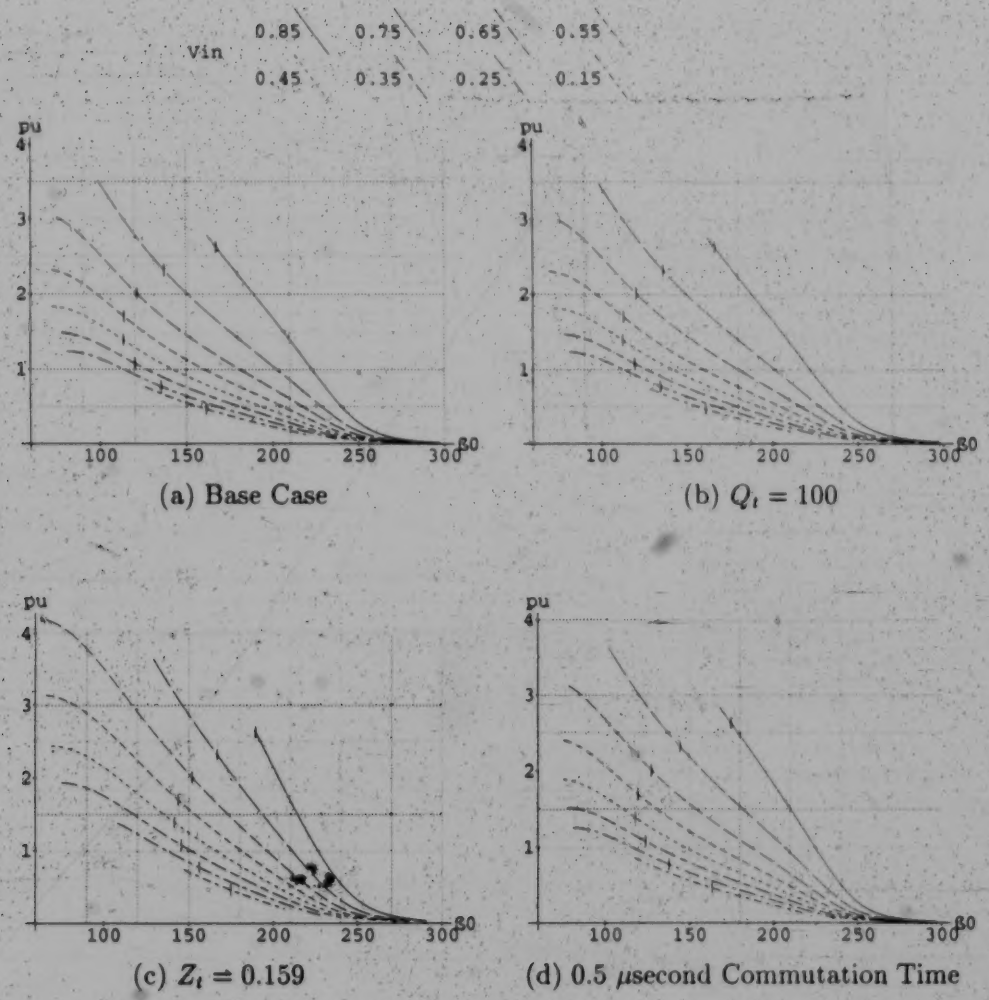

(a) Base Case

(b) $Q_t = 100$

(c) $Z_t = 0.159$

(d) 0.5 μsecond Commutation Time

Figure 5.5: DCSteadyState: Pulse Average Current $i_{b_{av}}$ versus RT Phase at Turn-on

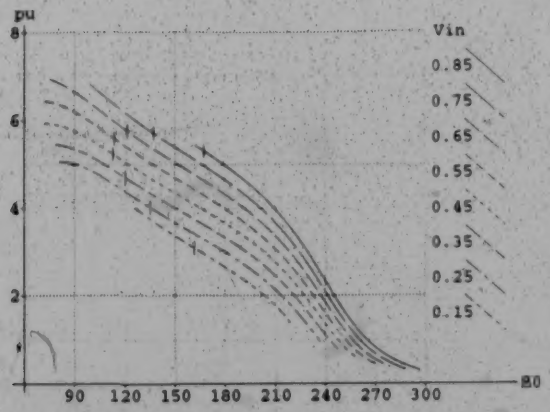

(a) DCSteadyState: $i_{b_{pk}}$ versus β_0

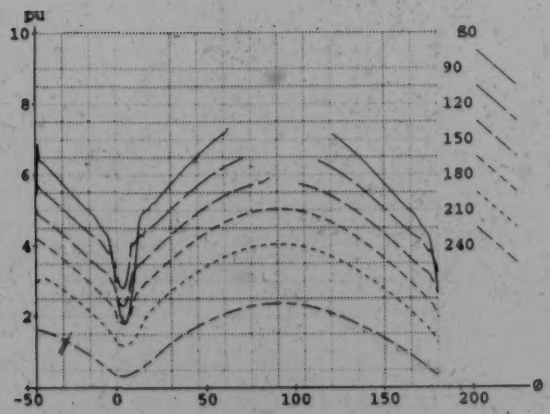

(b) ACLineCycle: $i_{b_{pk}}$ versus ϕ_V

Figure 5.6: Pulse Peak Current Simulations

5.3.2 Peak Input Pulse Current

The graph of i_{bpk} versus β_0 in Figure 5.6(a) is not as linear as the $i_{b_{av}}$ curve. This indicates that $i_{b_{av}}$ is not linearly proportional to i_{bpk} at any given V_{in}. As β_0 increases, the proportion of on time of i_b decreases, so $i_{b_{av}}$ decreases at a faster rate than i_{bpk}.

The peak input current that could be drawn by this RTBR is about 7 pu,

although a sinusoidal input current would require peaks below 6 pu. While this seems high, it is a value relative to the output current which is lower than the input current. 6 pu corresponds to 2.3 times the crest of the sinusoidal input current. This is as expected, since the peak of a sawtooth waveform is twice the average value.

The graph of i_{bpk} versus ϕ_V in Figure 5.6(b) appears similar to an elevated rectified sine wave. The values of i_{bpk} through the line cycle can be used to determine the rms current carrying capability required by the boost switch and boost diode.

5.3.3 Time at Switch Turn-off

The graph of t_2 versus β_0 in Figure 5.7(a) is also fairly linear, with t_2 decreasing as β_0 increases. Since t_2 decreases as β_0 increases, the switch on time decreases as the load decreases. With less on time and less peak current, the switch on-state losses will decrease as the load decreases.

The RTBR with decreased Z_t shows an increase of roughly 2 μseconds in t_2, as shown in Figure 5.7(b). This will result in increased on time switch losses of the RTBR.

The graph of t_2 versus ϕ_V in Figure 5.8 shows that t_2 has some variance through an ac line cycle with β_0 held constant. Again, t_2 decreases as β_0 increases. The dependence of t_2 on V_{in} is due to the time it takes for v_t to traverse from V_{in} to V_o.

The effect of a maximum on time is clearly illustrated for smaller values of β_0. For larger β_0's, near the input voltage cusps, the switch turn-off occurs at zero current turn-off (when i_b falls back down to zero current before commutation can occur). This explains the behavior of t_2 near $\phi_V = n\pi$.

5.3.4 Tank Phase at Turn-off

The graph in Figure 5.9(a) shows the RT phase at turn-off β_2 to be almost independent of V_{in} for smaller values of β_0 and almost linear with β_0 between $\beta_0 = 120^o$ and 210^o. β_2 is positive for low β_0's and negative for high β_0's.

Figure 5.9(b) shows decreased values of β_2 with decreased Z_t at the same β_0 when compared to Figure 5.9(a). This is in concordance with (4.35) and (4.36) and the lower values of V_{tp} as will be seen in section 5.3.5. This is a beneficial aspect of decreasing Z_t.

The graph of β_2 versus ϕ_V in Figure 5.10 shows that β_2 is fairly independent of V_{in} except for small values of V_{in} near the cusp of the input voltage. The dependence of β_2 on β_0 is confirmed. The effect of forced commutation and ZC turn-off of the current pulse can be seen in the behavior of β_2 near the input voltage cusps.

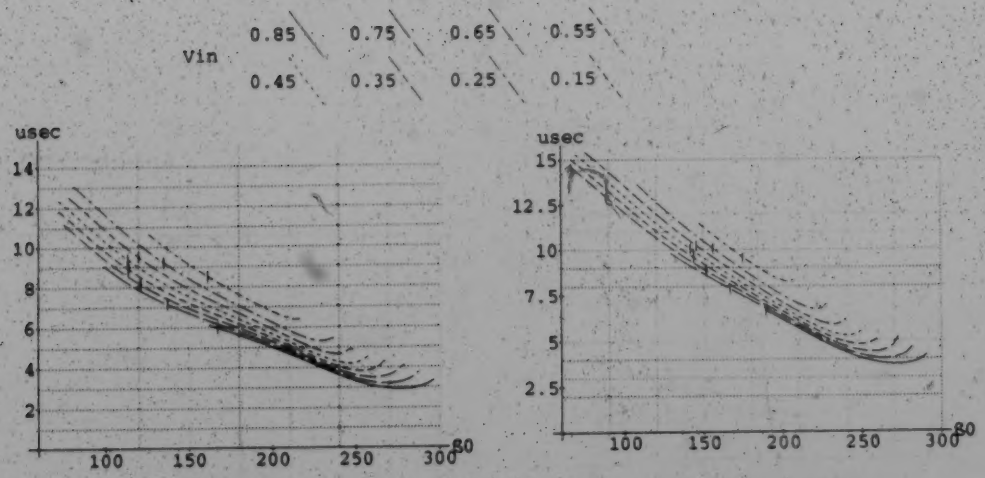

(a) Base Case (b) $Z_t = 0.159$

Figure 5.7: DCSteadyState: Time at Turn-off t_2 versus RT Phase at Turn-on

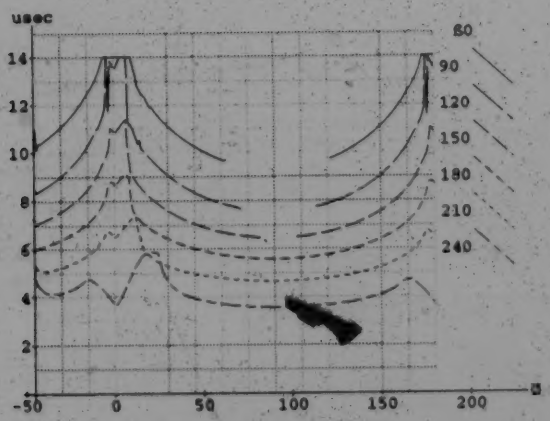

Figure 5.8: ACLineCycle: Time at Turn-off t_2 versus Phase ϕ_V of V_{ac}

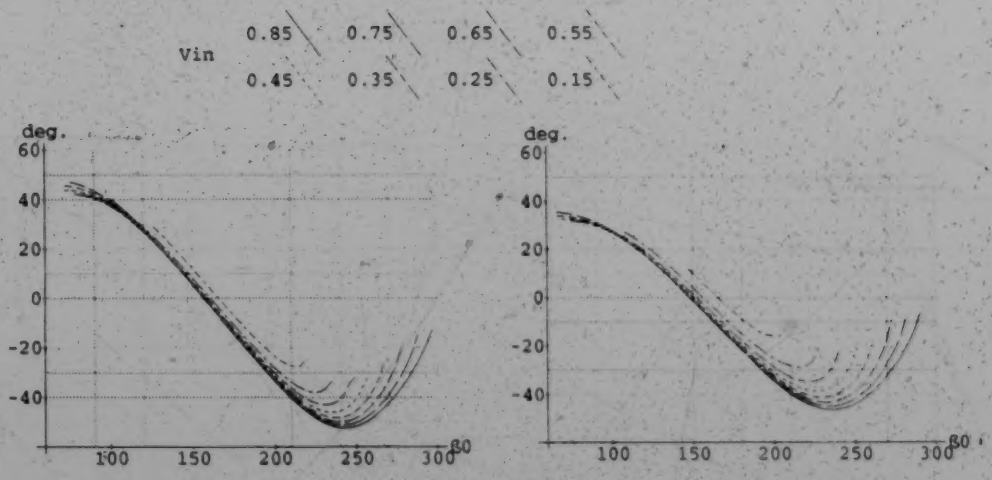

(a) Base Case (b) $Z_t = 0.159$

Figure 5.9: DCSteadyState: RT Phase at Turn-off β_2 versus RT Phase at Turn-on

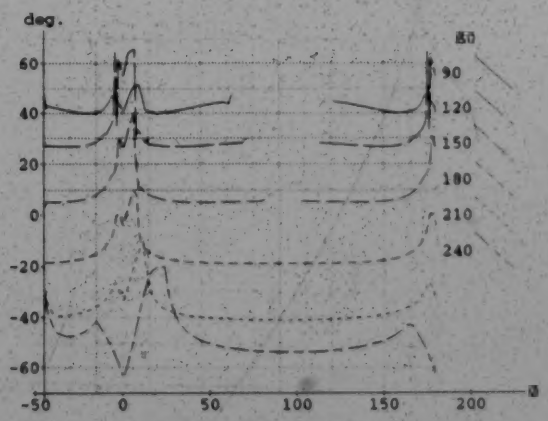

Figure 5.10: ACLineCycle: RT Phase at Turn-off β_2 versus Phase ϕ_V of V_{ac}

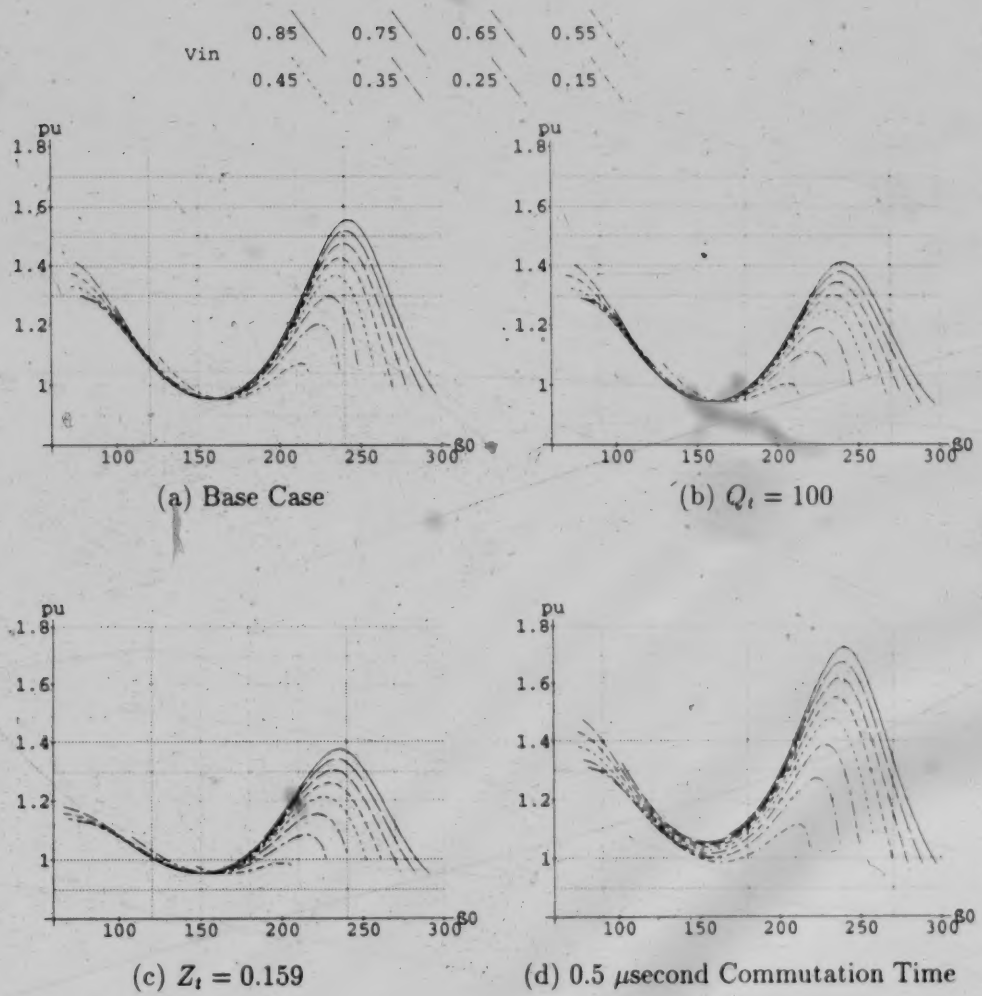

(a) Base Case (b) $Q_t = 100$

(c) $Z_t = 0.159$ (d) 0.5 μsecond Commutation Time

Figure 5.11: DCSteadyState: Peak Tank Voltage V_{tp} versus RT Phase at Turn-on

5.3.5 Peak Tank Voltage

V_{tp} is very dependent on β_0 and also affected by V_{in}, as can be seen in Figure 5.11(a). V_{tp} and β_2 are interrelated as seen in (4.35) and (4.36). The minimum V_{tp} occurs when β_2 is zero, and the maximum $V_{tp_{max}}$ occurs when β_2 is at it's lower limit.

Decreasing Q_t has a significant effect on V_{tp}, as shown in Figure 5.11(b). This is due to the inherent balancing of the energy gains and losses during each switching period, as discussed in section 4.6.1. The decrease in Q_t results in a decrease in $V_{tp_{max}}$, which results in lower voltage stresses and lower device voltage rating requirements. This effect will be more pronounced at lighter loads where β_0 is near 240°, and will be practically insignificant at heavier loads where V_{tp} is close to V_{out}.

Decreasing Z_t also has the effect of decreasing V_{tp}, as shown in Figure 5.11(c). This is due to an increase in RT tank losses as discussed in section 4.6.1, resulting in a lowering of the steady-state V_{tp}.

Adding the approximation of commutation time to the RTBR simulation produces a larger $V_{tp_{max}}$, as shown in Figure 5.11(d). This is due to the extra charging that occurs on C_t during the commutation period.

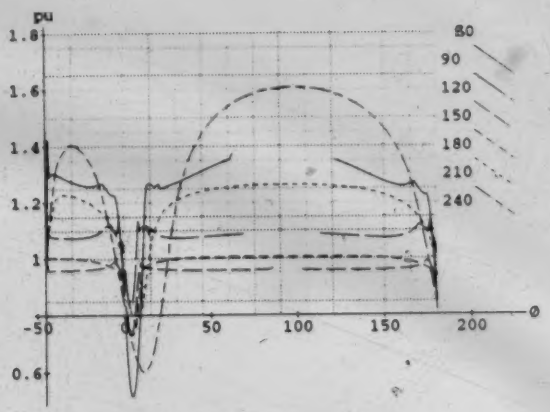

Figure 5.12: ACLineCycle: Peak Tank Voltage V_{tp} versus Phase ϕ_V of V_{ac}

The dependence of V_{tp} on β_0 is confirmed in Figure 5.12. The sensitivity of V_{tp} to turn-off timing is apparent in the behavior of V_{tp} near the input voltage cusps. The curves go through three regions as they approach $V_{in} = 0$. As V_{in} drops, forced commutation due to the v_t trigger begins to occur. In some cases, there is a harmless perturbation as turn-off alternates between natural and forced commutation in sequential switching periods. After a few switching periods of

forced commutation, the input current pulses stop commutating as they turn-off at ZC. The three regions then occur in reverse order as V_{in} increases from zero.

Figure 5.12 is useful in indicating the peak forward voltage which S_b must withstand and the peak reverse voltage which D_{sw} must withstand. This is discussed in section 6.2.

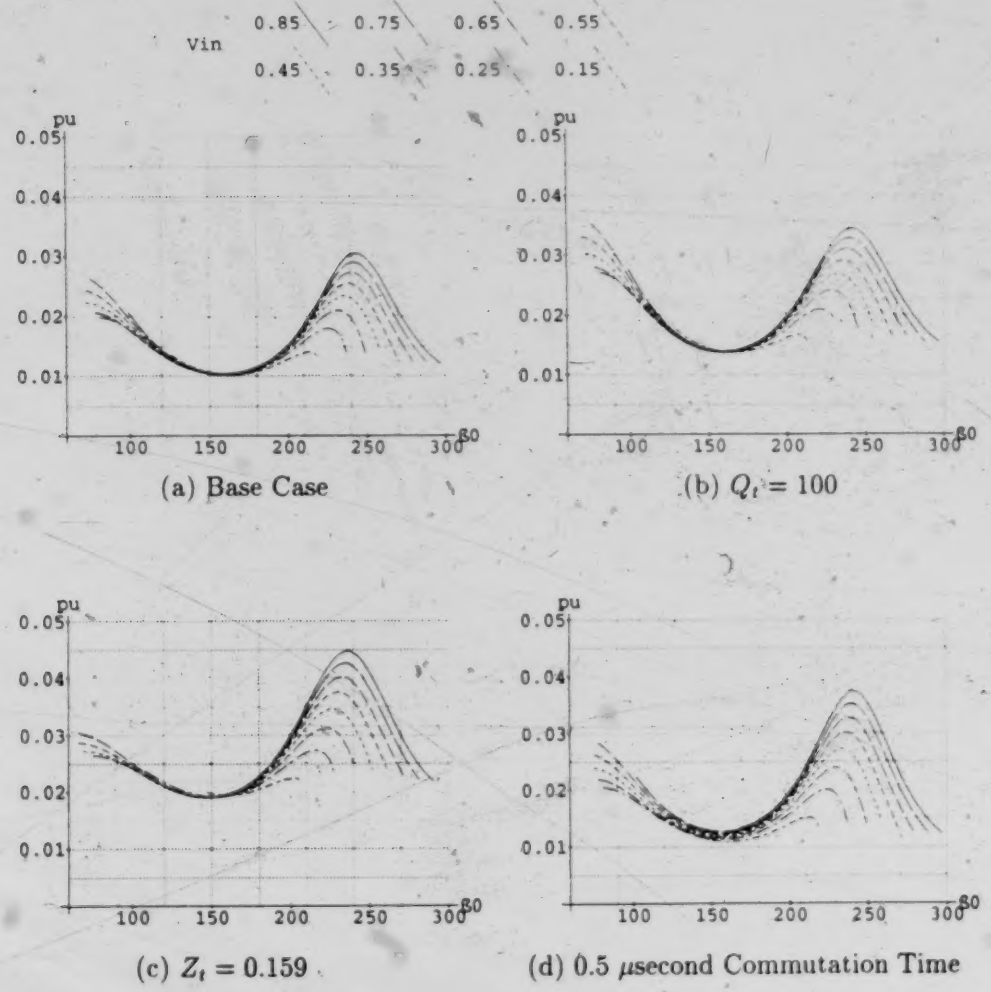

(a) Base Case (b) $Q_t = 100$

(c) $Z_t = 0.159$ (d) 0.5 μsecond Commutation Time

Figure 5.13: DCSteadyState: Switching Cycle RT Loss P_t versus RT Phase at Turn-on

5.3.6 Switching Cycle Tank Loss

The switching cycle tank loss graphs in Figure 5.13 are very similar to the graphs of V_{tp} since both are determined by the energy e_t in the RT. The tank losses increase as the load decreases until β_0 reaches roughly 240°, after which tank losses begin to decline. This increased RT losses at lighter loads is an undesirable characteristic of the RTBR resulting in greatly decreased efficiencies at lighter loads.

Equation (4.54), repeated below, holds true in Figures 5.13(b) and 5.13(c) where a decrease in Q_t or Z_t results in increased RT losses. In order to minimize RT losses, both Q_t and Z_t must be maximized within the constraints of other design limitations.

$$P_t \propto \frac{V_{tp}^2}{Q_t Z_t}$$

The RT losses are increased slightly by the addition of a commutation period to the RTBR simulation, as shown in Figure 5.13(d). This is due to the higher RT energy that occurs as a result of the higher V_{tp}.

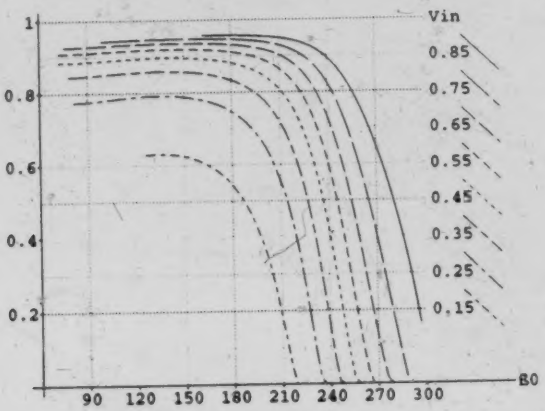

Figure 5.14: DCSteadyState: Pulse Efficiency η_p versus RT Phase at Turn-on

5.3.7 Pulse Efficiency

The graphs of pulse efficiency can be used as overall indicators of RTBR performance. The pulse efficiency η_p shown in Figure 5.14 is fairly good for low values of β_0 but decreases rapidly as β_0 increases. While switch on-state losses decrease with

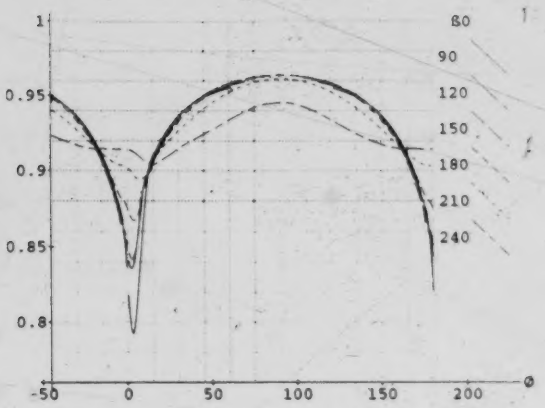

Figure 5.15: DCSteadyState: Pulse Efficiency η_e versus Phase ϕ_V of V_{ac}

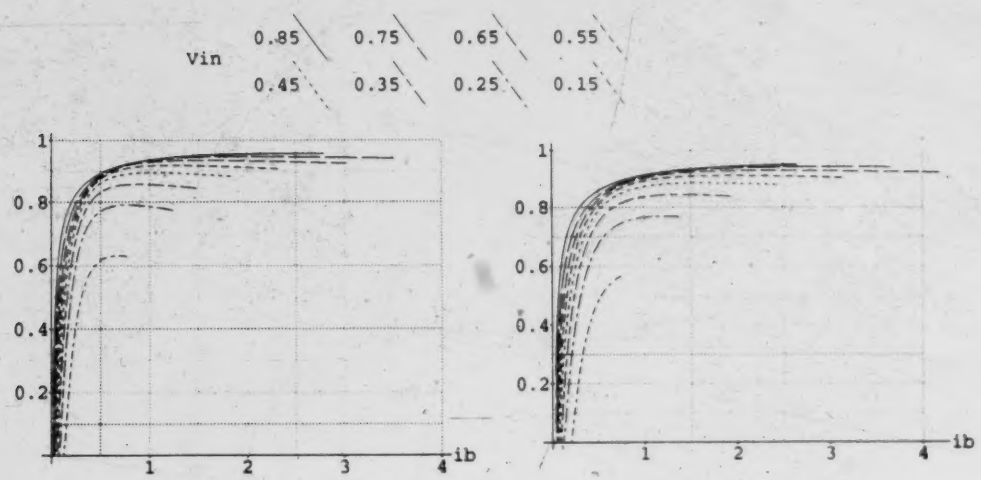

(a) Base Case (b) $Z_l = 0.159$

Figure 5.16: DCSteadyState: Pulse Efficiency η_p versus Pulse Average Current $i_{b_{av}}$

load, the tank losses increase significantly, causing the RTBR overall efficiency to fall as the load decreases.

The variance in the switching period energy efficiency η_e over an ac line cycle in Figure 5.15 shows the highest efficiencies near the input voltage crest. The energy efficiency appears lower than the power efficiency in Figure 5.14 because e_t is added to the numerator and the denominator as seen in equation (5.7). η_e shows less variance with β_0 than η_p.

The efficiency graphs in Figure 5.16 confirm the good efficiency at high currents, but low efficiency at low currents. The "sharpness" of the curves in the upper left corner of the graph can be used as an indication of the overall efficiency of a particular RTBR. A sharply bent 'elbow' indicates an efficient converter. Figure 5.16(b) shows the decrease in efficiency that occurs due to a decrease in Z_t. Similar decreases in efficiency were noted with a decrease in Q_t or with the addition of the commutation period.

5.3.8 Switching Frequency

The switching frequency decreases as β_0 increases as seen in Figure 5.17, and is almost independent of V_{in}. Therefore f_{sw} varies with load, but will remain fairly constant through a line cycle if the RTBR is operated at constant β_0, as confirmed in Figure 5.18. f_{sw} has more variance with V_{in} at smaller β_0's. With a sinusoidal input current, β_0 will vary throughout the ac line cycle, resulting in a greater variance in switching frequency.

Equation (4.47) shows that the switching period is affected by β_0 and β_2. However, increases in β_0 are partially cancelled by the resulting decreases in β_2. Therefore, the variance of the switching frequency is only roughly 20 % from minimal load to full load.

f_{sw} approaches the minimum of $\frac{1}{2}f_t$ as the load decreases and β_0 increases. For large β_0's, the RT oscillation is continuous and smooth through the On Period as the waveform approaches a continuation of the sinusoid from the previous Off Period. This will be apparent in Figures 6.15 and 6.16. At smaller β_0's, the RT oscillation is much more abruptly interrupted, as will be seen in Figures 6.11 and 6.12. The result is a shortening of the switching period, and a higher switching frequency.

Decreasing Z_t results in a significant reduction in the variance of the switching frequency with load, as shown in Figure 5.17(b). The resulting narrower switching frequency band is considered beneficial where stringent filtering of the switching frequency may be required.

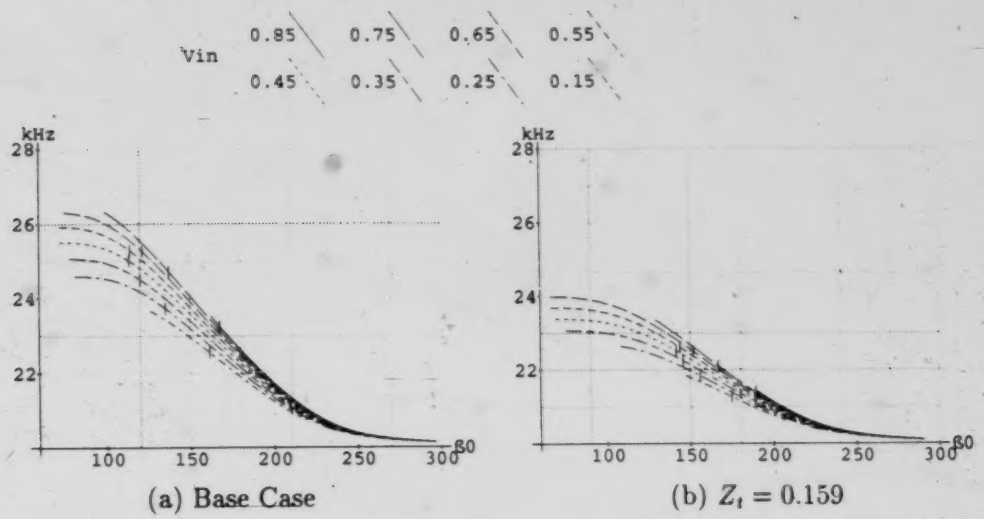

(a) Base Case (b) $Z_t = 0.159$

Figure 5.17: DCSteadyState: Switching Frequency f_{sw} versus Pulse Average Current $i_{b_{av}}$

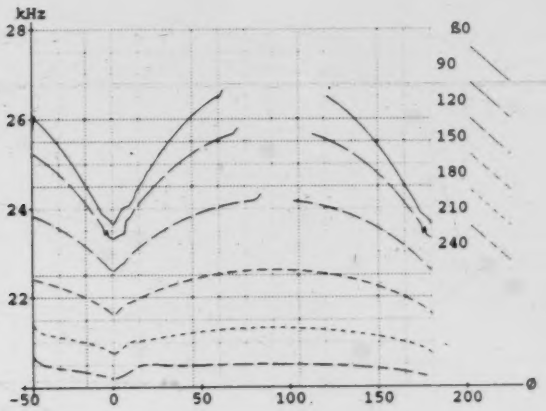

Figure 5.18: ACLineCycle: Switching Frequency f_{sw} versus Phase ϕ_V of V_{ac}

5.4 Simulation Limitations

5.4.1 Undamped On Period Calculations

In the determination of the formulae for circuit variables during the On Period, the neglection of losses in the "undamped" case will result in slightly elevated values over the "damped" case. Since the undamped case was used in **ACLineCycle**, the results are slightly erroneous. This error was generally found to be less than 5 %, and can often be considered insignificant when the results are being used to indicate trends or the feasibility of component changes. An equally great error can be expected between nominal component and resistance values and the actual values in the circuit.

5.4.2 Estimation of Losses

Steady-state occurs when the power added to the RT in a switching cycle equals the losses in the RT during that cycle. Hence, steady-state is very dependent on the losses in the circuit and will vary significantly as the estimates of component resistances vary. Inductor and capacitor resistances were estimated based on the expected currents and expected losses in each component.

The modelling of inductor losses by a lone resistance does not accurately portray the inductor core losses. Using a lone resistance gives the core losses a square relationship with the inductor current and ignores the effect of frequency. Actual core losses will become non-linear with current as saturation of the core is approached and will increase with frequency.

5.4.3 Switching Transients

In these simulations, switching transients are ignored. This is justified on the grounds that the vast majority of switchings are natural commutation without perturbation and those that are not are at low power levels. A real circuit will however have some switching transients regardless of the natural commutation and some associated losses.

The inclusion of a delay at the end of the On Period as an approximation of the effects of the commutation period is not expected to be completely accurate. However, the effects of the commutation period on the RTBR operation are not great at a 20 kHz switching frequency. The information that could be derived from the creation of an accurate commutation model would not justify the production effort required. Such a model is beyond the scope of this thesis. The approximation used shows the effects of the commutation delay, and that is sufficient for the purposes herein.

Chapter 6

Prototype Design and Performance

An 800 Watt, 120 Volt ac to 200 Volt dc resonant tank boost rectifier was built in the lab to demonstrate the feasibility of the topology and control philosophy and to analyze the rectifier performance. The design and construction of this RTBR is discussed in this chapter. Then the accuracy of the RTBR simulations is verified and the performance of the prototype RTBR is presented. The measurements of performance deal mainly with the observed ability of the RTBR to operate at unity power factor, and the efficiency achieved.

6.1 Design Criteria

The prime objective of the RTBR was to achieve operation at unity power factor with a sinusoidal input current from a sinusoidal line voltage. A power factor of better than 0.99 was targeted, including the effects of both the DPF and CHF as described in Chapter 1. Assuming a DPF of 1.00, a THD of 14 % or better would be required.

Many of the design specifications for the RTBR were not hard requirements to meet a specific input restriction or load characteristic. The intent was to achieve the best performance possible from the topology using economical and practical components and design methods. The input voltage was chosen as 120 Volts ac since that is the common single phase distribution voltage in North America. The output voltage was chosen as 200 Volts dc because:

- it is just above the minimum voltage feasible from a boost type rectifier with a 120 Volt ac input,
- it is a usable voltage for single phase inverter loads,

- a relatively low output voltage would bring out some of the inherent problems of boost converters and prove useful in resolving those problems in the RTBR.

The output voltage ripple requirements were not specified, but a constant V_o was required for accurate testing and analysis.

A power output of 800 Watts was chosen as sufficiently high to demonstrate the converter performance, while keeping it relatively small physically and economically. Therefore, full load would be 4 amps output current. The input power was designed for 900 Watts, or 7.5 amps so as to more than cover converter losses. A converter efficiency of better than 90 % at full load was desired.

A simple control system was preferable if the power factor objectives could be met. Stability and robustness under all reasonable load conditions would be required. Since the input current drawn with open loop current control would give a PF below 0.99, closed loop control was required.

Second cycle switching operation was chosen so as to minimize the resonant frequency f_t relative to the switching frequency f_{sw}, while still achieving a relatively small switch on-period. This was considered the best compromise between increasing RT losses as f_t increases (due to increasing core losses) and increasing switch conduction losses as the switch on-period increases. Whether or not second cycle switching actually results in optimum performance was not investigated.

The minimum desired f_{sw} was 20 kHz, which is just above the human audible range. f_t was set at 40 kHz since f_{sw} would always be greater than half f_t. In summary, the design values for the prototype RTBR are given in Table 6.1.

Table 6.1: Prototype RTBR Design Values

Parameter	*Value*
V_o	200 *volts*
I_o	4 *amps*
P_o	800 *watts*
V_s	120 *volts*
I_s	7.5 *amps rms*
P_{in}	900 *watts*
f_{sw}	40 *kHz*

6.2 Component Selection and Design

The determination of component values for the RTBR is discussed in this section. The selection of components for the RTBR was an interactive process involving calculation, simulation, and observation of actual RTBR behavior. First, rough estimates of component values were calculated. Then, a prototype RTBR was built using these component values, and the simulation program was developed. The desired results were compared with the actual results in the prototype as well as the simulation results, and components were adjusted accordingly. Since actual component values could be expected to vary by as much as 5 % and more accurate simulations would follow, the initial calculations were simplified and rounded.

Simulations were used in resolving the final component values for the prototype RTBR. The simulation results shown in this Chapter are all from the final simulation which accurately reflects the actual RTBR circuit. All parameters are expressed in per unit quantities. The base per unit quantities for the prototype RTBR were given in Table 5.1. Figure 6.1 shows the simulated RTBR, with the component values used in the simulations given in Table 6.2. These values are based on the actual prototype component values used as will be determined in sections 6.1 and 6.2. A summary of the actual experimental component values used in the prototype RTBR are listed in Table 6.3, complete with descriptions.

Boost Inductor

The size of the boost inductor was determined by the time required for the current to ramp down to zero at full load at the crest of the input voltage. The voltage across L_b during the Off Period is roughly:

$$V_{ramp} = V_o - \sqrt{2}V_s = 0.15\ pu \tag{6.1}$$

The peak pulse current required at not-quite-continuous conduction is:

$$I_{pk} \approx 2(\sqrt{2}I_s) = 5.3\ pu \tag{6.2}$$

At the crest of the input current waveform, β_0 will be near the start of the phase window, so a value of 90° or $\frac{\pi}{2}$ radians is used as an estimate. β_2 can be expected to be small and positive due to the low β_0, so a value of 30° or $\frac{\pi}{6}$ radians is used as an estimate. With second cycle switching at not-quite-continuous conduction, t_{ramp} can be estimated at:

$$t_{ramp} = \frac{[4\pi c - \beta_0 + \beta_2]}{\omega_t} \approx \frac{(4\pi - \frac{\pi}{2} - \frac{\pi}{6})}{\omega_t} = \frac{5}{3f_t} = 42\ pu \tag{6.3}$$

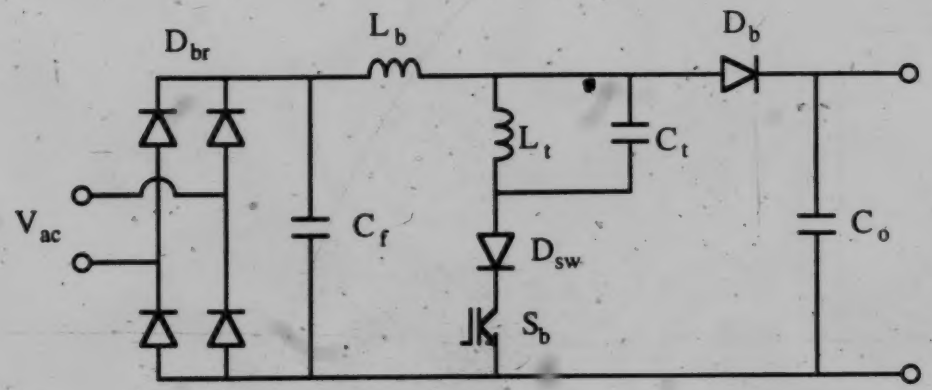

Figure 6.1: Resonant Tank Boost Rectifier Components

Table 6.2: Prototype RTBR Simulation Component Values

Parameter	*Per Unit Value*	*Actual Value*
L_b	1.15	57.5 μH
L_t	1.18	59 μH
C_t	13.3	266 nF
R_b	0.0050	0.25 Ω
R_t	0.0038	0.19 Ω
R_c	0.000188	0.0094 Ω
V_{br}	0.0100	2.0 *volts*
V_{sw}	0.0185	3.7 *volts*
V_{db}	0.0050	1.0 *volts*
Q_t	74.5	74.5
Z_t	0.298	14.9 Ω

The inductance L_b is approximately given by:

$$L_b \approx \frac{V_{ramp} t_{ramp}}{I_{pk}} = \frac{(0.15)(42)}{(5.3)} = 1.2\ pu \tag{6.4}$$

Figure 6.2(a) shows the graph of the simulated $i_{b_{pk}}$ versus β_0 of the final RTBR. The inductance of L_b in the prototype was found through the simulation, as the

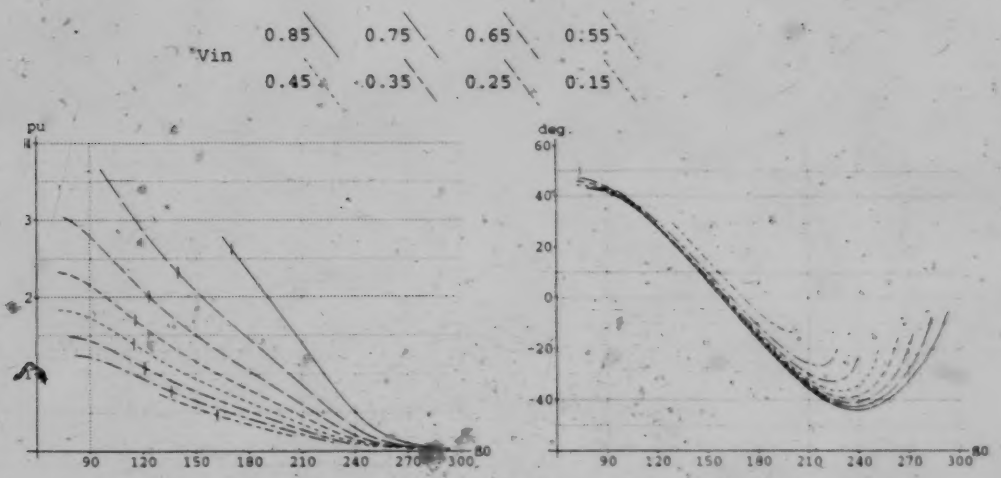

(a) $i_{b_{av}}$ versus β_0 (b) β_2 versus β_0

Figure 6.2: Prototype Simulated Pulse Average Current and RT Phase at Turn-off versus RT Phase at Turn-on

value that gave an $i_{b_{av}}$ of 2.7 at the left edge of the $V_{in} = 0.85$ curve. At this point, V_{in} is at the crest of V_{ac}, $i_{b_{av}}$ equals $\sqrt{2}I_s$, and the RTBR is almost just-continuous.

L_b was built with sheet copper and a ferrite core to minimize losses.

Resonant Tank

The choice of RT components affects the RTBR phase window, efficiency, and peak tank voltage V_{tp}. As discussed in section 4.6.1 and in Chapter 5, a higher tank impedance Z_t would result in lower tank losses. This would result in an increased V_{tp}, and a smaller $\beta_{0_{min}}$. A higher Q_t would also result in lower tank losses and an increased V_{tp}, but would produce a larger $\beta_{0_{min}}$. The optimum design would minimize losses while keeping V_{tp} at acceptable levels.

While the value of Q_t is a design variable, it's value was largely dictated by fixed losses in L_t. These losses are modelled by the series resistance R_t. L_t was built with sheet copper and a ferrite core to minimize the losses. However, once L_t was built, the value of R_t was essentially fixed. The value of L_t was changed by varying the air gap in the core.

The determining factor in resolving the RT component values was found to be $\beta_{0_{min}}$. When β_2 is positive, the switch is required to support a forward voltage ramp immediately upon turn-off as v_t begins to drop quickly. Since an earlier β_0

results in a more positive β_2, as shown in Figure 6.2(b), a decreased $\beta_{0_{min}}$ produces a greater positive $\frac{dv}{dt}$ across the switch. As the choice of $\beta_{0_{min}}$ is lowered, a point is reached where the switch can no longer recover sufficiently from turn-off to support the positive $\frac{dv}{dt}$.

A normal turn-off characteristic for an IGBT is for a "tail" of forward current to continue for two or more microseconds after forced gate turn-off, providing there continues to be a driving force. In the RTBR, the natural commutation generally removes that driving force at turn-off. However, a sufficiently large positive $\frac{dv}{dt}$ across the IGBT after turn-off re-instates a driving force for forward current. In these instances, it becomes crucial for gate turn-off to coincide exactly with natural commutation.

It would be extremely difficult to predict $\beta_{0_{min}}$. In the prototype, $\beta_{0_{min}}$ was found interactively using the actual circuit and simulations. The value is roughly 110^o. Z_t was decreased in the simulations until a value was found at which $\beta_{0_{min}}$ was close to 110^o. This value of Z_t was 0.298, corresponding to an L_t of 1.18 pu or 59 μH and a C_t of 13.3 pu or 266 nF.

The continuous oscillation of the RT dictated that C_t be a very low loss capacitor. The best capacitors available for this application are polypropylene film capacitors with metal foil electrodes, internally series-connected.

Switch

An IGBT with series ultrafast diode was chosen as the switch S_b and diode D_{sw}. The IGBT provided a low on-state V_{ce}, quick turn-on, and has the capacity for the largest current levels probable in a single phase rectifier. The ultrafast diode restricted the reverse recovery current in the switch, and provided reverse voltage capability, which was required during the negative tank voltage peaks.

During operation when β_2 is negative, v_t will continue to increase immediately after turn-off. At turn-off, i_t is negative and continues to flow into C_t, thereby increasing v_t. This results in an immediate requirement that the switch be able to sustain a reverse voltage. The greater the value of β_2, the greater both the reverse voltage and the $\frac{dV}{dt}$ will be. IGBT's normally have a turn-off time of a few microseconds, and therefore are not good candidates for an application requiring fast reverse recovery. This capability is provided by the ultrafast diode in series with the IGBT.

The peak and average currents in S_b and D_{sw} can be derived from Figure 6.3. Since components must be sized with considerable room for variances, rough calculations are sufficient. The peak current from Figure 6.3(a) is 6 pu or 24 amps. At full load, the average peak current in the switch is 5.4 pu. The average on period from Figure 6.3(b) is 9 microseconds. The average switching period from Figure 6.3(c) is 41 microseconds. This gives an approximate average S_b current of:

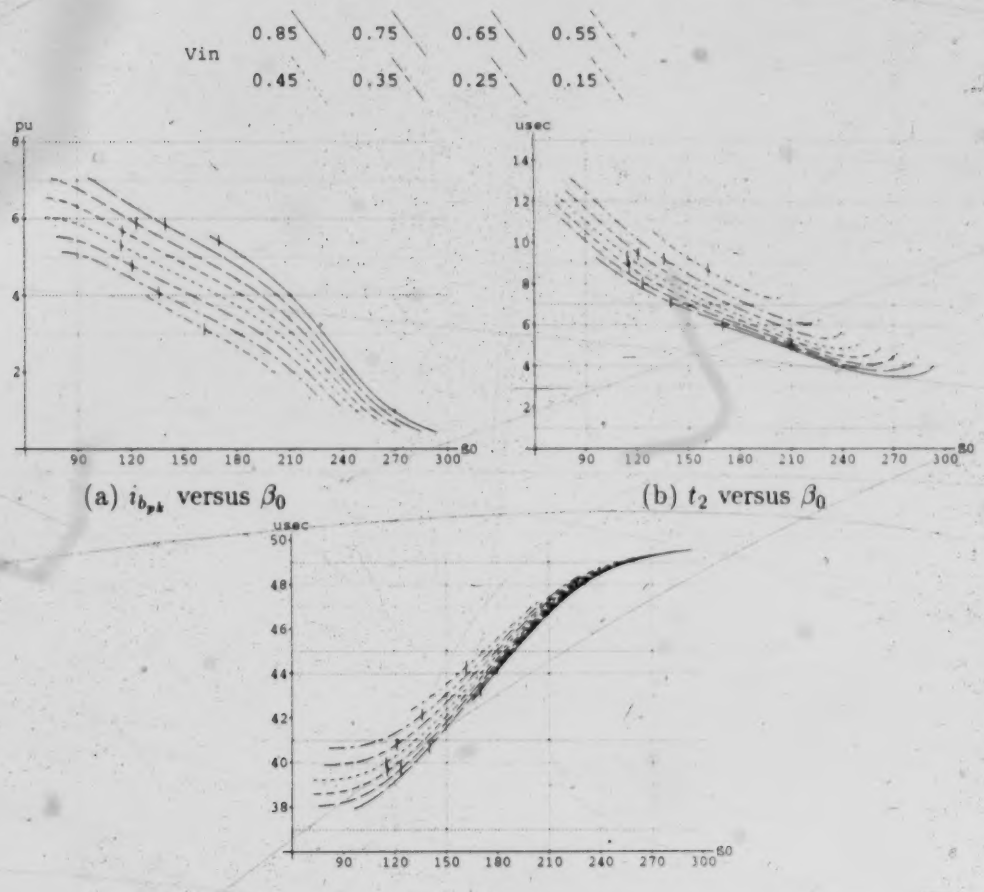

(a) $i_{b_{pk}}$ versus β_0

(b) t_2 versus β_0

(c) t_{sw} versus β_0

Figure 6.3: Prototype Simulated Switch Peak Current, Turn-off Time, and Switching Period versus RT Phase at Turn-on

$$i_{sw_{av}} = i_{b_{pk}} \frac{t_2}{t_{sw}} = 5.4 \frac{9}{41} = 1.2\ pu \approx 5\ amps$$

Figure 6.4 is useful in indicating the peak forward voltage which S_b must withstand and the peak reverse voltage which D_{sw} must withstand. The peak forward voltage is $V_o + V_{tp}$, which varies through the ac line cycle, and is at a maximum

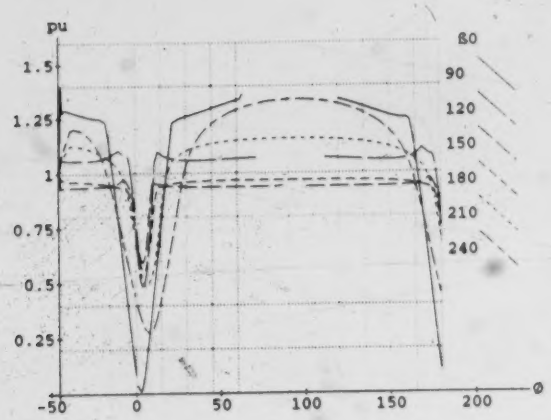

Figure 6.4: Prototype Simulated Peak Tank Voltage V_{tp} versus Phase of V_{ac}

when $\beta_0 = 240°$. The peak reverse voltage is $V_{tp_{max}} - V_{in}$, which will always be less than 1.4 pu.

The IGBT used in the prototype was an IXGH25N90, with a continuous collector current rating of 25 amps at 90° C, and a collector-emitter voltage rating of 900 volts [65]. This was chosen because it was available and had ratings well within those required. While this IGBT has a rated current fall time of 4000 nanoseconds, this current 'tail' would not normally be a factor in the RTBR due to the natural commutation of the IGBT, providing the gate turn-off coincided with the natural commutation.

The ultrafast diode used in series with the IGBT was a MUR840, with a continuous current rating of 8 amps, a peak current rating of 100 amps, and a reverse voltage rating of 400 volts.

Boost Diode

An ultrafast diode was used for the boost diode D_b, although a fast diode would have been sufficient. Since the diode turn-off is at ZC, and the reverse recovery current of the boost diode is restricted by L_b, the stresses are limited and an ultrafast diode is not necessary.

The peak current in D_b will be 6 pu as it is in the boost switch. The average current in D_b will be roughly given by half the peak current for half the switching period, or $\frac{1}{4} \times 6 = 1.5\ pu$ or 6 amps.

The peak reverse voltage that D_b must withstand occurs at turn-on when V_{tp0} is greatest. This is at a maximum of $V_o + V_{tp_{max}}$ when β_0 is near 240°. The peak

reverse voltage, determined from Figure 6.4, is under 1 pu + 1.5 pu = 2.5 pu or 500 volts.

The boost diode used was a DSEI 30-09A, with a continuous current rating of 30 amps, and a reverse voltage rating of 900 volts. This was chosen because it was available and had ratings well within those required.

Output Capacitance

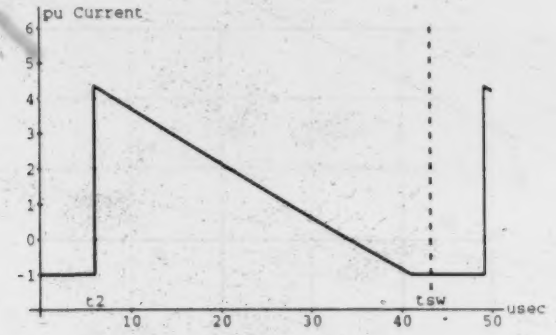

Figure 6.5: Output Capacitance Current at Input Voltage Crest

The determining factor in choosing the output capacitance C_o was the ripple current i_{rip} capability of the capacitor. The current through into C_o is the triangular boost diode current offset by the load current I_o. The waveform shown in Figure 6.5 is the capacitor current near the input voltage crest. The actual current will vary through the ac line cycle. An appropriate method to determine the rms value of this ripple current would be to simulate the capacitor current. Unfortunately, the **ACLineCycle** program developed only simulates the open loop current response (at a constant β_0) since it does not include a simulation of the closed loop control system. The ripple current in the closed loop case could be expected to be less than the open loop case since the peak currents would be less. The simulation of the closed loop control circuit was not attempted due to time constraints.

A rough estimate of the ripple current can be made based on the maximum ripple current $i_{rip_{max}}$ which would occur when the RTBR is operating at full load. At the crest of V_{in} at full load, with $I_o = 1$, the rms ripple current shown in Figure 6.5 can closely approximated by:

$$i_{rip_{max}} = \sqrt{\frac{(t_{sw} - t_2)}{t_{sw}} \left[\frac{(i_{b_{pk}} - 1)^3 + 1}{3 i_{b_{pk}}} \right] + \frac{t_2}{t_{sw}}}$$

With $i_{b_{pk}} = 5.4\ pu$, $t_2 = 6$ and $t_{sw} = 43$, as read from the graphs in Figure 6.3, this rms value is 2.2 pu. At the cusps of V_{in}, the ripple current will be slightly less than I_o or 1 pu. Therefore, the rms value of i_{rip} will be between 1 pu and 2.2 pu. The capacitor chosen, a CGS242T450X5L, has an equivalent series resistance (ESR) of 0.100 Ω and a maximum ripple current rating of 6.85 amps rms (1.71 pu) at 120 Hz.

Input Filter Capacitance

The purpose of the input filter capacitance C_f is to remove most of the switching frequency component from i_b so that the ac line current follows a waveform reasonably close to $i_{b_{av}}$. If the RTBR is considered as a source of current at the switching frequency, C_f must be made sufficiently large to offer a smaller impedance to ground than the ac utility supply at the switching frequency. This is dependent on the line impedance.

The amount of attenuation of the switching frequency was not considered of great importance for the prototype since it was only being built to verify the circuit concept. Therefore C_f was chosen experimentally at a value that removed a large portion of the switching frequency.

RC Filter

After the boost inductor current has fallen to zero and before the next switch turn-on occurs, there is a period where the only circuit activity is the oscillation of the tank. During this time, the voltage at the top of the RT would ideally be clamped at V_{in} since the current in the boost inductor is supposedly unchanging. In reality though, the boost inductance acts together with the input rectifier diode capacitances, the boost diode capacitance, and the boost switch capacitance, to produce a high frequency voltage oscillation at the top of the RT and across the switch.

This oscillation appears to have no serious negative effect on circuit operation, since the energy involved is small. However, to ensure that the oscillations do not influence voltage and current measurements made on the circuit, an RC filter was placed across the boost inductor to dampen the oscillation. The component values for the RC filter were determined experimentally to be 700 Ω and 470 pF.

The complete prototype RTBR circuit is shown in Figure 6.6. The actual experimental component values used in the prototype RTBR are listed in Table 6.3, complete with descriptions.

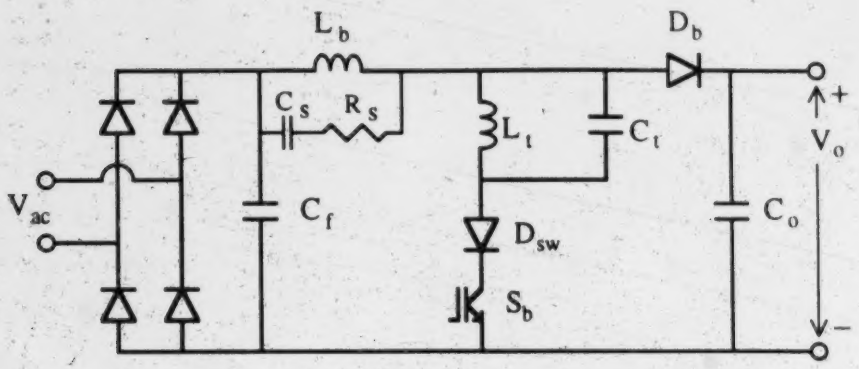

Figure 6.6: Complete Prototype RTBR Circuit

Table 6.3: Prototype RTBR Components

	Per Unit Value	*Actual Value*	*Description*
L_b	1.15	57.5 μH	ferrite core (Ferroxcube EC70-3C8) inductor with sheet copper coil
L_t	1.18	59 μH	ferrite core (Ferroxcube 1F5-3C6) inductor with sheet copper coil
C_t	13.3	266 nF	polypropylene film capacitors with internally series-connected metal foil electrodes (Wima FKP1, 1250Vdc, 400Vac); 2 × 100nF + 2 × 33nF
C_f	880	17.6 μF	metallized polyester film capacitor (Phillips 341 MKT, 250V); 2 × 2.2μF + 4 × 3.3μF
C_o	120 000	2400 μF	computer grade electrolytic capacitor (Mallory CGS242T450X5L, 450 Vdc)
C_s	0.0235	470 pF	general purpose capacitor
R_s	14	700 Ω	wound power resistor (PW10)
S_b			IGBT (Ixys IXGH25N90 9003, 900V, 25A)
D_{sw}			ultrafast diode (Motorola MUR840, 400V, 8A)
D_{br}			diode bridge (International Rectifier 250JB4L, 400V, 25A)
D_b			ultrafast diode (Ixys DSEI 30-09A, 900V, 30A)

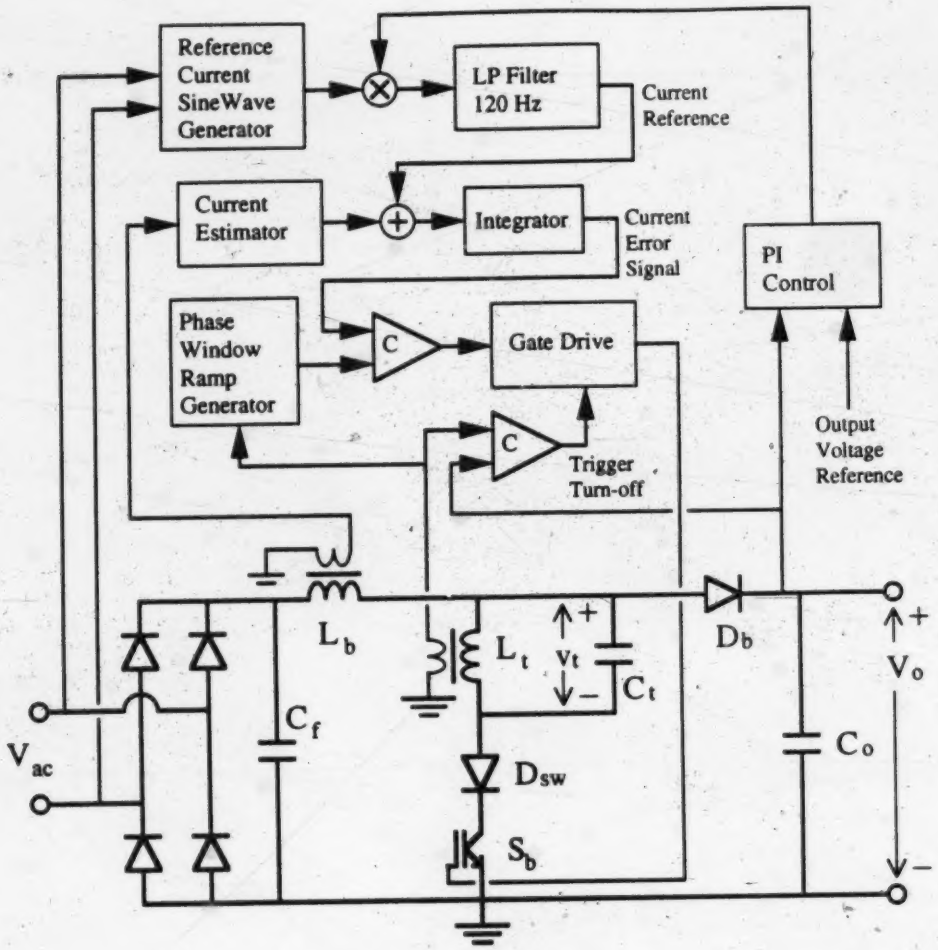

Figure 6.7: Control Overview

6.3 Control System Design

The requirements of the RTBR control system are outlined in section 4.5. The actual prototype RTBR control system is described in this section. The control system was constructed with analog op-amps and comparators due to their ease of use and their real-time speed of response. Switch timing and the circuit response once turn-off was initiated had to be accurate to a fraction of a microsecond.

The basic control of the RTBR consists of a switching period current control

circuit and an output voltage control loop, as shown in Figure 4.6. The switching period current control circuit consists of a reference current waveform generator, current estimator, current control loop, phase window ramp generator, and gate drive circuit, as shown in Figure 6.7. The complete control circuit schematic diagram appears in Appendix C.

Output Voltage Loop

The output voltage control loop takes the measured output voltage and the reference (desired) output voltage of the RTBR and produces a signal proportional to the magnitude of the desired input current. For the purposes of this prototype, a basic proportional, integral control was constructed using one op-amp. The time constant of the loop was set at a number of line cycles. This provided a reference signal that was essential constant throughout each ac line cycle, thereby ensuring that the current reference waveform itself would be free of harmonics. Fast output voltage loop response was considered unnecessary in this study of the RTBR, especially since C_o was sufficiently large to maintain output voltage regulation.

Reference Current Waveform

The reference current waveform is a pure sinusoid at the ac line frequency and in phase with the line voltage. It is proportional in magnitude to the current reference from the output voltage control loop.

The sinusoidal reference current is generated from the line voltage waveform, which is multiplied by the voltage error signal and then passed through a 120 Hz low pass filter and simple phase shifter to give a current reference signal to the inner current control loop. This was produced using op-amps and an Operational Transconductance Amplifier.

Current Estimation

The feedback of the actual input current can be achieved by current measurement, or by current estimation based on power circuit parameters. Actual current measurement is normally found to be more accurate, but requires an expensive current transformer, or lossy resistive current measurement techniques.

Theoretically, the input current could be accurately estimated by integrating the voltage across the boost inductor and adding the result to a differentiation of the voltage across the input filter capacitor. This would give a signal identical to the actual input current. In practice, noise introduced in the differentiator, in the voltage measurement, and elsewhere, will degrade the signal and necessitate the use of a low pass filter.

The current estimator in the prototype RTBR integrated the voltage across L_b and filtered out the switching frequency components with a 3.5 kHz low pass filter.

Current Control Loop

The input current control is implemented through an inner current control loop. The estimated and reference current waveforms are added and the result is integrated to give a stable signal proportional to the desired β_0. While this control is unsophisticated compared to possible adaptive control techniques, the result was quite adequate to produce unity power factor operation with the RTBR.

Phase Window Ramp

The phase window ramp circuit provides turn-on timing of S_b. This switch timing control circuit includes resonant tank phase detection and turn-on timing. The RT voltage v_t is fed in to the circuit from a secondary on L_t. The phase β of v_t is detected by triggering on the positive going zero crossing of v_t. A ramping voltage is then generated which corresponds to the phase window introduced in section 4.5. This ramp voltage is compared to the current error signal from the current control loop and turn-on is initiated when they cross. The start of the ramp is set so that the earliest turn-on of the switch will occur when β is at $\beta_{0_{min}}$. The slope of the ramp is set so that the latest turn-on will occur at $\beta_{0_{max}}$. In this way, turn-on is timed to occur at the appropriate β corresponding to the current reference signal.

$\beta_{0_{min}}$ and $\beta_{0_{max}}$ are determined from Figure 6.2(a). The vertical bars on the curves show the current and corresponding β_0 required for sinusoidal input current at full load at 90 % efficiency. $\beta_{0_{min}}$ can be read off the graph to be approximately 115°. The actual value of $\beta_{0_{min}}$ used is slightly smaller than that to allow for component variances, and for room for control variances. The value for $\beta_{0_{max}}$ is the point where the current has fallen close to zero for all values of V_{in}, which is roughly 280°. The result is the turn-on phase window shown in Figure 4.8.

While the normal operation of the RTBR was intended to be with closed loop current control, a switch was put in to allow operation at a constant β_0 so that the current waveform could be observed.

Switch Gate Drive Circuit

The switch gate drive circuit includes gate current injection, commutation detection and back-up turn-off timing. The gate current injection is a dual transistor totem pole arrangement. The lower voltage rail was set below zero at -5 volts to facilitate fast gate charge removal on turn-off. This was necessary so that the IGBT could support forward voltage as soon as possible after turn-off.

The commutation detection circuit was simply a comparator between V_o and v_t, providing trigger turn-off, as described in section 4.5.4. The detection of natural commutation would require current detection, which was considered undesirable. Therefore, the v_t trigger voltage was made adjustable so that gate turn-off could be timed to coincide as closely as possible with the natural commutation. This triggered gate turn-off does not constitute forced commutation in most cases since natural commutation occurs before the trigger turn-off signal has reached the gate of the IGBT. However, in most cases where natural commutation would not occur, the trigger signal would cause forced commutation.

The back-up turn-off timing, or maximum on time $t_{2_{max}}$, was instituted with an RC circuit which forces the gate low after the maximum time period has elapsed.

6.4 Experimental Accuracy

In measuring the performance of the prototype RTBR, it is necessary to qualify the accuracy of the measurements. Factors that might affect the accuracy of the test data are presented here.

Input Voltage harmonics

The operation of the RTBR is based on an assumption that the input voltage waveform is a clean sinusoid with no harmonic content. The utility supply used to power the prototype RTBR was not however clean. The background harmonic content of the input voltage waveform was found to vary between 1.5 and 1.8 % THD. Additional harmonics would also appear whenever the elevator was operating, resulting in a supply voltage THD of up to 2.2 % THD. These measurements were taken on the unloaded ac line at the point where the RTBR was to be tested.

All current waveforms and spectra in section 6.6 below were taken at times when the elevator(s) were not running. This was easy to determine since the harmonics induced by the elevator were audible from the RTBR.

Component Drift

All of the components used in the prototype RTBR are subject to component drift with temperature. The drift in component value of the inductors and capacitors has a significant effect on the RTBR behavior. The manufacturer's published information on the ferrite core used for L_t indicates an increase in the initial permeability of over 50 % from 25° to 75° [63]. The manufacturer's published information on the capacitors used for C_t indicates a capacitance drift with temperature of 0.07 % per degree [64].

While testing the RTBR in this simulation verification, it was found that the value of L_t decreased slightly as the inductor core heated up. Since the simulation component values were constant, it was necessary to attempt to maintain the prototype component values as constant as possible, so that the comparison could be valid. Therefore, for the purposes of the test results presented here, L_t was kept cool by using a fan and only operating the RTBR for long enough periods of time to take each measurement.

Measurement Instruments

Current and voltage measurements were taken using aemc multimeters. The measured dc currents and voltages generally contained ac ripple components. When these measurements were compared with the corresponding waveforms on the oscilloscope, the dc value given by the instrument was generally close to the midpoint of the ripple.

The oscilloscope used was a Tecktronix 2220. All time readings were made using the oscilloscope, including measurements of β_0. All peak voltage and current readings were made from the oscilloscope.

All harmonic spectra and the associated current waveforms were taken using the HP3660A Spectrum Analyzer.

6.5 Verification of the Simulation Accuracy

In order to justify the use of the simulation programs to predict the behavior of the RTBR, it is necessary to verify that the simulations are reasonably close to the actual circuit. In this section, experimental data from the prototype RTBR is compared to the results given by the simulation program **DCSteadyState**. The component values used in the simulation are given in Table 6.2.

The measured average input current data is plotted against the simulation in Figure 6.8(a). The measured curves are very close to the simulated curves, except for low values of β_0. These points were taken near the end of the testing, and the deviation may be due to the heating of L_t. The measured data confirms the linear relationship between $i_{b_{av}}$ and β_0.

The measured peak boost inductor current data is fairly close to the simulation, as shown in Figure 6.8(b). The actual $i_{b_{pk}}$ is close to 10 % higher than the simulated for low values of β_0, with less deviation at greater β_0's.

The actual and measured peak tank voltages in Figure 6.9 are also fairly close. Discrepancies are expected here due to the high susceptibility of V_{tp} to variances in β_0, V_{in}, Q_t, Z_t, and the turn-off timing. Q_t and Z_t are influenced by changes in the inductance and resistance of the RT inductor with heat. There is also some

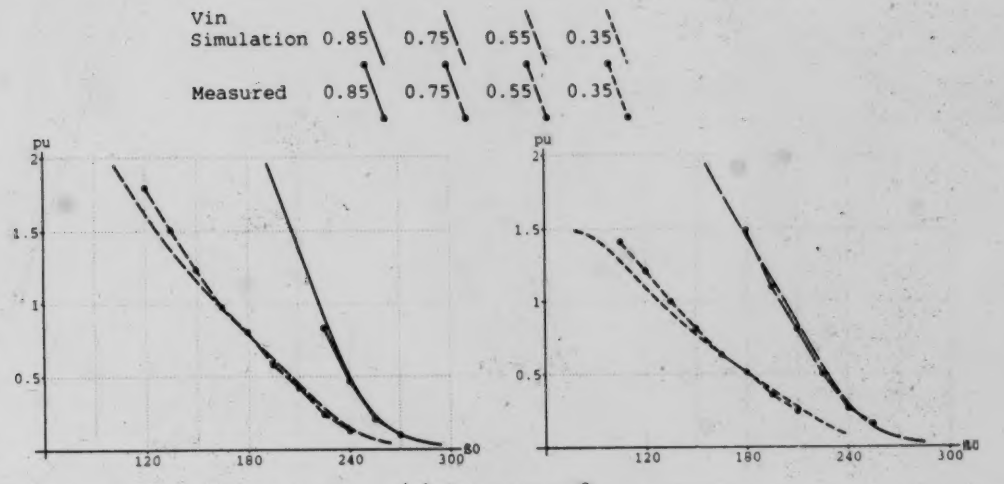

(a) $i_{b_{av}}$ versus β_0

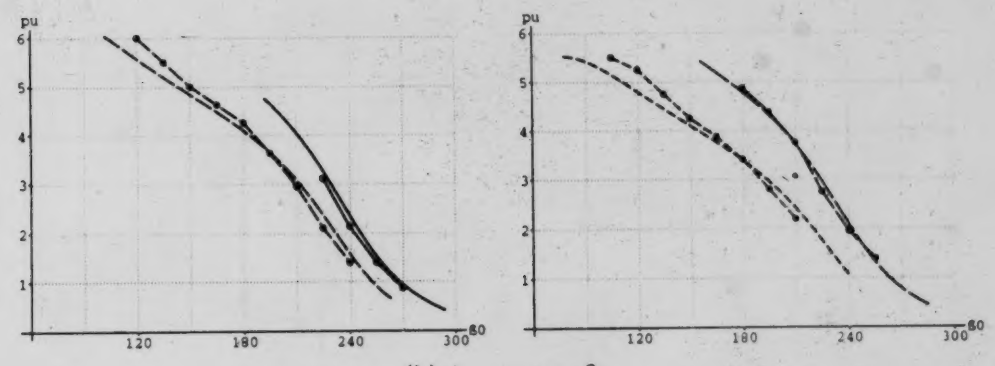

(b) $i_{b_{pk}}$ versus β_0

Figure 6.8: Comparison of Experimental Prototype RTBR Currents with the DC-SteadyState Performance

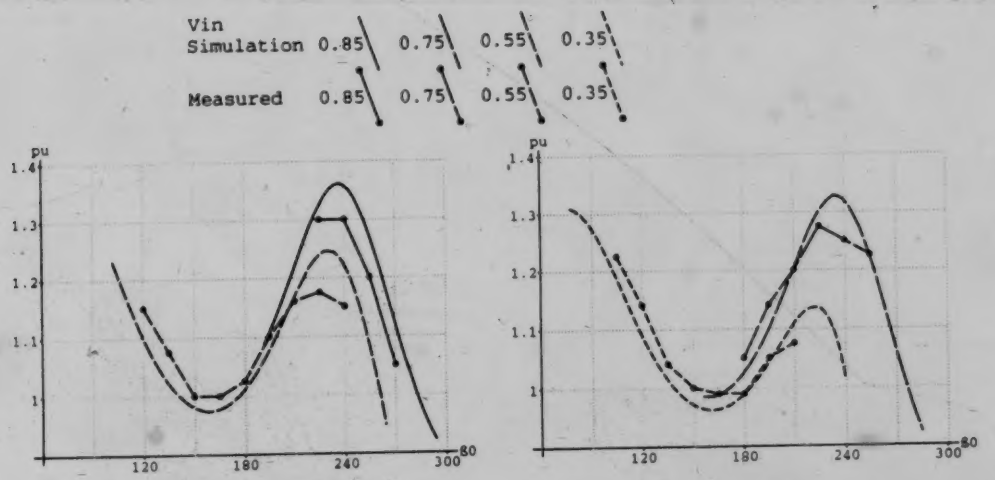

Figure 6.9: Comparison of Experimental Prototype RTBR Peak Tank Voltage with the DCSteadyState Performance: V_{tp0} versus β_0

error to be expected in the commutation period in the simulation, which will affect the simulated values for V_{tp}.

The measured turn-off times show general agreement with the simulated values, as shown in Figure 6.10(a). Discrepancies can be expected due to the difficulty in measuring β_0 accurately, and the error in the simulated commutation period.

The agreement between the measured and simulated switching periods shown in Figure 6.10(b) is a good final verification of the simulation accuracy.

Switching cycle waveforms from the prototype RTBR are shown in Figures 6.11, 6.13, and 6.15. The corresponding simulated switching cycle waveforms of the same RTBR are shown in Figures 6.12, 6.14, and 6.16 respectively. These waveforms show the general agreement between the simulation and the prototype in the switching period time frame.

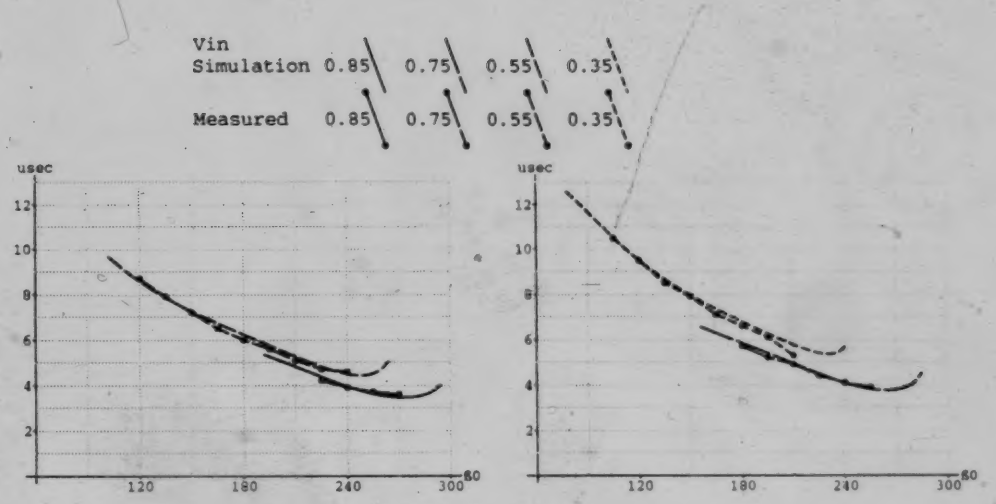

(a) t_2 versus β_0

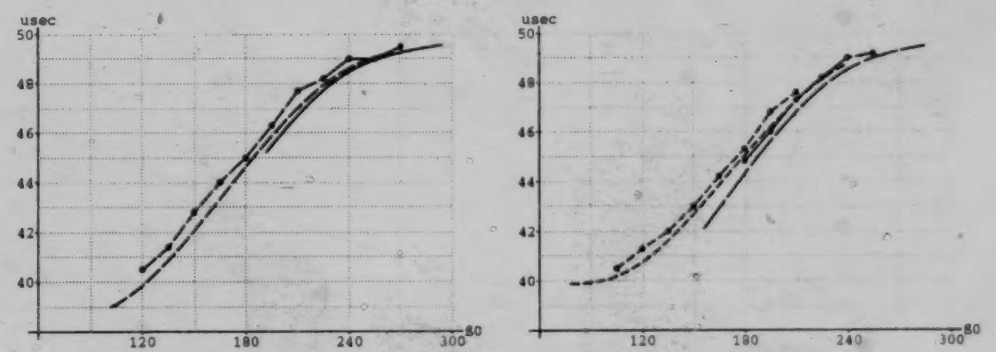

(b) t_{sw} versus β_0

Figure 6.10: Comparison of Experimental Prototype RTBR Time Periods with the DCSteadyState Performance

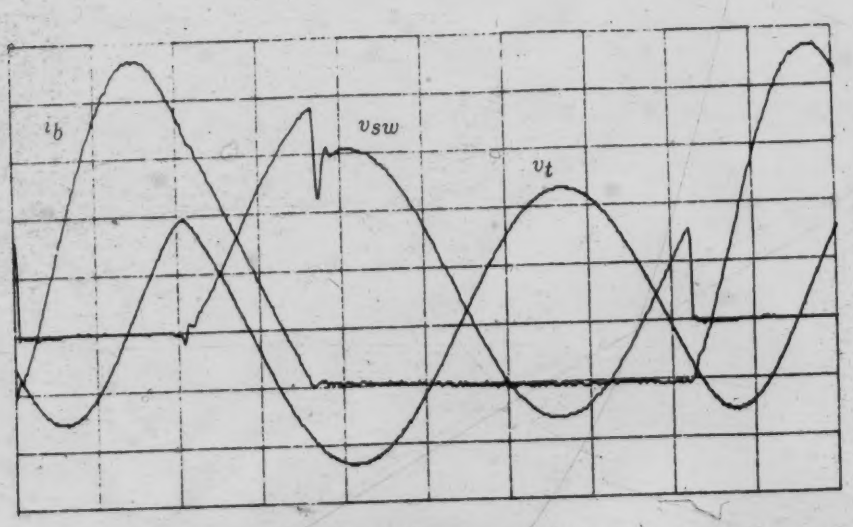

Figure 6.11: Prototype RTBR Switching Cycle Voltage and Current Waveforms, $\beta_0 = 120°$, $V_{in} = 0.42$ pu, div: 5 μsec, 100 volts, 4 amps

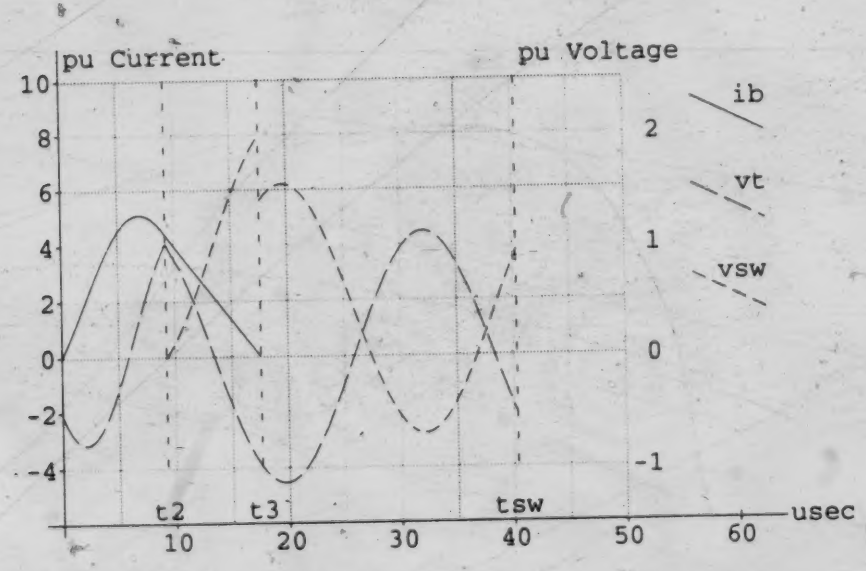

Figure 6.12: Simulated RTBR Switching Cycle Voltage and Current Waveforms, $\beta_0 = 120°$, $V_{in} = 0.42$ pu

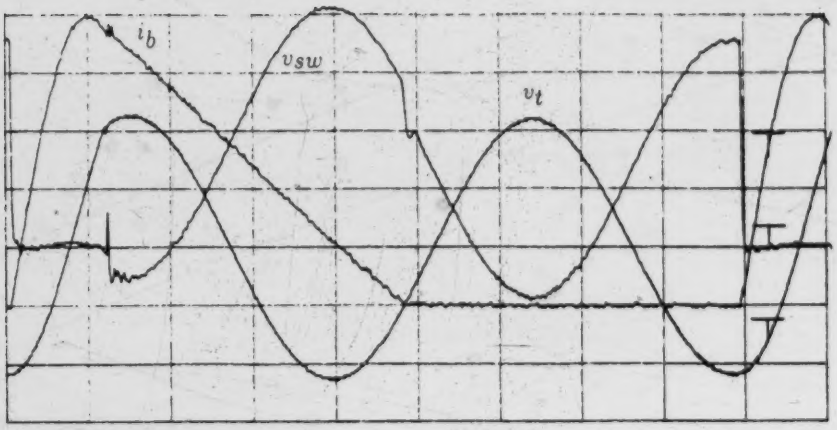

Figure 6.13: Prototype RTBR Switching Cycle Voltage and Current Waveforms, $\beta_0 = 180^o$, $V_{in} = 0.75$ pu, div: 5 μsec, 100 volts, 4 amps

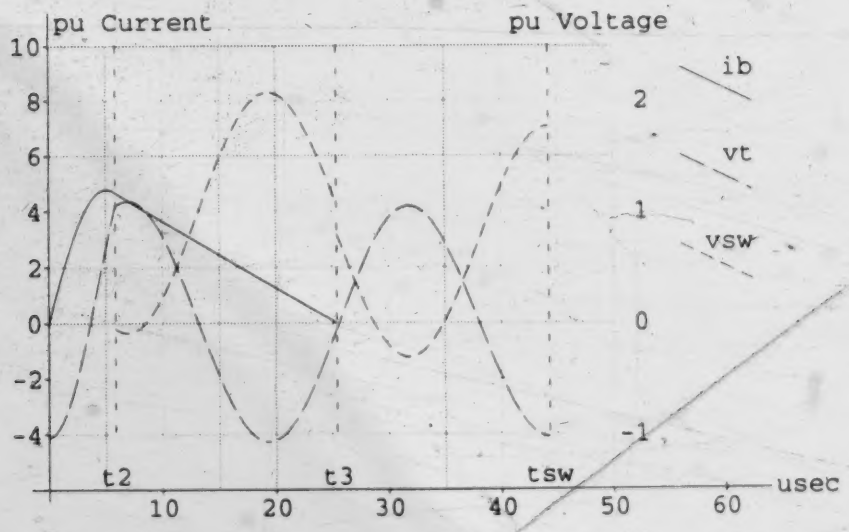

Figure 6.14: Simulated RTBR Switching Cycle Voltage and Current Waveforms, $\beta_0 = 180^o$, $V_{in} = 0.75$ pu

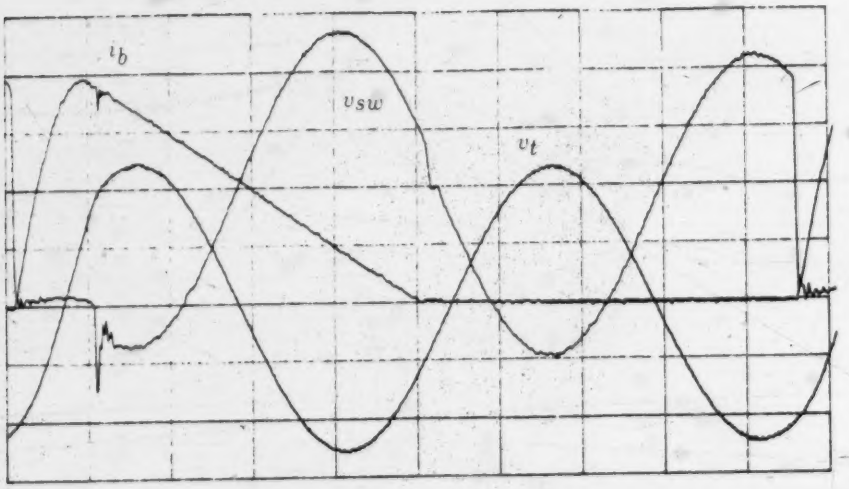

Figure 6.15: Prototype RTBR Switching Cycle Voltage and Current Waveforms, $\beta_0 = 220°$, $V_{in} = 0.84$ pu, div: 5 μsec, 100 volts, 4 amps

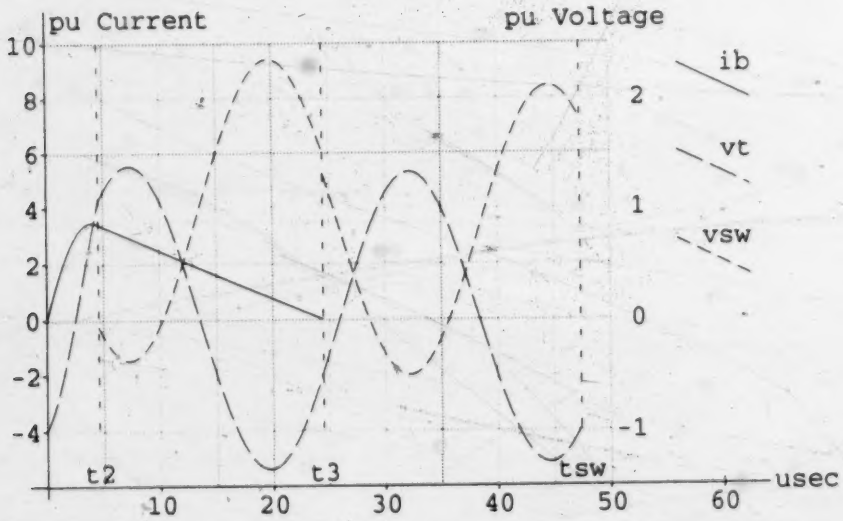

Figure 6.16: Simulated RTBR Switching Cycle Voltage and Current Waveforms, $\beta_0 = 220°$, $V_{in} = 0.84$ pu

6.6 Experimental Results

6.6.1 Zero Current and Zero Voltage Switching

The zero-current-switching of the boost switch at turn-on can be seen in each of the prototype and simulated current waveforms in Figures 6.11 through 6.16. The current starts at zero and is restricted from rising quickly by L_b.

The zero-voltage-switching of the boost switch at turn-off can also be seen in the waveforms in Figures 6.11 through 6.16. The voltage rises through the On Period, and reaches V_o just before turn-off. Then C_t restricts the switch voltage from increasing as the switch is turned off. In Figures 6.11 and 6.12, β_0 is near the start of the turn-on phase window and the voltage begins an upward ramp immediately after turn. In Figures 6.13 through 6.16, β_0 is larger and the switch is shown to support reverse voltage immediately after turn-off.

As expected, no current 'tail' was observed after the turn-off of the IGBT. This is attributed to the natural commutation of the switch where the switch current driving force has been eliminated. The RTBR is an application where the IGBT can be used at high switching frequencies without the switching losses that would normally be expected due to the hard-switched turn-off characteristics of the IGBT.

6.6.2 Closed Loop Power Factor

At full load, the RTBR was found to have a THD of just under 3 % considering the first 60 harmonics. This THD does not include the switching frequency and harmonics, since these are dependant on the size of the C_f which is a design variable. The input current waveform at full load is shown in Figure 6.17 along with the input voltage waveform. The sinusoidal nature of the waveform is apparent. The harmonic spectrum of the input current at full load showing the switching frequency is shown in Figure 6.18.

Input voltage and current waveforms at full, $\frac{3}{4}$, $\frac{1}{2}$, and $\frac{1}{4}$ load with their respective current harmonic spectra are shown in Figure 6.19.

The measured current distortion of the RTBR over its full load range is shown in Figure 6.20. The current distortion deteriorates at lower loads due to the effect of C_f close to the cusps of the rectified input voltage, where all of the RTBR current requirements are met by C_f and hence no line current is drawn. This is apparent in Figure 6.19(d) where the current is zero for a short period after the input voltage zero crossing.

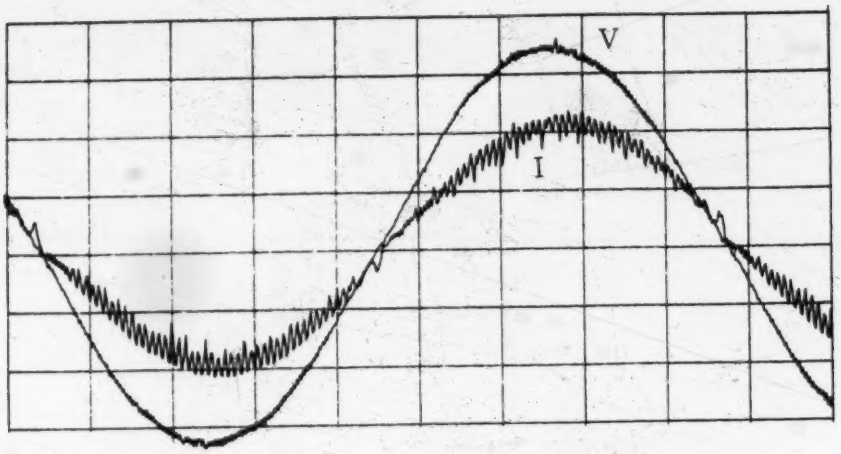

Figure 6.17: RTBR Input Voltage and Current at Full Load, div: 5 msec., 50 volts, 5 amps

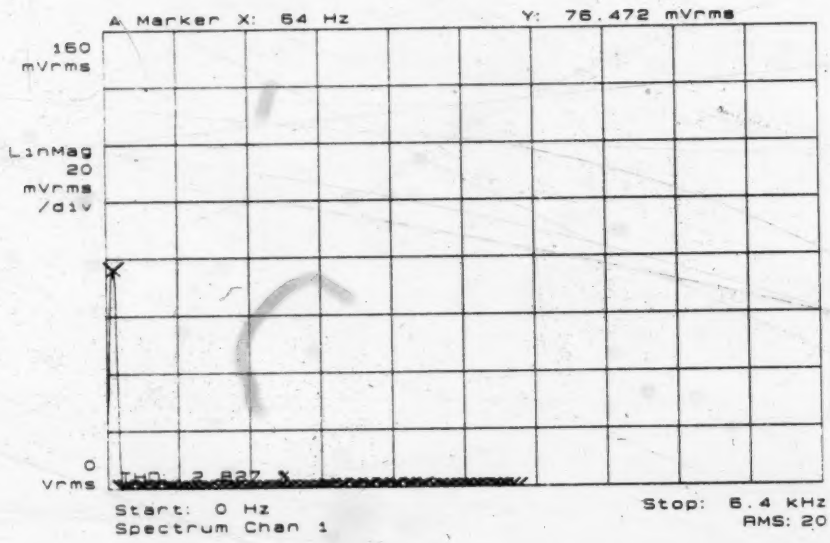

Figure 6.18: RTBR Input Current Harmonic Spectrum, div: 0.1 amp/mV

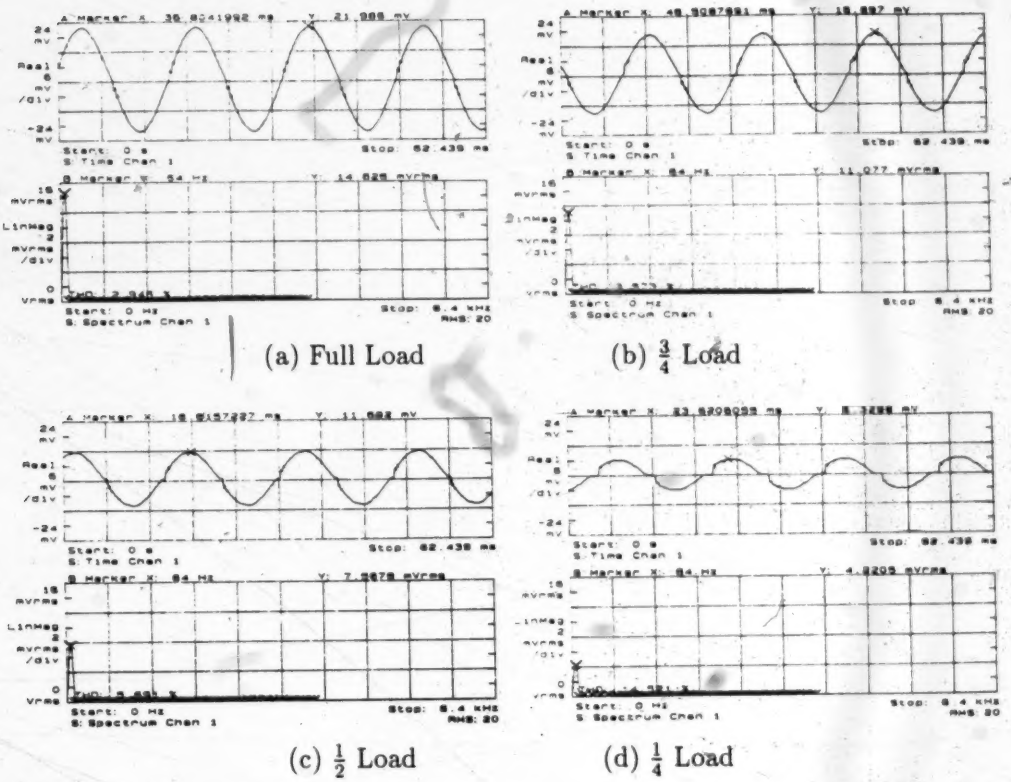

(a) Full Load (b) $\frac{3}{4}$ Load

(c) $\frac{1}{2}$ Load (d) $\frac{1}{4}$ Load

Figure 6.19: RTBR Input Current Waveforms and Spectra with Closed Loop Current Control, div: 0.5 amp/mV

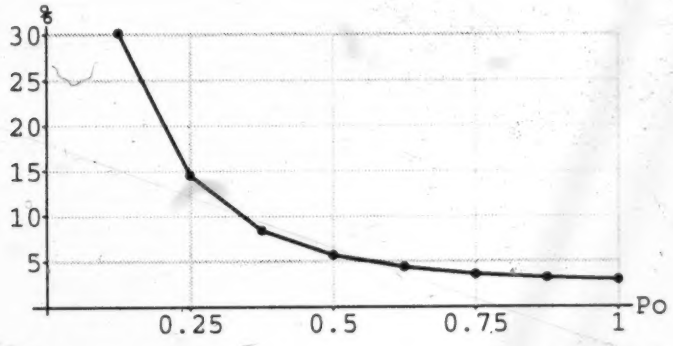

Figure 6.20: RTBR Measured Input Current Distortion versus Load

6.6.3 Open Loop Power Factor

Under open loop current control, a line current THD of 20 % was achieved with $\beta_0 = 170°$ as shown in Figure 6.21. This is the largest load possible with this RTBR while maintaining discontinuous conduction under open loop current control. The triangular nature of the waveform is apparent.

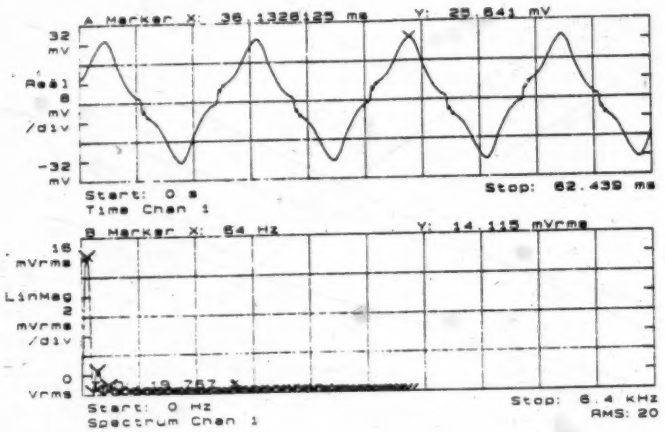

Figure 6.21: RTBR Input Current Waveform and Spectrum with Open Loop Current Control, div: 0.5 amp/mV

6.6.4 Efficiency

The efficiency of the RTBR (while operating under closed loop current control) was calculated from the measured input and output voltages and currents according to the formula below. I_1, the fundamental component of the input current, was measured by reading the magnitude of the 60 Hz component in the input current spectrum.

$$\eta_p = \frac{P_{out}}{P_{in}} = \frac{V_o I_o}{V_{ac} I_1}$$

At full load, the RTBR was found to have an efficiency of 91%. The measured efficiency over the full load range is shown in Figure 6.22. This graph shows a drop in efficiency as the load decreases. This is due to the nature of how RT losses vary with β_0, as shown in the simulation results in Figure 6.23. As the load decreases from full load, β_0 increases. When β_0 is between roughly 170° and 240°,

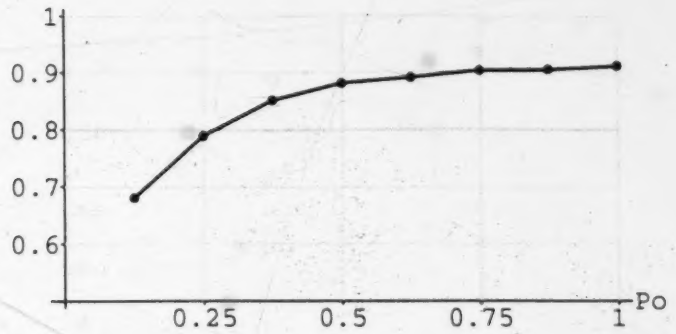

Figure 6.22: RTBR Measured Efficiency versus Load

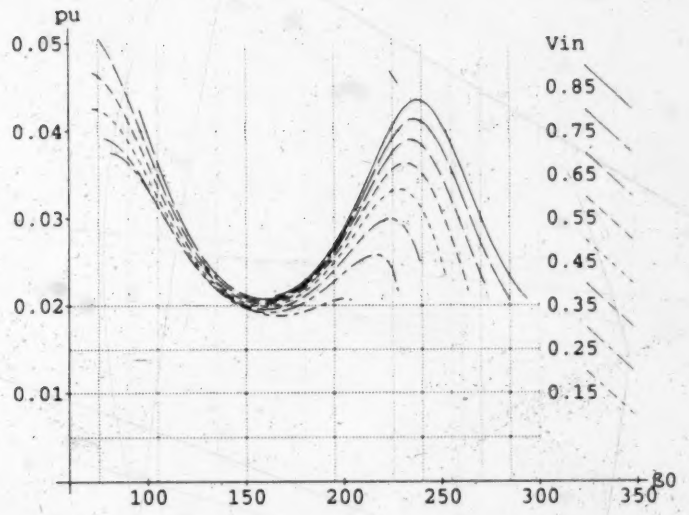

Figure 6.23: Simulated Switching Cycle RT Loss P_t versus RT Phase at Turn-on

the RT tank losses increase as the load decreases. While the switch on-time is coincidentally also decreasing, the savings in switch on period losses is not enough to offset the increases in RT losses.

Chapter 7

Conclusion

The work presented in this thesis concerns the design, simulation and experimental testing of a new type of resonant switch-mode rectifier conceived by the author. The technology of existing switch-mode rectifiers, including other resonant switch-mode rectifiers, is presented as relevant background material to the subject rectifier. Then, the operation of the RTBR is explained with a full mathematical analysis. The control system requirements are discussed, and the concept of dc steady-state as it applies to the RTBR is explained.

Software for the dc steady-state and ac line cycle mathematical simulation of the RTBR was written. Results from the simulations were used to verify the circuit operation, reveal the effects of component changes on the rectifier behavior, and optimize the prototype design. In a comparison with experimental results, the simulation results were found to be fully representative of the rectifier characteristics.

A prototype of the RTBR was designed, built, and tested in the laboratory. The operation was found to be close to the theoretical expectations. The performance of the RTBR in drawing unity power factor from the utility supply was shown to be very good at full load, and reasonably good at light loads. The efficiency was also found to be good at full load, although it deteriorated at lighter loads.

7.1 RTBR Performance

The "Resonant Tank Boost Rectifier" (RTBR) draws power from a single phase, 120 Volt, 60 Hz source at unity power factor. This is achieved by actively forcing the input current to follow a sinusoidal waveform, without directly measuring the current. The current distortion is much smaller than the requirements set out in present standards discussed in Chapter 1, such as IEEE 519-1981 [2], Transalta Utilities harmonic specification [4] and others mentioned by Arrillaga et al. [3].

7.1.1 Advantages

Under normal operation, the RTBR achieves rectification with sinusoidal input current at good efficiency near full load. It has the following distinguishing features:

- Under closed loop current control, the input current has less than 3 % THD at full load, falling to 30 % at 12.5 % load. This corresponds to a current harmonic factor (CHF) of 1.00 and 0.96 respectively.
- All components except the output capacitance are very small since they are sized above the switching frequency rather than at the ac line frequency. This is an improvement over most hard-switched and resonant switch-mode rectifiers which use an inductor sized to filter out the switching frequency.
- The input current is controlled by controlling the phase of the RT at turn-on of the boost switch. The current control loop uses current estimation based on the boost inductor voltage, eliminating the need for direct current measurement.
- The variance in switching frequency from 10 % of load to full load is less than 20 %. This is better than most resonant switch-mode rectifiers.
- The inherent current waveshaping (i.e. at a constant RT phase at turn-on) produces a THD of 20.7 %, corresponding to a CHF of 0.98.
- The switching losses are negligible. In normal operation the RTBR generally has ZCS at turn-on and ZVS at turn-off.
- The soft-switching conditions of the RTBR allow an IGBT to be used at higher switching frequencies than would normally be expected due to the elimination of the lengthy current fall time.
- Since the resonant circuit is used only as a turn-on and turn-off mechanism, it is decoupled from both the load and the input.

7.1.2 Disadvantages

The RTBR circuit has a number of disadvantages that reduce its effectiveness in certain applications. These include:

- The continuously oscillating resonant tank has losses which have proven to be significant. These losses are "regressive" since they are actually greater at lighter loads.

- As is typical with most resonant-mode power converters, the RTBR has relatively high peak and rms switch and diode currents.
- The discontinuous nature of the boost inductor current results in a high switching frequency component in the input current waveform. This is not a serious drawback since a relatively small input filter capacitor was used to eliminate the switching frequency component, with acceptable degradation in CHF at lighter loads.
- The current from the RTBR into the output capacitor is a sawtooth with a relatively higher rms component. The output capacitance must be chosen to handle this ripple current.
- A series ultrafast diode is required with the switch due in part to the very low reverse voltage capability of the IGBT used.
- The achievement of 3 % THD at full load requires a finely tuned control circuit.

7.1.3 Transient Operation

The operation of the RTBR under transient conditions was not fully investigated, but appears to be stable. On start-up, the circuit operates as a diode bridge LC rectifier. A surge of current is drawn as C_o is charged up, and then pulses proportional to the load are drawn as shown in Figure 1.2.

Once current control is initiated, the output voltage is boosted up to the specified level which was 200 volts in the prototype. The RTBR then operates as described in this thesis, with little resemblance to the diode bridge rectifier.

The circuit behavior under a load short circuit will be dominated by the boost inductance. The output capacitance will provide short circuit current until the output voltage has fallen to zero. Then the only impedance presented to the utility supply will be the boost inductance, which is very small. The RTBR does not have good short circuit current protection.

The circuit behavior under a load open circuit is also not good under normal operation since current is still drawn at $\beta_{0_{max}}$ at the input voltage crests. The logical way to handle a load open circuit would be to stop switching so there is no input current.

7.2 Suggestions for Further Work

There is a lot of work that could be undertaken on the RTBR circuit to produce a better rectifier. The main area requiring improvement is the efficiency at lighter loads.

Topology

The use of an IGBT with high reverse voltage capability could be investigated. This may eliminate the need for the switch series ultrafast diode if the lone IGBT can perform the necessary functions at turn-off. The switch must be capable of sustaining both forward and reverse voltage ramps immediately after turn-off.

Alternatively, topological changes that would restrict V_{tp} could be investigated. In the original concept for the RTBR, the switch contained a reverse diode (as in a MOSFET). The current i_{t2} in L_t at turn-off was expected to be negative, and hence would flow through the reverse diode to the output until it had ramped down to zero. The RT free oscillation would then always start with $V_{tp2} = V_o$ and $\beta_2 = 0$, and RT losses would be independent of β_0. This was abandoned when it was found that i_{t2} was positive for small β_0's, and when the MOSFET reverse diode was found to be too slow. However, there may still be a way of implementing the reverse diode idea.

Since the RT losses are so significant in the RTBR, work toward improving the efficiency of the RT would be very beneficial. Integrated L-C circuits, as proposed by Smit et al. [66], may prove useful in the RTBR. As the name suggests, an integrated L-C circuit combines the inductance and capacitance in one component. This should reduce the copper required and reduce the copper losses in the tank circuit.

Control

It may be possible to control V_{tp} by turning the switch off earlier than would occur under natural commutation. When β_0 is large (at lighter loads), i_t is positive and increasing in value at turn-off. If turn-off was triggered to occur earlier, i_{t2} would be lower, and the resulting V_{tp} would also be lower as mentioned in section 4.5.4. There would be trade-offs to consider such as the increase in switching losses, but an investigation is warranted.

Improvements could be made to the current estimator circuit to take into account the effects of C_f on the input current waveform. A voltage differentiator was tried but was found to be too noisy and actually caused a deterioration of the THD at full load. One possible method would be to generate a current that is proportional to the integrated L_b voltage. This current could be smoothed by

a capacitance proportional to C_f, and the result should be representative of the input current.

The prototype control system has no provision for no load operation. With β_0 at $\beta_{0_{min}}$, there is still a small current delivered to the output, and the output voltage will rise if there is no load. A relatively minor addition to the control circuit is required to stop the switching if the voltage rises above certain value.

Assuming that the problem of poor efficiency at lighter loads can be resolved, work could be undertaken to create a control circuit for the RTBR on an ASIC. The control may still require analog circuitry for those functions where fast response or timing precision is an absolute necessity, such as the switch gate turn-on and turn-off timing.

Bibliography

[1] Ned Mohan, Tore M. Undeland, and William P. Robbins, Power Electronics; Converters, Applications, and Design, John Wiley & Sons, New York, Toronto, 1989.

[2] IEEE Guide for Harmonic Control and Reactive Compensation of Static Power Converters, ANSI/IEEE Standard 519-1981.

[3] J. Arrillaga, D. A. Bradley, and P. S. Bodger, Power System Harmonics, TK3226.A77 1985, John Wiley, Toronto.

[4] Harmonic Specification for Harmonic Producing Customers Connected to the Transalta Utilities Corporation System, 1988-05-09, Transalta Utilities Corporation, Calgary.

[5] Electricity Council (1976). Limits for Harmonics in the United Kingdom Electricity Supply System, Engineering Recommendation G5/3, Electricity Council, London

[6] C. K. Duffey and R. P. Stratford, "Update of Harmonic Standard IEEE-519; IEEE Recommended Practices and Requirements for Harmonic Control in Electric Power Systems", IEEE/IAS Annual Meeting Conference Record 1989, TK4001, pp. 1618-1624.

[7] Mark A. Geisler, "Predicting Power Factor and Other Input Parameters for Switching Power Supplies", IEEE Applied Power Electronics Conference Proceedings 1990, TK7881.15, pp. 579-587.

[8] Arthur W. Kelly, William F. Yadusky, "Rectifier Design for Minimum Line Current Harmonics and Maximum Power Factor", IEEE Applied Power Electronics Conference Proceedings 1989, pp. 13-22.

[9] California Institute of Technology, Power Electronics Group, "Final Report, Input-Current Shaped Ac-to-Dc Converters", NASA-CR-176787, Prepared for NASA Lewis Research Center, May 1986.

[10] Alturi Rama Prasad, Phoivos D. Ziogas, and Stefanos Manias, "A Comparative Evaluation of SMR Converters With and Without Active Input Current Waveshaping", IEEE Transactions on Industrial Electronics, vol. IE-35, No. 3, August 1988, pp. 461-468.

[11] F. C. Lee, "High-Frequency Quasi-Resonant and Multi-Resonant Converter Technologies", IEEE Industrial Electronics Society Conference, 1988 (IECON '88), pp. 509-521.

[12] Fred C. Lee, "High-Frequency Quasi-Resonant Converter Technologies", Proceedings of the IEEE; Special Issue on Power Electronics, April, 1988, pp. 377-390.

[13] S. Singer, "The Application of 'Loss-Free Resistors' in Power Processing Circuits", IEEE Power Electronics Specialist's Conference Record 1989 (PESC'89), TL1100, pp. 843-846.

[14] Martin F. Schlecht, "Novel Topological Alternatives to the Design of a Harmonic-Free, Utility/DC Interface", IEEE Power Electronics Specialist's Conference Record 1983 (PESC'83), TL1100, pp. 206-216.

[15] Martin F. Schlecht, "Harmonic-Free Utility/DC Power Conditioning Interfaces", IEEE Transactions on Power Electronics, vol. PE-1, No. 4, October 1986, pp. 231-239.

[16] Martin F. Schlecht and Brett A. Miwa, "Active Power Factor Correction for Switching Power Supplies", IEEE Transactions on Power Electronics, vol. PE-2, No. 4, October 1987, pp. 273-281.

[17] Roger J. King, "Analysis and Design of an Unusual Unity-Power-Factor Rectifier", IEEE Transactions on Industrial Electronics, vol. IE-38, no. 2, April 1991, pp. 126-134.

[18] Walley E. Rippel "Optimizing Boost Chopper Charger Design", Sixth National Solid-State Power Conversion Conference (Powercon6), May 1979, TK2798, pp. D1-1 to D1-20.

[19] Ned Mohan, Tore M. Undeland, and Ralph J. Ferraro, "Sinusoidal Line Current Rectification with a 100 kHz B-SIT Step-Up Converter", IEEE Power Electronics Specialist's Conference Record 1984 (PESC'84), TL1100, pp. 92-97.

[20] Richard Keller and Gary Baker, "Unity Power Factor Off Line Switching Power Supplies", International Telecommunications Energy Conference 1984, (INTELEC'84), pp. 332-339.

[21] C. P. Henze and N. Mohan, "A Digitally Controlled AC to DC Power Conditioner that Draws Sinusoidal Input Current", IEEE Power Electronics Specialist's Conference Record 1986 (PESC'86), TL1100, pp. 531-540.

[22] J. Ch. Bendien, B. Fregien, and J. D. van Wyk, "High-efficiency on-board battery charger with transformer isloation, sinusoidal input current and maximum power factor", IEE Proceedings, Vol. 133, Pt. B, No. 4, July 1986, pp. 197-204.

[23] F. E. Spooner, "Switch Mode Power Supplies with Idealised Performance", International Telecommunications Energy Conference 1986, (INTELEC'86), pp. 89-95.

[24] Kalyan K. Sen and Alexander E. Emanuel, "Unity Power Factor Single Phase Power Conditioning", IEEE Power Electronics Specialist's Conference Record 1987 (PESC'87), TL1100, pp. 516-524.

[25] Alexander E. Emanuel and Kalyan K. Sen, "Steady-State Performance of the DC Motor Supplied from Single-Phase Rectifier with Step-Up Converter, A Unity Power Factor Converter", IEEE Transactions on Energy Conversion, vol. 3, No. 1, March 1988, pp. 172-178.

[26] Folke Eklund, "A Rectifier with an Internal Microprocessor, that is an Essential Part of a Very Flexible, Computer Controlled Power System", International Telecommunications Energy Conference 1988, (INTELEC'88), pp. 429-432.

[27] Chen Zou, Raymond B. Ridley, and Fred C. Lee, "Design and Analysis of a Hysteretic Boost Power Factor Correction Circuit", IEEE Power Electronics Specialist's Conference Record 1990 (PESC'90), TL1100, pp. 800-807.

[28] K. Mahabir, G. Verghese, and J. Thottuvelil, A. Heyman, "Linear Averaged and Sampled Data Models for Large Signal Control of High Power Factor AC-DC Converters", IEEE Power Electronics Specialist's Conference Record 1990 (PESC'90), TL1100, pp. 372-381

[29] Richard Redl and Nathan O. Sokal, "Current-Mode Control, Five Different Types, Used with the Three Basic Classes of Power Converters: Small-Signal AC and Large-Signal DC Characterization, Stability Requirements, and Implementation of Practical Circuits", IEEE Power Electronics Specialist's Conference Record 1985 (PESC'85), TL1100, pp. 771-785.

[30] M. Kazerani, G. Joos, and P. D. Ziogas, "Programmable Input Power Factor Correction Methods for Single Phase Diode Rectifier Circuits", IEEE Applied Power Electronics Conference Proceedings 1990, TK7881.15, pp. 177-184.

[31] M. Kazerani, P. D. Ziogas and G. Joos, "A Novel Active Current Waveshaping Technique for Solid-State Input Power Factor Conditioners", IEEE Transactions on Industrial Electronics, vol. IE-38, no. 1, Feb 1991, pp. 72-78.

[32] Bruce Carsten, "High Speed Control of Sinusoidal Input Current Converters for Minimal Energy Storage Requirements", PCI'87 Conference, September 1987, TK2551, pp. 296-303.

[33] James B. Williams, "Design of Feedback Loop in Unity Power Factor AC to DC Converter", IEEE Power Electronics Specialist's Conference Record 1989 (PESC'89), TL1100, pp. 959-967.

[34] Derek Chambers and Dee Wang, "Dynamic Power Factor Correction in Capacitor Input Offline Converters", Sixth National Solid-State Power Conversion Conference (Powercon6), May 1979, TK2798, pp. B3-1 to B3-6.

[35] J. H. Mulkern and N. Mohan, "A Sinusoidal Line Current Rectifier Using a Zero-Voltage Switching Step-up Converter", IEEE/IAS Annual Meeting Conference Record 1988, TK4001, pp. 767-771.

[36] Kwang-Hwa Liu and Yung-Lin Lin, "Current Waveform Distortion in Power Factor Correction Circuits Employing Discontinuous-Mode Boost Converters", IEEE Power Electronics Specialist's Conference Record 1989 (PESC'89), TL1100, pp. 825-829.

[37] Robert Erickson, Michael Madigan, and Sigmund Singer, "Design of a Simple High-Power-Factor Rectifier Based on the Flyback Converter", IEEE Applied Power Electronics Conference Proceedings 1990, TK7881.15, pp. 792-801.

[38] T. S. Latos and D. J. Bosack, " A High Efficiency 3 kW Switchmode Battery Charger", IEEE Power Electronics Specialist's Conference Record 1982 (PESC'82), TL1100, pp. 341-349.

[39] Stefanos Manias and Phoivos D. Ziogas, "An SMR Topology with Suppressed DC Link Components and Predictive Line Current Wave Shaping", IEEE Transactions on Industry Applications, vol. IA-23, No.4, July/August, 1987, pp. 644-653.

[40] R. Itoh and K. Ishizaka, "Single-phase Sinusoidal Convertor Using MOSFETs", IEE Proceedings, Vol. 136, Pt. B, No. 5, September 1989, pp. 237-242.

[41] Takami Kagotani, Kazou Kuroki, Junichi Shinohara, and Akira Misaizu, "A Novel UPS Using High-Frequency Switch-Mode Rectifier and High-Frequency PWM Inverter", IEEE Power Electronics Specialist's Conference Record 1989 (PESC'89), TL1100, pp. 53-57.

[42] A. Chibani and M. Nakaoka, "A New Control Topology of Single-Stage HF Link Switch-Mode-Rectifier with Sinusoidal Line Current", IEEE/IAS Annual Meeting Conference Record 1990, TK4001, pp. 1157-1162.

[43] Sayed-Amr El-Hamamsy, "Coupled-Inductor Rectification and Cycloconversion", IEEE Applied Power Electronics Conference Proceedings 1988 (APEC'88), TK7881.15, pp. 258-266.

[44] Eric Destobbeleer, Guy Seguier, and Andre Castelain, "AC-DC Converter Minimizing Induced Harmonics in Industrial Power Systems", IEEE Transactions on Power Electronics, vol. PE-2, No. 4, October 1987, pp. 320-327.

[45] Teruo Kataoka, Kazuhiro Mizumachi, and Shota Miyairi, "A Pulsewidth Controlled AC-to-DC Converter to Improve Power Factor and Waveform of AC Line Current", IEEE Transactions on Industry Applications, vol. IA-15, No. 6, November/December 1979, pp. 670-675.

[46] Mark J. Kocher and Robert L. Steigerwald, "An AC-to-DC Converter with High Quality Input Waveforms", IEEE Transactions on Industry Applications, vol. IA-19, No. 4, July/August 1983, pp. 586-599.

[47] David Thimmesch, "An SCR Inverter with an Integral Battery Charger for Electric Vehicles", IEEE Transactions on Industry Applications, vol. IA-21, No. 4, July/August 1985, pp. 1023-1029.

[48] Shigeyuki Funabiki, "A Single-Phase PWM Controlled AC to DC Converter Based on Control of Unity Displacement Power Factor", IEEE/IAS Annual Meeting Conference Record 1990, TK4001, pp. 1012-1016.

[49] Iftikhar A Khan and Robert W. Erickson, "Control of Switched-Mode Converter Harmonic-Free Terminal Waveforms Through Internal Energy Storage", IEEE Power Electronics Specialist's Conference Record 1986 (PESC'86), TL1100, pp. 13-26.

[50] R. Mahadevan, S. El-Hamamsy, W. M. Polivka, and S. Cuk, "A Converter with Three Switched-Networks Improves Regulation, Dynamics, and Control", Tenth International Power Electronics Conference (Powercon10), March 1983, TK2798, pp. E-1 Page 1 to 19.

[51] Stefanos Manias, Phoivos D, Ziogas, and Guy Olivier, "An AC-DC Converter with Improved Input Power Factor and High Power Density", IEEE Transactions on Industry Applications, vol. IA-22, No. 6, November/December 1986, pp. 1073-1081.

[52] J. T. Boys and A. W. Green, "Current-forced Single-phase Reversible Rectifier", IEE Proceedings, Vol. 136, Pt. B, No. 5, September 1989, pp. 205-211.

[53] Omar Stihi and Boon-Teck Ooi, "A Single-Phase Controlled-Current PWM Rectifier", IEEE Transactions on Power Electronics, vol. PE-3, October 1988, pp. 453-459.

[54] Y. Y. Tzou and H. J. Wu, "Design and Implementation of a Mulitprocessor-based Uninterruptible Power Supply", IEEE Power Electronics Specialist's Conference Record 1988 (PESC'88), TL1100, pp. 650-657.

[55] N. Mohan, "Power Electronic Circuits, An Overview", IEEE Industrial Electronics Society Conference, 1988 (IECON '88), pp. 522-527.

[56] Derek Chambers, "A New High Frequency Resonant Technique for Dynamic Correction of Offline Converter Input Current Waveforms", Tenth International Power Electronics Conference (Powercon10), March 1983, TK2798, pp. F-1 Page 1 to 7.

[57] Harold Seidel, "A High Power Factor Tuned Class D Converter", IEEE Power Electronics Specialist's Conference Record 1988 (PESC'88), TL1100, pp. 1038-1042.

[58] E. B. G. Nijhof, "Resonant Power Supply (RPS) Converters. The Solution for Mains/Line Pollution Problems", PCI'86 Conference, June 1986, TK2551, pp. 104-139.

[59] Jin He and Ned Mohan, "Input-Current Shaping in Line-Rectification by Resonant Converters", IEEE/IAS Annual Meeting Conference Record 1987, TK4001, pp. 990-995.

[60] Ivo Barbi and S. A. Oliveira da Silva, "Sinusoidal Line Current Rectification at Unity Power Factor with Boost Quasi-Resonant Converters", IEEE Applied Power Electronics Conference Proceedings 1990, TK7881.15, pp. 553-562.

[61] R. W. DeDoncker and G. Venkataramanan, "A New Single Phase AC to DC Zero Voltage Soft Switching Converter", IEEE Power Electronics Specialist's Conference Record 1990 (PESC'90), TL1100, pp. 206-212.

[62] D. M. Divan and G. Skibinski, "Zero Switching Loss Inverters for High Power Applications", IEEE/IAS Annual Meeting Conference Record 1987, TK4001, pp. 627-634.

[63] Linear Ferrite Materials and Components, Ferroxcube Division of Amperex Corp., Saugerties, New York, 1984.

[64] Capacitors for electronic equipment, Wilhelm Westermann, Spezialvertrieb elektronischer Bauelemente, Manheim, Germany, 1989.

[65] IXYS Product Selector Guide, Ixys Corporation, San Jose, California, September, 1989.

[66] M. C. Smit, J. A. Ferreirs, and J. D. Van Wyk, "A New Ultrasonic Series Resonant Converter with Integrated L-C-T", IEEE Power Electronics Specialist's Conference Record 1990 (PESC'90), TL1100, pp. 729-733.

Appendix A

DCSteadyState Simulation Program Listing

This section contains the program listings for **DCSteadyState**. This simulation program was performed in **Mathematica, Version 1.2** on the **Next** computer. A full description and flowchart of **DCSteadyState** is contained in section 5.

Description

DC Steady-State RTBR Switching Periods with undamped or natural damped "On Period" response, and varying β_0 for a fixed value of input voltage.

RTBR Parameters

```
vbase = 200 (* Used to determine pu diode drops. *)
vout = 1 (* "vout" set at 1 pu. *)
vbr = 2.0/vbase;   vsw = 3.7/vbase;   vdb = 1.0/vbase
lb = 1.15
lt = 1.18
ct = 13.3
zt = Sqrt[lt/ct]
rb = 0.004
rc = N[(1 / (400 ct)), 3]
qfixed = 0      (* "qt" is the Q of the RT. *)
If[qfixed == 1, qt = 136, rt = (0.004 - rc)]
If[qfixed == 1, rt = N[(zt / qt - rc), 3], qt = N[(zt / (rt + rc)), 3]]
```

Input Parameters and Limits

Initial starting values and desired calculation direction is given.

```
runsToDo = 8 (* A run determines data for curves of all steady-state
 parameters versus "beta0" for a specific input voltage. *)
pulsesToDo = 0 (* This overrides "runsToDo" and generates
 data for the number of pulses specified. *)
damping = yes

(* Curve starting values: *)
vin = 0.85;   beta0start = 170

(* Curve constants: *)
vinstep = 0.1;  beta0step = 3;  cycle = 2;  tcom = 0.3

(* Curve limits: *)
beta0left = 60;  beta0right = 300;  error = .0005 vout
```

Characteristic Calculations

The characteristic matrix "charm" and its' eigenvalues "eig" are determined. A check is done to ensure that the imaginary pair eigenvalues are the first two of "eig". The resonant frequencies and other parameters are determined.

```
charm = {{ -(rb+rc)/lb, rc/lb, -1/lb},
 {rc/lt, -(rt+rc)/lt, 1/lt}, {1/ct, -1/ct, 0 }}
sIch = s IdentityMatrix[3] - charm
phis = Inverse[sIch]
eig = Eigenvalues[charm]

If[Im[eig[[3]]] == 0, Goto[normal]]
AppendTo[eig, eig[[1]]]
eig = Drop[eig, 1]

Label[normal]
chareqn2 = Expand[ (s - eig[[1]]) (s - eig[[2]]) ]
aloss = - Coefficient[chareqn2,s,1] / 2
wb = Sqrt[Coefficient[chareqn2,s,0] - aloss^2 ]
wtn = 1/ Sqrt[lt ct]
zeta = (rt + rc)/(2 zt)
wt = wtn Sqrt[1 - zeta^2]
k = lt/(lb + lt)
wbn = Sqrt[(lb + lt)/(lb lt ct)]
ft = N[1000 wt/(2 Pi)]
```

State-Transition Matrix

Inverse Laplace Transform

This is a function to Perform the Inverse Laplace Transform of the characteristic frequency matrix, or resolvent, "phis" to get the state-transition matrix, "eAt".

```
If[damping == no, Goto[endinvLap]]
(* The inverse Laplace Transform only needs to be
 determined if damped calculations are being done. *)

invLap[l_,m_,phis_,chareqn2_,eig_,aloss_,wb_] :=
Block[{ph2, eat, a0, a1, a2, ls, rs, eqa, eqb, eqc, an, ph, b1, b2},
ph2 = phis[[l,m]];   eat = 0;   Clear[a0,a1,a2];

ls = Numerator[ph2];
rs = a2 chareqn2 + (a1 s + a0) (s - eig[[3]]);
eqa = Coefficient[ls,s,0] - Coefficient[rs,s,0];
eqb = Coefficient[ls,s,1] - Coefficient[rs,s,1];
eqc = Coefficient[ls,s,2] - Coefficient[rs,s,2];
an = Solve[{eqa, eqb, eqc} == {0,0,0}];

ph = (((a1/.an) s + (a0/.an))/chareqn2 + (a2/.an)/(s - eig[[3]]));
eat = (Numerator[ph[[1,1]]]
 E^( - Coefficient[Denominator[ph[[1,1]]], s, 0] t ));
ph2 = ph[[1,2]];
b1 = Coefficient[Numerator[ph2],s,1];
b2 = aloss + (Coefficient[Numerator[ph2],s,0]/ b1);
eAt[[l,m]] = eat + (b1 E^(aloss t) (Cos[wb t] + b2/wb Sin[wb t]))
]

Label[endinvLap]
```

Determination of the State-Transition Matrix eAt

```
If[damping == no, Goto[endDo]]
(* "eAt" only needs to be determined if damped calcs are being done.*)

Clear[l,m]; eAt = IdentityMatrix[3]
Do[invLap[l,m,phis,chareqn2,eig,aloss,wb], {l, 3}, {m, 3} ]

Label[endDo]
```

Pulse Calculations

This program simulates a RTBR, calculating DC steady- state pulse characteristics for constant values of input voltage as β_0 (tank phase at turn-on) varies. The characteristics for each pulse (corresponding to one switching period) are determined iteratively until the final value of RT peak voltage matches the starting value at a particular V_{in} and β_0. Pulse currents, voltages, times, power, efficiency and other RTBR parameters for a pulse are determined.

Only pulses that can reach DC steady-state through natural commutation or turn-off at zero current are stored. The data is stored in files outside Mathematica for later retrieval by the MakeGraph program.

```
(* Counters *)
runsDone = pulsesDone = inc = 0;

rtbrvalues = pulses = swperiods = {}
pulselist = swperiodlist = vinlist = curvlist = {}
If[pulsesToDo != 0, Goto[force]]

(* If curve data has already been calculated for this
 RTBR, this data will be retrieved, so that the new
  data can be added to it. *)
Print["Reading rtbrvalues from memory."]
rtbrvalues = <<DCss.cyc2/vout1pu/file/rtbrvalues
If[rtbrvalues[[1]] == yes || rtbrvalues[[1]] == no,
 Print["File with prior data exists."],
  Goto[force], Goto[force]]
vinlist = rtbrvalues[[27]]
curvlist = rtbrvalues[[28]]
runsDone = rtbrvalues[[29]]

Label[force]
(* Start of a run at a certain "vin". *)
vimp = vin - vbr - vsw        (* voltage impressed across the RT. *)
vtcom = vout + vdb - vsw      (* "vt" when natural commutation occurs. *)
vlbramp = vout + vdb - vin + vbr
 (* voltage across "lb" during the "ib" ramp down. *)
beta0 = beta0start

AppendTo[vinlist, vin]
If[pulsesToDo == 0 , Print["Curves starting with Vin = ", vin V,
  ", runs = ", runsToDo],
 Print["Pulses with Vin = ", vin V, ", pulses = ", pulsesToDo]]
If[damping == no, Goto[flow]]

elam = Inner[Times, eAt, {{vimp/lb}, {0}, {0}}]
conv = elam/. t -> (t - lam)
```

```
int = Integrate[Collect[conv, {E^lam}], {lam, 0, t}]
forced = Collect[int, {E, Cos, Sin}]
 (* The forced response is determined here.  It is dependent only on "vin",
  so it is determined only once for each curve. *)

Label[flow]
(* Program flow control.  For one curve at constant "vin", "beta0" starts
 at "beta0start" and increases until steady-state can no longer be
  achieved.  Then "beta0" is decreased from "beta0start" until either
   steady-state can't be achieved or continuous conduction occurs. *)
lastfour = {};   vtp0 = vtcom
If[beta0 < beta0start, Goto[curveReady]]
 (* In this case, the curve left endpoint has been
  reached and the curve data is ready to be stored. *)
If[beta0 > beta0start, beta0 = beta0start - beta0step]
(* Continue with "beta0" values below "beta0start". *)

Label[phase]
(* Start of calculations for one switching period. *)
beta0rad = N[beta0 Degree]
Clear[t2, ton, tonUnd, tibpk, tibpkUnd, tvtpk, tosc, tsw, tramp, t3, ibpk,
 ib2, it2, ibav, vtp2, vt2, vtpk, vtpkUnd, fsw]
vtp0max = 2.5 vout;   vtp0min = 0.5 vout   (* These
 are starting absolute maximum and minimum values. *)
tdel = 0    (* MakeGraph expects a value for "tdel". *)
errlist = {}
cc = 1;   ss = 0;   ssUnd = 0

(* Extrapolate a guess for steady-state "vtp0" by curve fitting to the
 previous four "vtp0"'s.  If there are not already four, use the last
  "vtp0". *)
If[Length[lastfour] < 4, Goto[ontime]]
vtp = Fit[lastfour, {1, x, x^2, x^3}, x]
vtp0 = vtp /. x-> 5
lastfour = Drop[lastfour, 1]

Label[vtp0maxCheck]
vt0 = vtp0 Cos[beta0rad]
If[vt0 > vimp, vtp0 = vtp0max = vimp/Cos[beta0rad]]
 (* If "vt0" > "vimp", the boost inductor will not be forward biased.
  Therefore, "vtp0" and "vtp0max" are set so that "vt0" will equal "vimp".
   DC steady-state can not be reached if "vtp0" > this value. *)

Label[ontime]
(* Determine terms used in the undamped (non-resistive) case. *)
vt0 = vtp0 Cos[beta0rad]
avt = vt0 - k vimp
bvt = - vtp0 Sqrt[1-k] Sin[beta0rad]
cvt = Sqrt[avt^2 + bvt^2]
```

```
(* Terms used in determining whether "vt" would reach certain values in
 the undamped case, and the time at which those values would be reached.
  Since the damped "vt" will not rise as high as the undamped "vt", a
   damped pulse that fails the "mn" test below will not reach DC
    steady-state either. *)
ln = (1 - k) vimp / cvt; aln = Re[ArcSin[ln]]
mn = (vtcom - k vimp) / cvt; amn = Re[ArcSin[mn]]
nn = avt/cvt; ann = Re[ArcSin[nn]]

If[mn >= 1, vtp0 = vtp0min = 1.01 mn vtp0, ssUnd = 1]
 (* If mn > 1, "vt" won't reach "vtcom" and natural
  commutation will not occur.  The minimum "vtp0" that
   might produce natural commutation is determined. *)
If[mn >= 1, If[vtp0min > vtp0max, Goto[flow], Goto[ontime]]]
  (* If "vtp0min" > "vtp0max", DC steady-state can not
   be achieved, and the curve is at it's endpoint.  If
    not, re-iterate using "vtp0min". *)

tibpkUnd = If[beta0 < 180, N[(aln + Pi + ann) / wbn], N[(aln - ann)/wbn]]
  (* The peak of ib occurs when "vt" = "vimp". *)
tonUnd = If[beta0 < 180, N[(amn + Pi + ann) / wbn], N[(amn - ann)/wbn]]
  (* The switch is on until "vt" = "vtcom". *)
vtUnd = (k vimp + bvt Sin[wbn t] + avt Cos[wbn t])
vtpkUnd = k vimp + Sqrt[bvt^2 + avt^2]
it0 = vtp0 / zt Sin[beta0rad]

If[damping == yes, Goto[dampedcalcs]]
tibpk = tibpkUnd;   t2 = tonUnd + tcom/2
vt = vtUnd;   vtpk = vtpkUnd
it0 = vtp0 / zt Sin[beta0rad]
ib = vimp t/(lb + lt) - (avt Sin[wbn t] + bvt (1 - Cos[wbn t])) / (wbn lb)
it = vimp t/(lb + lt) + (avt Sin[wbn t] +
 bvt (1 - Cos[wbn t]))/(wbn lt) + it0
Goto[time2]

Label[dampedcalcs]
xt1 = Collect[Inner[Times, eAt, {{0}, {it0}, {vt0}}],
 {E, Cos, Sin}] (* natural response *)
xt = Collect[xt1 + forced, {E, Cos, Sin}]
ib = xt[[1]][[1]] (* current in Lb *)
it = xt[[2]][[1]] (* current in Lt *)
vt = xt[[3]][[1]] (* voltage across the RT. *)

(* Even though the pulse passes the "mn" test above, it may still not reach
 DC steady-state.  The actual peak tank voltage "vtpk" is found to determine
  if "vt" can reach "vtcom", and "vtp0" is increased if it can't.
   "tibpkUnd" and "tonUnd" are used as starting values for the damped
    (lossy) case. *)
```

```
tvtpk = Re[t/. FindRoot[D[vt, t] == 0,
 {t, (vtpkUnd - vt0)/(vtcom - vt0) tonUnd}]]
  (* time when "vt" reaches its peak. *)
vtpk = Re[vt/. t-> tvtpk]

If[vtpk < vtcom, vtp0 = vtp0min = 1.01 vtp0, ss = 1]
(* If "vt" can't reach "vtcom", then natural commutation
 won't occur.  Try again with a larger "vtp0". *)
If[vtpk < vtcom, If[vtp0min > vtp0max, Goto[flow], Goto[ontime]]]
  (* If "vtp0min" > "vtp0max", DC steady-state can
   not be achieved, and the curve is at it's endpoint.
    If not, re-iterate using "vtp0min". *)

ton = Re[t/. FindRoot[(vt - vtcom == 0), {t, tonUnd}]]
  (* The switch is on until "vt" = "vtcom". *)
t2 = ton + tcom/2 (* "tcom" is used as a crude
 way to simulate the continued circuit activity during
  the finite time it takes for commutation to occur. *)
tibpk = If[ton == 0, 0, Re[t/. FindRoot[(D[ib, t] == 0), {t, tibpkUnd}]]]

Label[time2]
ib2 = Re[N[ib/. t -> t2]]  (* check "ib" at time "t2". *)
If[ib2 < 0, t2 = Chop[Re[t/. FindRoot[(ib == 0), {t, 1.5 tibpk}]]]]
  (* New "t2" at "ib" = 0 if "ib" reaches zero before
    the boost diode turns on. *)
it2 = N[it/. t -> t2]
vt2 = N[vt/. t -> t2]
vtp2 = Re[Sqrt[vt2^2 + (zt it2)^2]]
beta2rad = Re[ArcSin[it2/vtp2 zt]]
beta2 = N[beta2rad / Degree]

tosc = Re[N[( 2 (cycle - 1) Pi + beta0rad - beta2rad) / wt]]
  (* length of time of RT free oscillation. *)
vtp4 = vtp2 E^(-zeta wtn tosc) (* vtp at "tsw" and at next turn-on.*)
err = vtp0 - vtp4
If[Abs[err] < error, Goto[timing]]    (* DC steady-state has been found. *)

If[vtp4 > vtp0max, Print["Boost inductor reverse biased."]]
  (* If "vtp4" > "vtp0max", then steady-state can not
   be achieved and the curve has passed its endpoint. *)
If[vtp4 > vtp0max, Goto[flow]]

If[vtp4 > vtp0min, Goto[errorExtrapolation]] (* Go find a better "vtp0". *)

(* End of curve reached because the min. "vtp0" can not be maintained. *)
Print["Steady-state not achievable."]
If[beta0 != beta0start, Goto[flow], Goto[end]]

Label[errorExtrapolation]
```

```
(* This routine speeds up the convergence of "vtp0" to its steady-state
 value.  A linear extrapolation based on the last two iterations of "vtp0"
  is used to estimate a "vtp0" at which the error will be zero. *)
AppendTo[errlist, {err, vtp0}]
vtp0 = vtp4 - err
If[Length[errlist] < 2, Goto[vtp0maxCheck]]
e1 = errlist[[1]][[1]];   e2 = errlist[[2]][[1]]
v1 = errlist[[1]][[2]];   v2 = errlist[[2]][[2]]
vtp0 = (e2 v1 - e1 v2) / (e2 - e1)
errlist = Drop[errlist, 1]
(* Head back up to re-iterate with the new "vtp0". *)
Goto[vtp0maxCheck]

Label[timing]
AppendTo[lastfour, vtp0]
ib2 = Chop[N[ib/. t -> t2], 10^-6]
tramp = Re[-lb/rb Log[ 1/( 1 + rb ib2 / vlbramp)]]
  (* time taken for ib to ramp down to zero. *)
t3 = t2 + tramp (* Lb conduction period *)
tsw = t2 + tosc (* switching period *)
If[t3 < tsw, Goto[here]]
Print["Continuous Conduction."]
If[pulsesToDo == 0, Goto[flow]]

Label[here]
cc = 0
fsw = 1000/tsw
ibpk = Chop[N[ib/. t -> tibpk], 10^-6]
intibon = NIntegrate[ib, {t, 0, t2}]
 (* Integral of ib during the "On Period". *)
ibramp = - vlbramp/rb +
 (ib2 + vlbramp/rb) E^(-rb/lb (t-t2))
intibramp = NIntegrate[ibramp, {t, t2, t3}]
 (* Integral ib during the ramp down time. *)
ibav = (intibon + intibramp)/tsw
pin = vin ibav
pout = vout intibramp/tsw
eff = pout / pin
 (* Pulse power efficiency.  This ignores the energy in the RT, which is
  the same at "t0" as at "tsw" since steady-state has been reached. *)

itosc = (E^(-zeta wtn (t-t2)) vtp2  Sin[wt (t-t2) + beta2rad] / zt )
intit2 = NIntegrate[it^2, {t, 0, t2}]
 (* Integral of it^2 during the "On Period". *)
intitosc2 = NIntegrate[itosc^2, {t, t2, tsw}]
 (* Integral of it^2 during the "Off Period". *)
tankloss = (rc + rt) (intit2 + intitosc2)/tsw

pulsesDone++
```

```
If[pulsesDone >= pulsesToDo && pulsesToDo != 0, Goto[end]]

onepulse = N[{beta0, tibpk, vtpk, ibpk, t2,
 tsw, beta2, eff}, 6]
oneswperiod = N[{beta0, vtp0, ibav, tankloss, cc, ss, ssUnd}, 6]
If[beta0 < beta0start, Goto[beta0minus]]

Label[beta0plus]
AppendTo[pulselist, onepulse]
AppendTo[swperiodlist, oneswperiod]
beta0 = beta0 + beta0step
If[beta0 < beta0right, Goto[phase], Goto[flow]]

Label[beta0minus]
PrependTo[pulselist, onepulse]
PrependTo[swperiodlist, oneswperiod]
beta0 = beta0 - beta0step
If[beta0 > beta0left, Goto[phase], Goto[flow]]

Label[curveReady]
If[runsDone == 0, Goto[storeCurve]]
Print["Reading pulses and swperiods from memory."]
pulses = <<DCss.cyc2/vout1pu/file/pulses
swperiods = <<DCss.cyc2/vout1pu/file/swperiods

Label[storeCurve]
inc++;   runsDone++
AppendTo[pulses, pulselist]
AppendTo[swperiods, swperiodlist]
AppendTo[curvlist, runsDone]
Print["Writing to pulses and swperiods."]
pulses >> DCss.cyc2/vout1pu/file/pulses
swperiods >> DCss.cyc2/vout1pu/file/swperiods
pulses = swperiods = pulselist = swperiodlist = {}

rtbrvalues = {damping, lb, lt, ct, rb, rt, rc,
 vout, N[vbr, 4], N[vsw, 4], N[vdb, 4], qt, zt, 1,
  wbn, wb, wtn, wt, zeta, k, cycle, runsDone,
   "beta0", beta0left, beta0right, "Vin", N[vinlist, 3],
    curvlist, runsDone, NA, 0, 0, tcom}
Print["Writing to rtbrvalues."]
rtbrvalues >> DCss.cyc2/vout1pu/file/rtbrvalues

vin = vin - vinstep
If[inc < runsToDo && vin >= 0, Goto[force]]

Label[end]
Print["The Mathematica program has finished."]
```

Appendix B

ACLineCycle Simulation Program Listing

This section contains the program listing for **ACLineCycle**. This simulation program was performed in **Mathematica, Version 1.2** on the **Next** computer. A full description and flowchart of **ACLineCycle** is contained in section 5.

Description

RTBR actual line cycle behaviour with undamped "On Period" response and fixed values of β_0.

RTBR Parameters

```
vbase = 200   (* Used to determine pu diode drops. *)
vout = 1 (* "vout" set at 1 pu. *)
vbr = 2.0/vbase;    vsw = 3.7/vbase;    vdb = 1.0/vbase
lb = 57.5/50
lt = 1.18
ct = 13.3
zt = Sqrt[lt/ct]
rb = 0.004
rc = N[(1 / (400 ct)), 3]
qfixed = 0  (* "qt" is the Q of the RT. *)
If[qfixed == 1, qt = 136, rt = (0.004 - rc)]
If[qfixed == 1, rt = N[(zt / qt - rc), 3],
 qt = N[(zt / (rt + rc)), 3]]
```

Input Parameters and Limits

Initial starting values and desired calculation direction is given.

```
runsToDo = 6 (* A run determines data for curves of all steady-state
 parameters versus "beta0" for a specific input voltage. *)
pulsesToDo = 0 (* This overrides "runsToDo" and generates data for the
 number of pulses specified. *)

(* Curve starting values: *)
beta0 = 90
vin = 0.75 (* Starting Vin for a few pulses. *)
vtp0start = vout
If[pulsesToDo == 0, phiVstart = -45, phiVstart =
 N[ ArcSin[(vin / Sqrt[2] vbase/120)] / Degree ] ]

(* Curve constants: *)
beta0step = 30;   cycle = 2
vttrig = 0.9 vout   (* RT voltage at which the control circuit triggers
 turn-off.*)
tod = 1.0 (* Control circuit turn-off delay. *)

(* Curve limits: *)
t2max = 12 (* On Period time-out. *)
ib0max = 0.5 (* Arbitrary limit to suppress excessive output values. *)
changelimit = 0.1
phiVend = 180;
```

Characteristic Calculations

The characteristic matrix "charm" and its' eigenvalues "eig" are determined. A check is done to ensure that the imaginary pair eigenvalues are the first two of "eig". The resonant frequencies and other parameters are determined.

```
charm = {{ -(rb+rc)/lb, rc/lb, -1/lb},
 {rc/lt, -(rt+rc)/lt, 1/lt}, {1/ct, -1/ct, 0 }}
eig = Eigenvalues[charm]

If[Im[eig[[3]]] == 0, Goto[normal]]
AppendTo[eig, eig[[1]]]
eig = Drop[eig, 1]

Label[normal]
chareqn2 = Expand[ (s - eig[[1]])*(s - eig[[2]]) ]
aloss = - Coefficient[chareqn2,s,1] / 2
wb = Sqrt[Coefficient[chareqn2,s,0] - aloss^2 ]
wtn = 1/ Sqrt[lt ct]
zeta = (rt + rc)/(2 zt)
wt = wtn Sqrt[1 - zeta^2]
```

```
k = lt/(lb + lt)
wbn = Sqrt[(lb + lt)/(lb lt ct)]
ft = N[1000 wt/(2 Pi)]
```

Pulse Calculations

This program simulates a RTBR through 5/8 of a line cycle (from $\phi_V = -45$ to 180) for constant values of β_0 (tank phase at turn-on). Each pulse (corresponding to one switching period) is simulated using the final values of the last pulse as it's initial conditions. Pulse currents, voltages, times, power, efficiency and other RTBR parameters for a pulse are determined. AC steady-state is expected to be reached before ϕ_V reaches zero.

Numerous conditionals are used in the program to allow calculations to be included or omitted depending on the type of current pulse being generated. Four types of pulses are possible, differentiated by the turn-off mechanism;

1. Turn-off at zero current, with no output current.
2. Forced commutation due to the turn-off trigger.
3. Natural commutation when "vt" reaches "vtcom".
4. Turn-off due to timeout.

In addition, if the RT voltage is higher than the impressed voltage "vimp" at the turn-on instant, the pulse may be delayed for a time "tdel". The pulse will begin as soon as "vt" drops below "vimp".

The data is stored in files outside Mathematica for later retrieval by the MakeGraph program. Data for a pulse is only stored if "changetest" indicates that there has been sufficient change in the slope of the curves to warrent saving another point.

```
(* Counters *)
runsDone = pulsesDone = numCurves = lineCurves = inc = 0;

rtbrvalues = linecycle = pulses = swperiods = {}
pulselist = swperiodlist = beta0list = curvlist = {}
If[pulsesToDo != 0, Goto[beta0curves]]

(* If curve data has already been calculated for this RTBR, this data will
 be retrieved, so that the new data can be added to it. *)
Print["Reading rtbrvalues from memory."]
rtbrvalues = <<AClc.cyc2/voutipu/file/rtbrvalues
If[rtbrvalues[[1]] == 1, Print["File with prior data exists."],
```

```
  Goto[beta0curves]]
numCurves = rtbrvalues[[22]]
beta0list = rtbrvalues[[27]]
curvlist = rtbrvalues[[28]]
runsDone = rtbrvalues[[29]]
lineCurves = rtbrvalues[[31]]
Print["Reading linecycle from memory."]
linecycle = <<AClc.cyc2/vout1pu/file/linecycle

Label[beta0curves]
(* Start of a linecycle run at a certain "beta0". *)
ibsqt = ibavsqt = itsqt = pinsum = poutsum = 0
phiVflip = ib0 = ib0abort = cc = 0
t2ch = ibavch = vtp0ch = 0
ibavb1 = ibavb2 = vtp0b1 = vtp0b2 = 1
mag = t2b1 = t2b2 = 1
runsDone++

phiVrad = N[phiVstart Degree]
beta0rad = N[beta0 Degree]
vtp0 = vtp0start

AppendTo[beta0list, beta0]
If[pulsesToDo == 0 ,
 Print["Curves starting with beta0 = ", beta0,
  ", runs = ", runsToDo],
 Print["Pulses with beta0 = ", beta0,
  ", pulses = ", pulsesToDo]]

Label[force]
(* Start of calculations for one switching period. *)
tdel = ton = t2 = t2nat = t2trig = t3 = tosc = tramp = 0
ib = ib2 = ibav = it = itdel = it2 = vt = intibon = intibramp = 0
intit2 = intitdel2 = 0
tibpk = vtpk = ibpk = beta2rad = tsw = eff =.
changetest = 1;  trigger = 0

phiV = N[phiVrad/Degree]
vin = N[Sqrt[2]] 120/vbase Abs[Sin[phiVrad + N[2 Pi 60/3 t2max 10^-6]]]
  (* The value for "vin" is calculated 1/3 through
   the potential "On Period" for greater accuracy. *)
vimp = vin - vbr - vsw     (* voltage impressed across the RT. *)
vlbramp = vout + vdb - vin + vbr
 (* voltage across "lb" during the "ib" ramp down. *)
vtcom = vout + vdb - vsw    (* "vt" when natural commutation occurs. *)

(* Determine initial condition values. *)
it0 = vtp0 / zt Sin[beta0rad]
vt0 = vtp0 Cos[beta0rad]
```

```
If[vt0 < vimp, Goto[pulse]]  (* The diode bridge is forward biased. *)
If[-vtp0 < vimp, Goto[delay]]  (*  The diode bridge will become forward
 biased as the RT oscillates, assuming "t2max" > "(Pi - beta0) /wt". *)

Label[nopulse]
(* This switching period will consist only of the specified number of
 cycles of RT oscillation.   Time "t2" is zero. *)
it2 = it0;   vt2 = vt0;   vtp2 = vtp0
beta2rad = beta0rad
tsw = tosc = Re[N[( 2 cycle Pi) / wt]]
vtp4 = vtp2 E^(-zeta wtn tosc) (* vtp at "tsw" and at next turn-on.*)
Print["No current pulse."]
Goto[freewheel]

Label[delay]
(* "ib" and current in the switch are delayed until
 "vt" drops below "vimp". *)
tdel = (ArcCos[vimp/vtp0] - beta0rad) / wt
If[tdel > t2max, Goto[nopulse]]
Print["Delayed current pulse."]
itdel = (E^(-zeta wtn t) vtp0 / zt Sin[wt t + beta0rad])
intitdel2 = NIntegrate[itdel^2, {t, 0, tdel}]
 (* Integral of "it"^2 during the delay time. *)

(* Re-assign initial condition values. *)
vtp0 = vtp0 E^(-zeta wt tdel)
it0 = vtp0 / zt Sin[beta0rad + wt tdel]
vt0 = vimp

Label[pulse]
(* Start to determine terms to be used in the formulae
 for "ib", "it", and "vt". *)
t2 = t2nat = t2max
avt = vt0 - k vimp
bvt = ib0/(wbn ct) - vtp0 Sqrt[1-k] Sin[beta0rad + wt tdel]
cvt = Sqrt[avt^2 + bvt^2]

(* Terms used in determining whether "vt" reaches certain values, and the
 time at which those values are reached. *)
ln = (1 - k) vimp / cvt; aln = Re[ArcSin[ln]]
lmn = (vttrig - k vimp) / cvt;  almn = Re[ArcSin[lmn]]
mn = (vtcom - k vimp) / cvt; amn = Re[ArcSin[mn]]
nn = avt/cvt; ann = Re[ArcSin[nn]]
tibpk = If[0 < beta0 < 180, N[(aln + Pi + ann) / wbn], N[(aln - ann)/wbn]]
  (* The peak of "ib" occurs when "vt" = "vimp". *)
If[lmn >= 1, Goto[formulae]]  (* If lmn > 1, then vt won't reach vttrig. *)
If[mn >= 1, Goto[forcedCommutation]] (* If mn > 1, "vt" won't reach "vtcom"
 and natural commutation will not occur. *)
ton = If[0 < beta0 < 180, N[(amn + Pi + ann) / wbn], N[(amn - ann)/wbn]]
```

```
  (* The switch is on until "vt" = "vtcom". *)
t2 = t2nat = ton + tdel

Label[forcedCommutation]
(* The control circuit will commence turn-off when "vt" passes vttrig.
  The circuit imposes a delay,  "tod", in actual turn-off. *)
tvttrig = If[0< beta0 <180, N[(almn + Pi + ann)/wbn], N[(almn - ann)/wbn]]
t2trig = tvttrig + tod + tdel
If[t2trig < t2nat, trigger = 1]
If[t2trig < t2nat, t2 = t2trig]
If[t2 > t2max, t2 = t2max]

Label[formulae]
ib = ib0 + vimp (t - tdel)/(lb + lt) - ( avt Sin[wbn (t - tdel)] +
  bvt (1 - Cos[wbn (t - tdel)]) ) / (wbn lb)
it = vimp (t - tdel)/(lb + lt) + (avt Sin[wbn (t - tdel)] +
  bvt (1 - Cos[wbn (t - tdel)]))/(wbn lt) + it0
vt = k vimp + bvt Sin[wbn (t - tdel)] + avt Cos[wbn (t - tdel)]
vtpk = k vimp + Sqrt[bvt^2 + avt^2]

ib2 = Re[N[ib/. t -> t2]]    (* check ib at time t2 *)
ibch = Re[N[ib/. t -> (t2 + tibpk)/2]]
 (* check "ib" at an intermediate time as well, in case
  "t2" is at "t2max" and "ib2" has become positive. *)
If[ib2 < 0 || ibch < 0, ib2 = 0, Goto[time2]]

(* Since "ib" would fall below zero before the boost
 diode turns on, a new "t2" at "ib" = 0 is determined. *)
Print["Pulse with no output current."]
t2 = Chop[Re[t/. FindRoot[(ib == 0), {t, (tdel + 1.5 tibpk)}]]]

Label[time2]
If[trigger == 1 && ib2 != 0, Print["Trigger Forced Commutation."]]
it2 = N[it/. t -> t2]
vt2 = N[vt/. t -> t2]
vtp2 = Re[Sqrt[vt2^2 + (zt it2)^2]]
If[ vt2 >= 0, beta2rad = Re[ArcSin[it2/vtp2 zt]],
 beta2rad = N[Re[ -ArcSin[it2/vtp2 zt]] -Pi]]
  (* "vt2" < 0 only in rare cases when "vtp0" is very small. *)
beta2 = N[beta2rad/Degree]

tramp = Re[-lb/rb Log[ 1/( 1 + rb ib2 / vlbramp)]]
  (* time taken for ib to ramp down to zero. *)
t3 = t2 + tramp (* Lb conduction period *)
tosc =  Re[N[(( 2 (cycle - 1) Pi + beta0rad - beta2rad) / wt]]
  (* length of time of RT free oscillation. *)
tsw = t2 + tosc (* switching period *)

ib0 = 0  (* Re-set to zero for the next pulse in case
```

```
 discontinuous conduction has returned. *)
If[t3 > tsw, cc = 1, Goto[power]]
Print["WARNING!  Continuous Conduction!"]

(* The following saves the value of "phiV" and "vtp0" when continuous con-
 duction first occurs so that a flip can be performed if "ib" runs away. *)
If[phiVflip == 0, vtp0flip = vtp0]
If[phiVflip == 0, phiVflip = N[Pi - phiVrad + 120 Pi tsw 10^-6]]
ib0 = Chop[N[ibramp /. t -> tsw], 10^-6]
t3 = tsw
If[ib0 < ib0max || pulsesToDo != 0, Goto[power], ib0abort = 1]

(* Aborting calculations since "ib" is running away due to continuous
 conduction.  Will re-start at the last "vin" of discontinuous conduction,
  but on the other side of the input voltage crest. *)
Print["ib0max exceeded.  Flip performed."]
ib0 = 0
phiVrad = phiVflip;   vtp0 = vtp0flip
Goto[curveReady]  (* Will store the curve points, and
 start a new curve on the flipside. *)

Label[power]
ibramp = - vlbramp/rb + (ib2 + vlbramp/rb) E^(-rb/lb (t-t2))
intibon = NIntegrate[ib, {t, tdel, t2}]
 (* Integral of "ib" during the "On Period". *)
intibramp = NIntegrate[ibramp, {t, t2, t3}]
 (* Integral "ib" during the ramp down time. *)

ibpk = Chop[N[ib/. t -> tibpk], 10^-6]
 (* The peak of the input current pulse. *)
ibav = (intibon + intibramp)/tsw
 (* Average current of the input current pulse. *)
pin = vin ibav (* Input Power. *)
pinsum = pinsum + vin (intibon + intibramp)
pout = vout intibramp/tsw (* Output Power. *)
poutsum = poutsum + vout intibramp

vtp4 = vtp2 E^(-zeta wtn tosc) (* vtp at tsw and at next turn-on.*)
et0 = ct vtp0^2 / 2 (* RT energy at t0. *)
et4 = ct vtp4^2 / 2 (* RT energy at tsw. *)
eff = (pout tsw + et4) / (pin tsw + et0)
 (* Energy efficiency is used rather than power
  efficiency since pout > pin for some pulses. *)

Label[freewheel]
itosc = (E^(-zeta wtn (t-t2)) vtp2 Sin[wt (t-t2) + beta2rad] / zt )
intitosc2 = NIntegrate[itosc^2, {t, t2, tsw}]
 (* Integral of "it"^2 during the "Off Period". *)
intit2 = NIntegrate[it^2, {t, tdel, t2}]
```

```
 (* Integral of "it"^2 during the "On Period". *)
tankloss = (rc + rt) (intitdel2 + intit2 + intitosc2)/tsw

phiVmid = phiV + N[60 Pi tsw 10^-6 / Degree]
 (* values awill be stored with the line cycle
  phase at the midpoint of the switching period. *)
pulsesDone++
If[pulsesDone >= pulsesToDo && pulsesToDo != 0, Goto[end]]

(* Parameters to check for the amount of change in
 the variables from one pulse to the next.  If
  "changetest" is large enough, the data will be stored.
   Otherwise, it is not. This reduces the amount of data
    generated and the time taken to make the graphs. *)
t2ch = t2ch + (t2b2 - 2 t2b1 + t2)^2
ibavch = ibavch + (ibavb2 - 2 ibavb1 + ibav)^2
vtp0ch = vtp0ch + (vtp0b2 - 2 vtp0b1 + vtp0)^2
changetest = mag^2 (t2ch + ibavch + vtp0ch)

If[changetest < changelimit && vin > 0.1 vout, Goto[phiVplus]]
onepulse = N[{phiVmid, tibpk, vtpk, ibpk, t2, tsw, beta2, eff}, 6]
AppendTo[pulselist, onepulse]
oneswperiod = N[{phiVmid, vtp0, ibav, tankloss, cc}, 6]
AppendTo[swperiodlist, oneswperiod]

(* Shifting of the changetest parameters. *)
t2b2 = t2b1;    ibavb2 = ibavb1;    vtp0b2 = vtp0b1
t2b1 = t2;  tswb1 = tsw
ibavb1 = ibav;  vtp0b1 = vtp0
t2ch = ibavch = vtp0ch = mag = 0
Print["Point Saved"]

Label[phiVplus]
phiVrad = phiVrad + N[120 Pi tsw 10^-6]
vtp0 = vtp4  (* "vtp" at the end of this switching
 period is the "vtp" at the start of the next one. *)
mag++
If[phiVrad < 0, Goto[force]]
 (* Calculations while "phiV" < 0 are only done to reach AC steady-state,
  so no further calculations or storage of data need be done. *)

If[N[120 Pi tsw 10^-6] < phiVrad < N[phiVend Degree], Goto[force]]
 (* This allows the program to reach  [curveReady] when "phiV" is closest
  to 0 and then again when "phiV" = "phiVend". *)

Label[curveReady]
If[numCurves == 0, Goto[storeCurve]]
Print["Reading pulses and swperiods from memory."]
pulses = <<AClc.cyc2/vout1pu/file/pulses
```

```
swperiods = <<AClc.cyc2/vout1pu/file/swperiods

Label[storeCurve]
AppendTo[pulses, pulselist]
AppendTo[swperiods, swperiodlist]
AppendTo[curvlist, runsDone]
Print["Writing to pulses and swperiods."]
pulses >> AClc.cyc2/vout1pu/file/pulses
swperiods >> AClc.cyc2/vout1pu/file/swperiods
pulses = swperiods = pulselist = swperiodlist = {}
numCurves++

rtbrvalues = {1, lb, lt, ct, rb, rt, rc, vout, N[vbr, 4], N[vsw, 4],
 N[vdb, 4], qt, zt, 1, wbn, wb, wtn, wt, zeta, k, cycle, numCurves,
  "phiV", phiVstart, phiVend, "beta0", beta0list, curvlist, runsDone, t2max,
   (lineCurves + 1), vttrig, tod}
Print["Writing to rtbrvalues."]
rtbrvalues >> AClc.cyc2/vout1pu/file/rtbrvalues

If[phiVrad < N[phiVend Degree], Goto[force]]
inc++;   beta0 = beta0 + beta0step
If[inc < runsToDo, Goto[beta0curves]]

Label[end]
Print["The Mathematica program has finished."]
```

Appendix C

Control Circuit Schematic Diagram

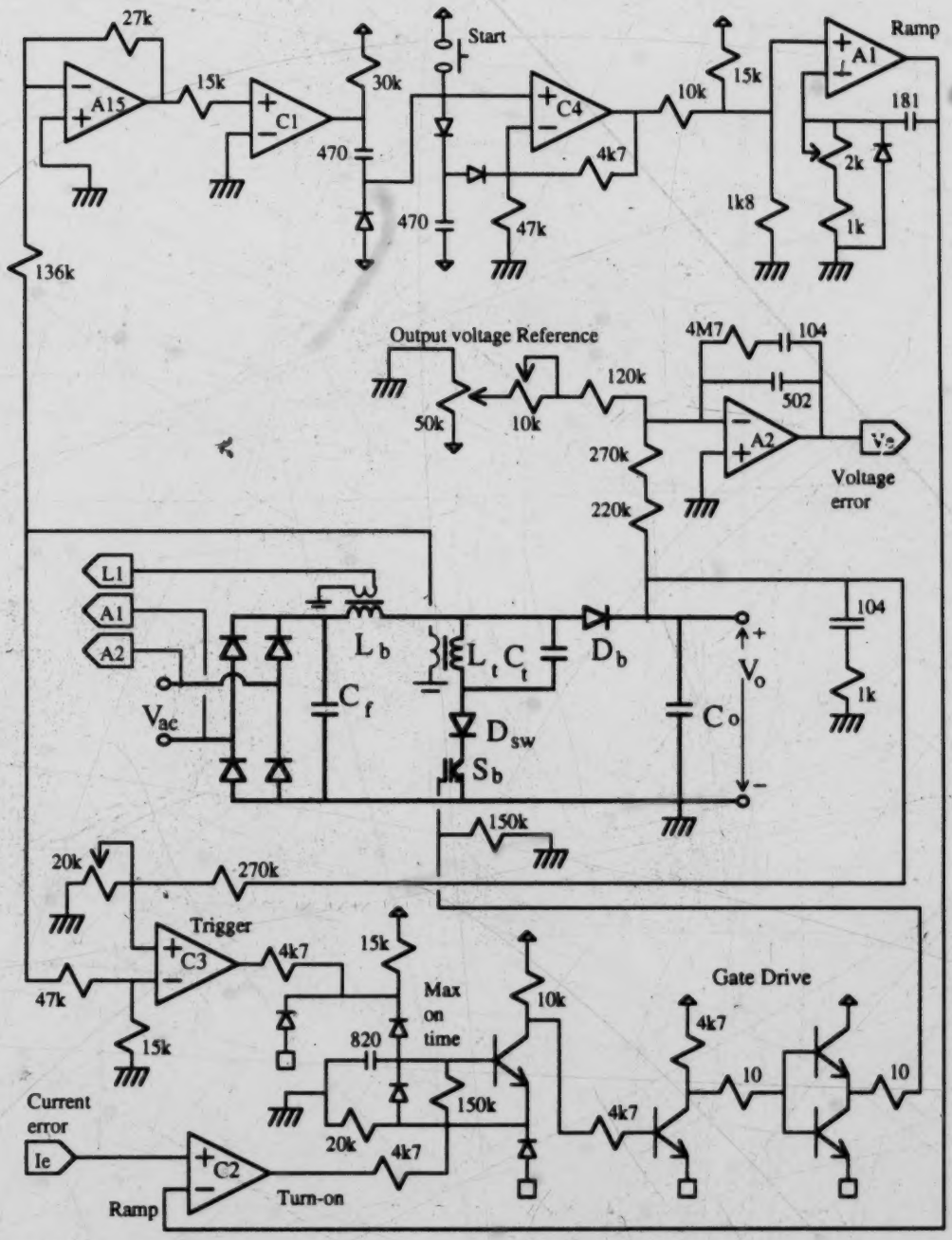

Figure C.1: Control Circuit Schematic Diagram, sheet 1.

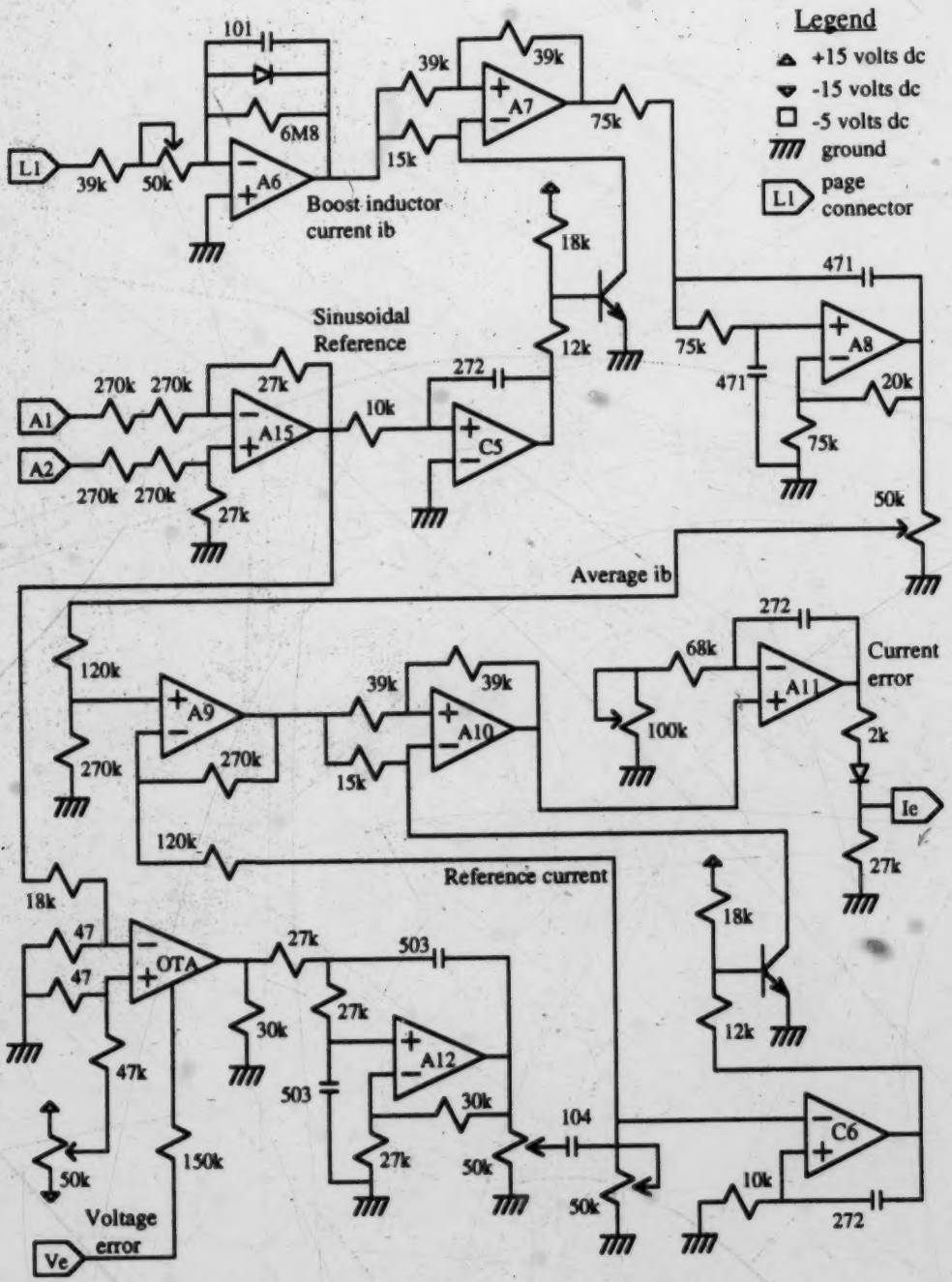

Figure C.1: Control Circuit Schematic Diagram, sheet 2.